Aerodynamic Analysis of a Blended-Wing-Body Aircraft Configuration

A thesis submitted in fulfilment of the requirement for the degree of Master of Engineering by Research.

Toshihiro Ikeda

Bachelor of Engineering

School of Aerospace, Mechanical and Manufacturing Engineering
Science, Engineering and Technology Portfolio
RMIT University

March 2006

Declaration

The author certifies that except where due acknowledgement has been made, the work is that of the author alone, the work has not been submitted previously, in whole or in part, to qualify for any other academic award; the content of this thesis is the result of research which has been carried out since the official commencement date of the approved research program, and any editorial works, paid or unpaid, carried out a third party are acknowledged.

Signed: 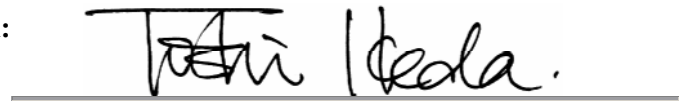

Toshihiro Ikeda

March 2006

Acknowledgements

There are so many who have helped both directly and indirectly in assisting with this research that it is difficult to thank everyone. The author's sincere thanks and appreciation are extended to:

▪ Associate Professor Cees Bil of RMIT University and Mr. Robert Hood of GKN Aerospace Engineering Services for their unceasing positive guidance and sage advices, and RMIT IT staff for their support.

▪ Mr. Hawk Lee of Fluvius Pty Ltd for his professional advice regarding CFD simulation, and maintaining engineering workstations, as well as to the staff of Fluent Asia Pacific Co., Ltd. for their services.

▪ Mr. Tony Gray of Altair Engineering Inc. for his assistance and useful guidance of computational methodologies of HyperWorks applications.

▪ Mr. Adrian Baker of one of author's friends and Associate Professor Cees Bil of RMIT University for taking the time to read, advise and make constructive comments on the document at various stages of its production.

▪ Finally, the author would like to thank his parents for their encouragement and support for his studies in Australia.

Abstract

In recent years unconventional aircraft configurations, such as Blended-Wing-Body (BWB) aircraft, are being investigated and researched with the aim to develop more efficient aircraft configurations, in particular for very large transport aircraft that are more efficient and environmentally-friendly. The BWB configuration designates an alternative aircraft configuration where the wing and fuselage are integrated which results essentially in a hybrid flying wing shape.

The first example of a BWB design was researched at the Loughead Company in the United States of America in 1917. The Junkers G. 38, the largest land plane in the world at the time, was produced in 1929 for Luft Hansa (present day; Lufthansa). Since 1939 Northrop Aircraft Inc. (USA), currently Northrop Grumman Corporation and the Horten brothers (Germany) investigated and developed BWB aircraft for military purposes. At present, the major aircraft industries and several universities has been researching the BWB concept aircraft for civil and military activities, although the BWB design concept has not been adapted for civil transport yet. The B-2 Spirit, (produced by the Northrop Corporation) has been used in military service since the late 1980s. The BWB design seems to show greater potential for very large passenger transport aircraft. A NASA BWB research team found an 800 passenger BWB concept consumed 27 percent less fuel per passenger per flight operation than an equivalent conventional configuration (Leiebeck 2005).

The purpose of this research is to assess the aerodynamic efficiency of a BWB aircraft with respect to a conventional configuration, and to identify design issues that determine the effectiveness of BWB performance as a function of aircraft payload capacity. The approach was undertaken to develop a new conceptual design of a BWB aircraft using Computational Aided Design (CAD) tools and Computational Fluid Dynamics (CFD) software. An existing high-capacity aircraft, the Airbus A380

was modelled, and its aerodynamic characteristics assessed using CFD to enable comparison with the BWB design.

The BWB design had to be compatible with airports that took conventional aircraft, meaning a wingspan of not more than 80 meters for what the International Civil Aviation Organisation (ICAO) regulation calls class 7 airports (Amano 2001).

From the literature review, five contentions were addressed;

- **i.** Is a BWB aircraft design more aerodynamically efficient than a conventional aircraft configuration?
- **ii.** How does the BWB compare overall with a conventional design configuration?
- **iii.** What is the trade-off between conventional designs and a BWB arrangement?
- **iv.** What mission requirements, such as payload and endurance, will a BWB design concept become attractive for?
- **v.** What are the practical issues associated with the BWB design that need to be addressed?

In an aircraft multidisciplinary design environment, there are two major branches of engineering science; CFD analysis and structural analysis; which is required to commence producing an aircraft. In this research, conceptual BWB designs and CFD simulations were iterated to evaluate the aerodynamic performance of an optimal BWB design, and a theoretical calculation of structural analysis was done based on the CFD results.

The following hypothesis was prompted;

A BWB configuration has superior in flight performance due to a higher Lift-to-Drag (L/D) ratio, and could improve upon existing conventional aircraft, in the areas of noise emission, fuel consumption

and Direct Operation Cost (DOC) on service. However, a BWB configuration needs to employ a new structural system for passenger safety procedures, such as passenger ingress/egress.

The research confirmed that the BWB configuration achieves higher aerodynamic performance with an achievement of the current airport compatibility issue. The beneficial results of the BWB design were that the parasite drag was decreased and the spanwise body as a whole can generate lift. In a BWB design environment, several advanced computational techniques were required to compute a CFD simulation with the CAD model using pre-processing and CFD software.

Nomenclature

A	Statistical Empty Weight Fraction
a	Speed of Sound
AR	Aspect Ratio
B	Fuselage Width of Aircraft
b	Wing Span
b_{vert}	Tail Length
C	Negative Exponent of Relationship between Empty Weight and TOGW
c	Specific Fuel Consumption (SFC)
C.G.	Centre of Gravity
C_L	Lift Coefficient
C_D	Drag Coefficient
C_{Dtotal}	Total Drag Coefficient
$C_{Dpressure}$	Pressure Drag Coefficient
$C_{Dfriction}$	Friction Drag Coefficient
C_{Dwave}	Wave Drag Coefficient
C_M	Momentum Coefficient
C_{Dp}	Parasite Drag Coefficient
C_{DI}	Induced Drag Coefficient
D	Drag
d	Mission Segment Range
e	Aircraft Efficiency
g	Gravity (= 9.8 m/s^2)
K_{VS}	Variable Sweep Constant
K_s	Scale Factor of Cabin Area
k	Turbulent Kinetic Energy
L	Lift
L/D	Lift to Drag Ratio
M	Mach number
N_{ult}	Ultimate Load Factor
N_{seat}	Number of Passenger Seat
P	Maximum Pressure Differential
R	Range
R	Universal Gas Constant (287.05 J/Kg/K for Air)
Re	Reynolds number
S	Reference Area
S_{cabin}	Cabin Area
S_{fuse}	Gross Wetted Area of Fuselage
S_{gw}	Gross Wing Area
S_{ref}	Reference Area of Aircraft
S_{vert}	Vertical Tail Area
T	Absolute Temperature (Kelvin)
T	Engine Thrust
TOGW	Take-Off Gross Weight
T/W	Thrust-to-Weight Ratio

$(t/c)_{avg}$ Average Airfoil Thickness

u Velocity of Fluid

V Velocity

V/c Propulsion Capacity Efficiency

$W_{air\ con}$ Air Conditioner and Anti-Icing System Weight

W_{apu} Auxiliary Power Unit Weight

W_{cabin} Cabin Weight

W_{crew} Crew Weight

W_{deng} Dry Engine Weight

W_{elecp} Electrical Equipment Weight

W_{empty} Empty Weight

W_{fuel} Fuel Weight

W_{furni} Furnishing Weight

W_{fuse} Fuselage Weight

W_{gear} Landing Gear Weight

W_{hp} Hydraulics and Pneumatics Weight

W_{sc} Surface Control Weight

$W_{takeoff}$ Take-Off Weight

$W_{payload}$ Payload Weight

W_{pro} Propulsion Weight

W_{vert} Vertical Tail Weight

W/S Weight Loading Ratio

W_{wing} Wing Weight

W_{ZFW} Zero Fuel Weight

ρ Density

κ Aircraft Shape Factor

δ Parameter of Wing Shape

λ Taper Ratio of Wing

Λ_{ea} Swept Angle of Structural Axis

μ Dynamic Viscosity

μ_t Turbulent Kinetic Viscosity

δ_{ij} Kroenecker Delta

G_b Generation of Turbulent Kinetic Energy due to Bouyancy

G_k Generation of Turbulent Kinetic Energy due to Mean Velocity Gradient

G_v Production of Turbulent Viscosity

Y_M Contribution of Fluctuating Dilation

Y_v Destruction of Turbulent Viscosity

γ Adiabatic Index (1.402 for Air)

ν Kinetic Viscosity

π 3.14159

Table of Contents

List of Figures

List of Tables

Chapter 1 Introduction

Aircraft technologies that could give greater performance include a large improvement in Lift-to-Drag ratio of a wing coupled to evolutionary improvement in composite structure and engines, such as Blended Wing Body aircraft configuration. This next generation airlifter has been researched with a high L/D ratio wing configuration design, engineered materials, composite fabrication and fastening, and next generation material for airframe and skin. A Blended-Wing-Body (BWB) design approach is to maximise overall efficiency by integrated the propulsion systems, wings, and the body into a single lifting surface. This BWB configuration is a new concept in aircraft design which expects to offer great potential to substantially reduce operating costs while improving an aerodynamic performance and flexibility for both passenger and cargo mission.

1.1 Definition of Blended-Wing-Body Aircraft Configuration

A BWB aircraft is a configuration where the wing and fuselage are integrated which essentially results in a large flying wing. BWB aircraft were previously called ‘tailless airplanes’ and ‘Flying-Wing aircraft’.

The BWB configuration has shown promise in terms of aerodynamic efficiency, in particular for very large transport aircraft, because the configuration has a single lifting surface that means an aerodynamically clean configuration.

1.2 Historical Background

BWB aircraft have been on the drawing board for more than a half century. Today such a concept has only been applied to military aircraft to obtain a low radar cross-section. However, in a presentation later in the 20th century the Boeing Company and Cranfield College of Aeronautics drew detailed

pictures of a BWB concept model where the idea has been addressed - and where it might be headed. In the past, also, several pioneers in the United States of America (USA) and Germany tried to produce an aerodynamically efficient aircraft, such as tailless aircraft and Flying-Wing concepts (Bolsunovsky 2001 & Ikeda 2005a).

In history, research groups, such as the Northrop Corporation in the UAS and the Horten Brothers in Germany and several investigators have made a design without a fuselage section as aerodynamically clean as the Flying-Wing design which has a big advantage over conventional aircraft configuration.

- **Northrop Corporation in the USA** (Currently known as the Northrop Grumman Corporation)

  In January, 1927, John Northrop and three other engineers formed the Lockheed Aircraft Company. It was at that time that he designed the famous Lockheed Vega using high wing cantilever monocoque framework. As years passed he drew the Flying-Wing design and became the leading exponent of Flying-Wing design in the United States. In 1928 the Northrop's first semi-Flying-wing plane (Fig. 1.1) was flown and made use of external control surfaces and curried outrigger twin booms. After 11 years a new Flying-Wing design, the N1M 'Jeep' (Fig. 1.2), was built and tested at Muroc Dry Lake in July 1940. During 1940 and 1941, over 200 flights were made in this aircraft to gather data. In 1941 the XB-35 design of the first Flying-Wing series of large Flying-Wing Bomber was made, which was a bombardment type of exceptionally long range and with a heavy load capacity for the United States Air Force. The YB-49 (Fig. 1.3) was introduced in 1947 which would prove to be the most successful Flying-Wing aircraft (History of Northrop Corporation 2005, Monash University 2005, pilotfriend 2005).

  Since the improvement of Flying-Wing technology, the most famous Flying-Wing and the only successful one has been, the Northrop-Grumman B-2 Spirit Stealth Bomber (Fig. 1.4)

made in 1981. The bomber had sophisticated modern computer control systems installed, and the 21 of these planes were in service in the 1999 bombing of Yugoslavia (pilotfriend 2005).

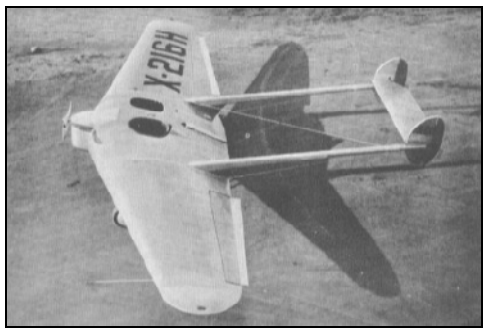

Fig. 1.1 Northrop Semi-Flying-Wing

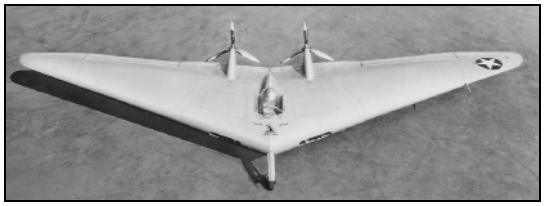

Fig. 1.2 Northrop N1M 'Jeep'

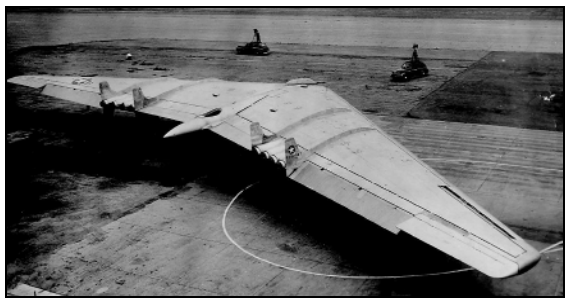

Fig. 1.3 Northrop YB-49

Fig. 1.4 Northrop B-2 Spirit Stealth Bomber

▪ **Horten Brothers in Germany** (aerostories 2005 & Horten Bros's Flying Wing 2005)

The Horten brothers, Walter Horten and Reimar Horten, are one of the virtuosos of the Flying-Wing manufacture, testing with stubbornness their machines without neither fuselage nor tail section in gliding flight in the 1930's in Germany. When hostilities began in World War II (WWII), the Horten brothers were assigned to the Luftwaffe. During the entire period of WWII, the Horten brothers conceived machines with constantly improved performance. Their first glider, the Horten Ho I (Fig. 1.5), was tested at Bonn-Hagelar in 1933. However, it was not success in flight. After evaluating their Flying-Wing design, the Horten Ho IV was a complete successful to fly. At the same time their Ho III (Fig. 1.6) successfully soared to 7,000 meters altitude in 1938 and the Horten Ho IX with turbojet engines made its second gliding flight, but the configuration had an insurmountable problem with the then

technologies. On 14th of April in 1945, the American army arrived at the production factory and captured the Gothear Go 229, and construction was discontinued of what had been the first jet propelled Flying-Wing after 10 years of the achievement of Flying-Wing aircraft with turbojet engines. The Horten Ho IX-Go 229 (Fig. 1.7) was never operational, but it came very close to completion.

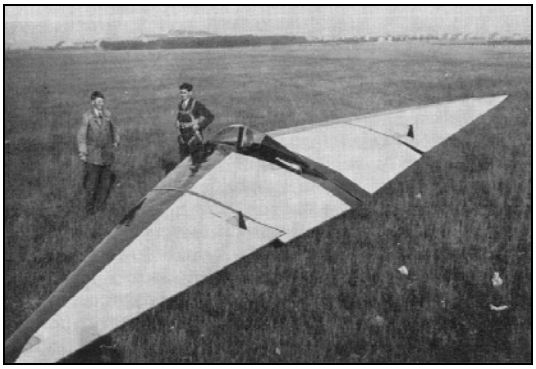

Fig. 1.5 Horten Ho I

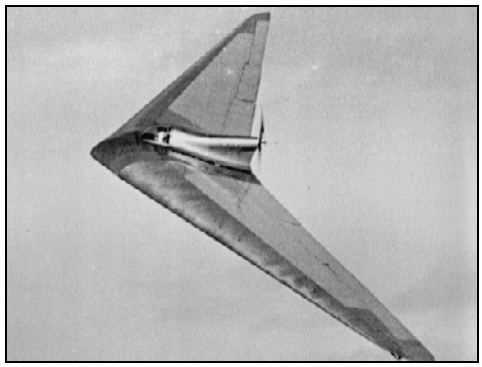

Fig. 1.6 Horten Ho III

Fig. 1.7 Horten Ho IX-Go 229

▪ **Other Previous Flying-Wing Projects**

In the United States, Sir W. G. Armstrong Whitworth Aircraft Ltd., designed the Armstrong Whitworth A.W. 52 (Fig. 1.8) in 1947 (British Aircraft 2005), and General Dynamics/McDonnell Douglas was also selected to develop a subsonic twin jet carrier, A-12 Avenger II, based on Advanced Tactical Aircraft concept (ATA) for attack at night or in bad weather in 1990 (GloablSecurity.org 2005).

In Japan there were several Flying-Wing concept aircraft, such as the HK 1 (Fig. 1.9) which

was the first Japanese tailless aircraft produced by the Ito Aircraft Laboratory in 1939 (BWB World 2005). Since the first test flight the HK 1 had been flown at 116 times, and the chief engineer Mr. Kimura reported that the HK 1 has a quiet, stable flight control in test flight at 1,000 meters altitude.

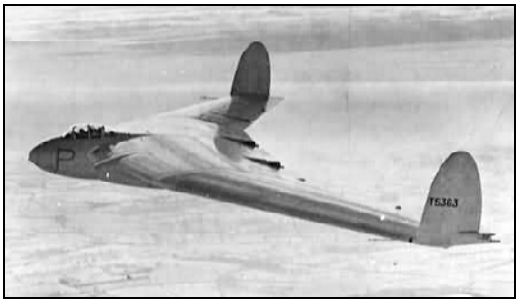

Fig. 1.8 Armstrong Whitworth A.W. 52

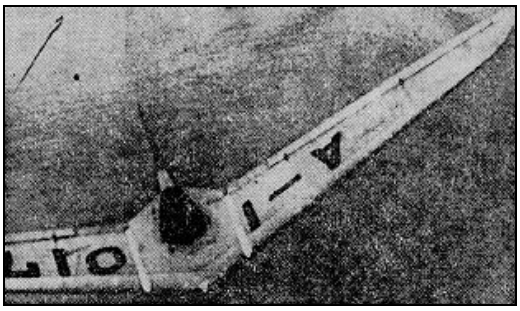

Fig. 1.9 Kayaba HK 1

In more recent years major aeronautical industries and universities have been researching and developing performance of BWB configuration for commercial aircraft. In regards to the research project at Cranfield College of Aeronautics, the preliminary design project of the Blended Wing Body Airliner is currently at the cutting edge of aircraft design technology exploring and evaluating a new configuration. This research has discovered a great deal of advantages and these concepts can be summarised as Fig. 1.10.

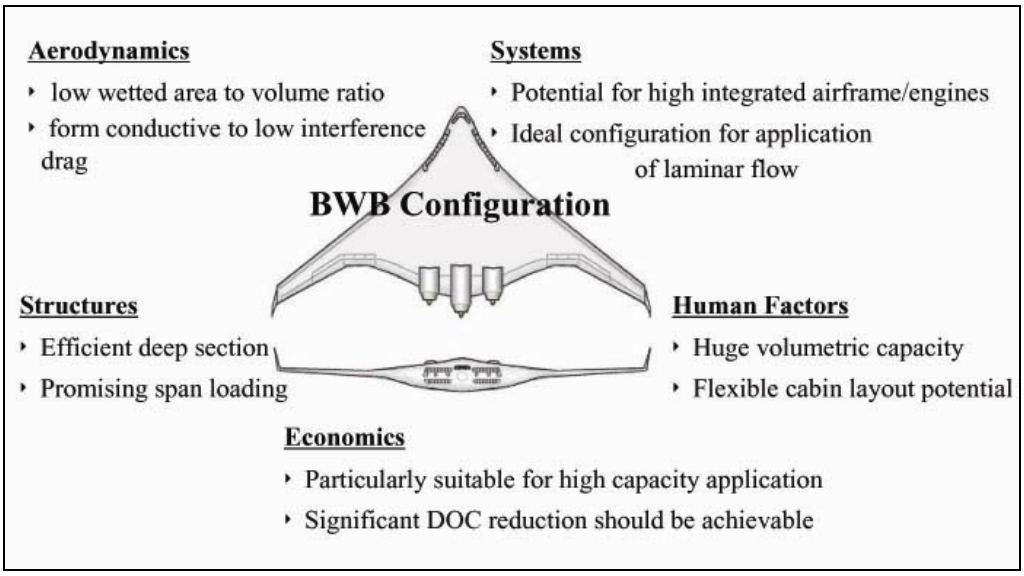

Fig. 1.10 Features of BWB Aircraft Configuration

In 1991, the NASA Langley Research Centre built a model of a BWB aircraft which had three engine nacelles on the aft of the top surface. Regarding the nose emission of this BWB aircraft, Dr. Lorenzo noticed that this aircraft model could reduce noise. The noise radiated downward was reduced by 20 dB to 25 dB overall in the full scale frequencies from 2,000 to 4,000 Hz, decreasing to 10 dB or less at the lower frequencies (Sandilands 2002).

NASA Langley Research Centre has stated that a BWB configuration will be more of a 600 than an 800 passenger airliner. Concerning this BWB aircraft, aeroelastic deflection will be severe for the wing span and will be counteracted by active surface as well as for verticals to provide a directional stability, control and to act as winglets to increase the effective aspect ratio (Guynn et al. 2004).

The leader of the aircraft industry, the Boeing Company, has announced that a BWB aircraft would climb an extremely steep angle, even compared to the gun-ho steep climb out experienced in the successful passenger flights today. In regards to the comparison between BWB configuration and conventional aircraft which have the same number of passengers and range for particularly large airliners, the BWB would be lighter and have a higher Lift-to-Drag (L/D) ratio and less fuel burn. For example, the BWB-450 which has been designed by the McDonnell Douglass team since 1988 would use 32 percent less fuel per seat and be 18 per cent lighter at its maximum Take-Off Gross Weight (TOGW) if both jets carried 480 passengers for an 8,700 nautical mile flight. In reference to the structural analysis of BWB aircraft, the configuration would require 30 percent fewer parts than conventional aircraft, because there are no complex wing-fuselage and fuselage-empennage joints (Sandilands 2002).

In regards to the high-lift-wing design for a Megaliner aircraft of Airbus A380-800 (Reckzen 2002), powered high-lift systems (e.g. externally blown flaps) of the Airbus Company showed an impressive

maximum lift potential beyond the performance of the familiar conventional high-lift systems. The high-lift performance aircraft, such as the A380 prototype, contributed better benefits than conventional aircraft which can be summarised as;

- 5 percent in maximum lift leads to 12-15 percent increase of payload,
- 5 percent of take-off L/D leads to 20 percent increase of payload,
- 5 percent of maximum lift in landing configuration leads to 25 percent increase of payload.

To conclude, the BWB aircraft configuration, synthetically, has the ability to provide a great number of benefits through its structural concepts, such as its aerodynamically low interface drag, high lift-to-drag ratio, structurally favourable span loading, and the reduction of green house emissions.

1.3 Multidisciplinary Design Study of a BWB Aircraft Configuration

The current knowledge of engineering technologies related to the A380 prototype and a BWB configuration will be covered from engineering perspectives.

1.3.1 Specifications of Airbus A380-800

The Airbus A380 is manufactured by Airbus S.A.S. (AIRBUS S.A.S 2004) and utilises novel approaches to the application of technologies, especially composite materials for weight saving proposes, in order for it to meet its guarantees of flight performance. During much of its development phase, the aircraft was commonly known as the Airbus A3XX, and the term ‘Superjumbo’ has become synonymous with the A380. The A380 is now the largest commercial airliner (Fig. 1.11).

The new A380 was initially manufactured in two versions: 1. The A380-800, carrying 555 passengers in a three class configuration (of up to 800 passengers in a single class economy layout), expected range for the A380-800 model is 8,000 nautical miles (14,800 km); 2. The A380-800F dedicated freighter will carry 150 tonnes of cargo and reach 5,600 nautical miles (10,400 km). For the propulsion

systems, either the Rolls-Royce Trent 900 (Rolls-Royce Company 2005) or Engine Alliance GP7200 (Engine Alliance 2005) turbofan engines are installed (Kennedy et. al 2003). The Trent 900 engine is the scale version of the Trent 800 incorporating sweptback fan and counter-rotating spools of the stillborn, and the GP7200 is derived fan and low-pressure turbo-machinery. The most improved technology employed for the A380 is the composite structure. The new material 'GLARE', which is an aluminium-glass-fibre laminate has superior corrosion-resistance, impact-resistance and lighter than common aluminium alloys used in aviation and is also utilised in the upper fuselage and on the landing edges of its stabiliser. Furthermore, the carbon-fibre reinforced plastics, glass-fibre reinforced plastic and quartz-fibre reinforced plastic are applied extensively to wings, fuselage sections and on doors. In addition, this is the first time that carbon fibre has been used to make the central wing box of a commercial airliner. (Airbus Company 2005a, AIRBUS S.A.S 2004). Table 1.1 shows the characteristics of the A380-800.

Additionally, procedures and handling characteristics are similar to those of other Airbus aircraft in regards to the cockpit design of the A380, but several features include improved glass cockpit, and fly-by-wire flight control linked to side-sticks as well as the eight 6-by-8 inch liquid crystal display (LCD) which are physically identical and interchangeable. The Multi-Function Displays (MFDs) are a new development, and provide an easy-to-use interface to the flight management system. Moreover, the MFDs units include QWERTY keyboards and trackballs are interfaced with a graphical 'point-and-click' display navigation system (Airbus Company 2005a, AIRBUS S.A.S 2004).

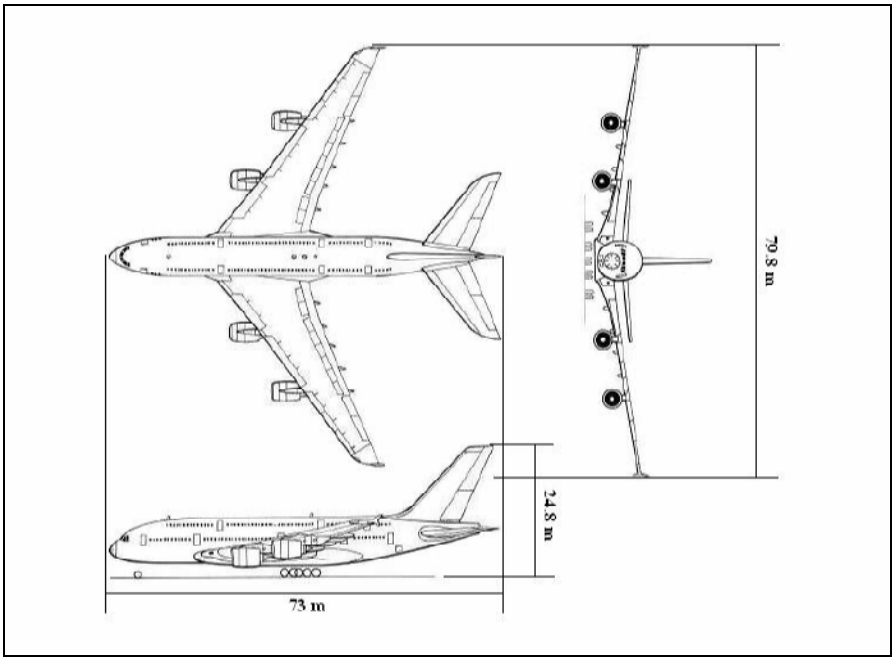

Fig. 1.11 Layout of Airbus A380-800 (AIRBUS S.A.S 2005)

Table 1.1 Characteristics of the A380-800 (AIRBUS S.A.S 2005)

Overall Length	73 m	239.3 ft
Cabin Length	50.68 m	166.3 ft
Fuselage Width	7.14 m	23.5 ft
Height	24.1 m	79.7 ft
Wingspan	79.8 m	261.8 ft
Wing Area (Reference)	845 m^2	9,100 ft^2
Swept Angle (25 % chord)	33.5 deg.	
Aspect Ratio	7.54	
Max. TOGW	560 ton	1,235,000 lbs
Max. ZFW	361 ton	796,000 lbs
Fuel Weight	310 ton	684,000 lbs
Payload	66.4 ton	145,500 lbs
Thrust Range	Four 70,000 lbs thrust	
Passengers	555	
Max. Operating Velocity	Mach 0.89	
Cruising Velocity	Mach 0.85	
Endurance	8,000 nm	15,000 km
W_e/W_0 Ratio	0.6868	
T/W	0.2268~0.2356	
Lift-to-Drag Ratio (L/D)	13.97	
TOGW Specific Range	0.014	
Requesting Thrust	305,000 lbs thrust	
Operating Thrust	88,200 lbs thrust	
FS Range	0.014 nm/lb	

The A380 has around a 13 percent lower fuel burn over Boeing B747 and is the first long-haul aircraft to consume less than 3 litres of fuel per passenger over 100 km which makes it as efficient as an average family car. Moreover, the large number of carbon fibre components and fuel-efficient technology also means that the cost per passenger is expected to be up to 20 percent less than on the B747 (netcomposites 2005). The most improved technology is that the flight performance and economics of the A380 is optimised by incorporating cutting-edge technologies in systems and materials. It benefits from the significant weight savings brought about by composite and other advanced materials which comprise 25 percent of its structure, 22 percent of which is carbon fibre reinforced plastic and 3 percent of GLARE and from the weight, reliability and cast benefits of new systems, such as its 5,000 psi pressure hydraulic system (Considerably more powerful than the 3,000 psi system normally used on commercial aircraft, and the greater pressure means that smaller pipes and hydraulic components can be used to transmit power) (JET Composites 2005).

In regards to the entire development phase, Airbus states that much work has been done to ensure that the large double-decker configuration will be able to operate on existing runways capable of accepting the B747 without requirements for any significant infrastructure adaptations. Airbus predicts that some 60 airports will be ready to welcome the A380 operations by 2010, and more will join as the number of operators continues to increase in the coming years (Airbus Company 2005b).

The marketing sector of the Airbus Company has announced that the A380 with 555 seats has been ordered by 15 customers with a commitment for a total of 154 A380 family aircraft, 127 passengers' aircraft from 13 customers and 27 freighters from 4 customers. The freighter version of the A380F will enter into service in 2008 (netcomposites 2005).

1.3.2 Current BWB Configuration Designs

In recent years BWB concept aircraft have been investigated and developed by many aeronautical

industries and institutions around the world. The most famous BWB project is the X-48 project (NASAexplores 2005) with both NASA and the Boeing Company designs suggesting that BWB concept configuration for passenger flight could carry from 450 to 800 passengers and achieve fuel savings of over 20 percent compared to the same flight missions of conventional aircraft (Sandilands 2002).

1.3.3 BWB Design of NASA and the Boeing Company, USA

The revolutionary BWB design (Fig. 1.12) was conceived by the McDonnell Douglass Corporation and has been newly proposed by the Boeing Company. Its flying-wing shape configuration has a thick airfoil shaped fuselage section to maximise overall efficiency by integrating the engines, wings, and the body into a single lifting surface. This BWB design houses a wide double-deck passenger compartment that actually blends into the wing. Adjacent to the passenger section is ample room for cargo.

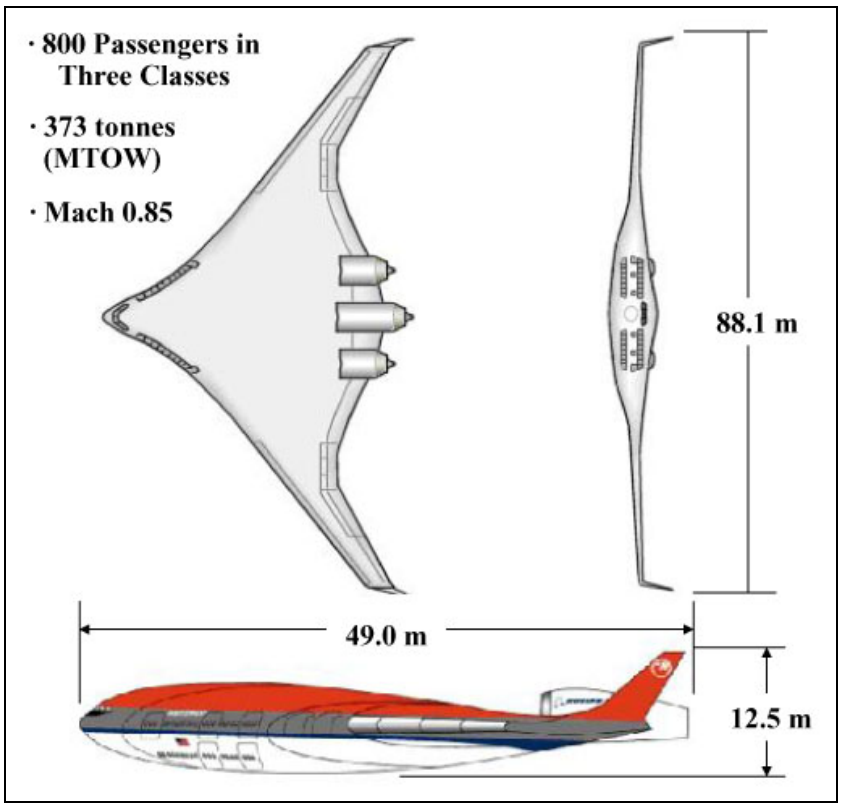

Fig. 1.12 Boeing BWB Concept Design (Aerosite 2005)

The BWB concept target of this research is to produce an advanced long-range ultra-high-capacity airliner, which is predicted to enter service between 2010 and 2020, and to carry 800 passengers with mixed classes over a range of 8,000 nautical miles at a cruise Mach number 0.85. In resent years the Boeing phantom work team, NASA and the Air Force Research Libratory (AFRL) have been developing X-48 as a BWB concept aircraft, and the X-48 prototype will be closely in flight testing phase later 2006 (Boeing News Release 2006). The principle of the BWB includes none-cylindrical section which is integrated within the wing, and this reduced surface area provides improved span loading which essentially resembles the Northrop B-2, and offers dramatic improvements in aerodynamic and structural efficiency. Moreover, the potential advantage indicates a fuel burn saving of 28 percent relative to a conventional aircraft of equivalent technology. The outline of the BWB design is 1.5 times the passenger capacity of the A380 and 69 precent larger than the A380 (Bowers 2000 & Liebeck 2005).

Fig. 1.13 Boeing Joined-Wing Concept Configuration (Steinke 2001)

In regards to its control stability, the stable all-wing configuration (Fig. 1.13) is difficult to trim without resorting to download at the wingtip which increases drag. The BWB concept design relies on advanced flight control systems to provide stable flight control allowing the centre-of-gravity to move the aft without trim problems. Furthermore improvement of the concept design is realised through use of boundary layer integration in the engines. This engine installation which is on the aft of the body

allows the engines to scavenge a sizable portion of the boundary air of the shape reducing the inlet ram drag and increasing efficiency. With the body shape of the BWB concept, the BWB configuration is predicted to be a 'clean' and more 'environment friendly' from of transport.

In addition, many American institutions such as Stanford University and George Washington University have been collaborating on investigations of a BWB concept design with the Boeing Company and NASA based on the NASA Science and Technical Information (STI) program (Kim 2003).

1.3.4 Conceptual Flying Wing Configuration of the Airbus Company, France

The Airbus Company has been investigating and developing an ecological version of the Airbus Flying Wing, Three Surface Aircraft (TSA) or a successor to Concorde with unusual designs aimed at increasing efficiency and environmental acceptability. Today these ideas are little more than intellectual exercises. However, these technologies could form the basis of an Airbus type in foreseeable future (Steinke 2001).

A different BWB conceptual design (Fig. 1.14) was presented by Airbus Deutschland GmbH (a partner in the Airbus project and member of the European Aeronautic Defence and Space Company (EADS) and is a user in the SafeAir project and participates in the user requirements definition for the process improvement techniques and the integrated toolset ASDE (Avionics System Development Environment) (Airbus Deutschland GmbH 2005)). The project aim was to compare a 'Flying Wing Two-deck configuration' to the configuration of the A380 structures with the flight mission of 7,650 nautical miles and with 750 passengers (22 First Class Seats/136 Business Class Seats/592 Economy Class Seats) (Lee 2003). For this conceptual design, the A380 based design is bigger than the A380 baseline: the wingspan will be 100 meters with top mounted wing and 23 meters' fuselage width. As it is a wide cabin design, the emergency procedure is a critical issue to consider, because of cabin

layout and the need to evacuate safely in an accident. When comparing the double and the single cabin design, the double deck cabin layout is more efficient because the cabin space which will be a dead space in the single cabin design is utilised effectually.

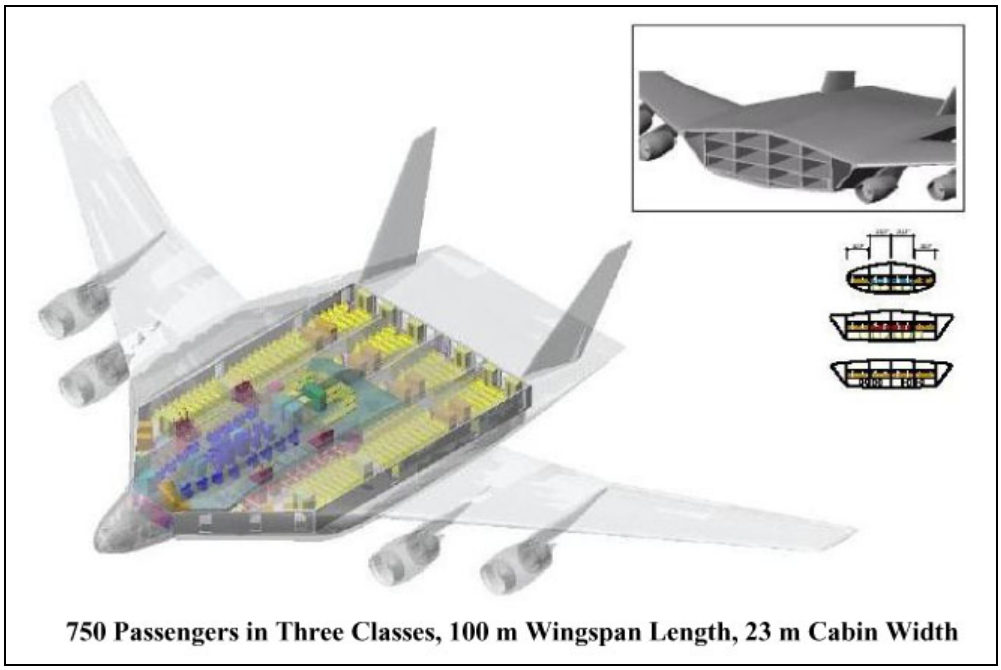

Fig. 1.14 Conceptual Flying Wing Design with the A380 Structures (Lee 2003)

As the two jointed wing concept of BWB design (Fig. 1.14), the Airbus Company has been investigating a large aircraft which potentially carries around 1,000 passengers. This design predicts radical reduction of fuel consumption compared with conventional wing-fuselage concepts. The main aerodynamic challenge in such a BWB is to obtain a clean flow of air over the thick midsection of the fuselage in which the payload area is located. From a design point of view, this approach poses some special challenges as it would entail combining wing design and fuselage design, whereas up to now these have been two distinct and separate design disciplines. Another drawback is the limited scope for modification of a flying wing from a technical view point whereas a conventional aircraft configuration can simply be stitched, so it is likely that every model of a BWB concept, and every side of every model, would require a dedicated design with the associated cost implications. Due to the complex structure, it would not be possible to insert or remove segments of the fuselage. In

addition, the complex BWB structure has to bear cabin pressurisation loads. Nevertheless, Airbus optimistic that it will be able to offer several variations of this aerodynamically clean model in 30 years time at the latest (Steinke 2001).

From an interview with FLUGREVUE (Steinke 2001), the chief engineer for new ideas in the subsonic area from the Department of Future Projects at EADS Airbus, mentioned the new conceptual designs of Airbus. There is a clear objective for a new Airbus concept for the next generation as;

> *A whole family of new Airbus concepts as Flying Wing design - the Low Noise Aircraft (LNA) - is concerned with the goal of noise reduction. The development engineers are using relatively conventional fuselage wing structures from the existing Airbus range as the starting point. Moreover, the unconventional features is the positioning of the jet engines, which have been moved from their traditional position underneath the wings to locations on the top of the wings or even above the fuselage where less noise is deflected downwards. The 'Joined Wing Concept', whose aerodynamics are particularly complex, of one variation of the LNA was designated to achieve a significant reduction in the weight and structure of the wing with a quite different primary objective.*

The 'Joined Wing' would be able to manage with a small wing span and space requirement due to the relatively reduction in the weight and structure of the wing. Therefore, Airbus is hoping with this modern variation of an idea that was the first developed in the 1930s to achieve a significant reduction in fuel consumption (Steinke 2001). Moreover, the altered and significantly taller fuselage cross-section is not necessarily aimed at holding hydrogen tanks, but at preventing unwanted interference between the pairs of wings through their spatial separation.

1.3.5 Feasibility studies of BWB Aircraft by Cranfield College of Aeronautics, UK

Cranfield College of Aeronautics in the UK is an advocate of the flying wing or BWB as offering a

major step forward in overall efficiency. Moreover, he states that this future vision of aircraft design is very impressive as he said (Birch 2001),

> *By using nuclear fuel to power what is essentially a closed-cycle stream engine driving propellers, there would be no atmospheric emissions to cause concern. Therefore, there would probably be some degradation in airliner cruising speed - about Mach 0.7 would be typical - but the efficiency of the aircraft, without the need to carry an enormously heavy fuel load on take-off, would be very high.*

Cranfield College said that while the researchers fully understand that public and political unease about nuclear-powered aircraft would be considerable, and nevertheless feel that the use of nuclear power should be considered as a serious alternative aviation fuel.

Considerable interest has been raised by the fact that the BWB layout may confer substantial overall advantages when applied to a transport aircraft in the ultra-high-capacity category. The most famous BWB design of the Cranfield College of Aeronautics is the College of Aeronautics BW-98 project illustrated in Fig. 1.15 (Howe 2001 & Smith 2000). This Cranfield baseline BWB configuration is similar to the Boeing concept in configuration, and currently represents the only UK National project of its scale.

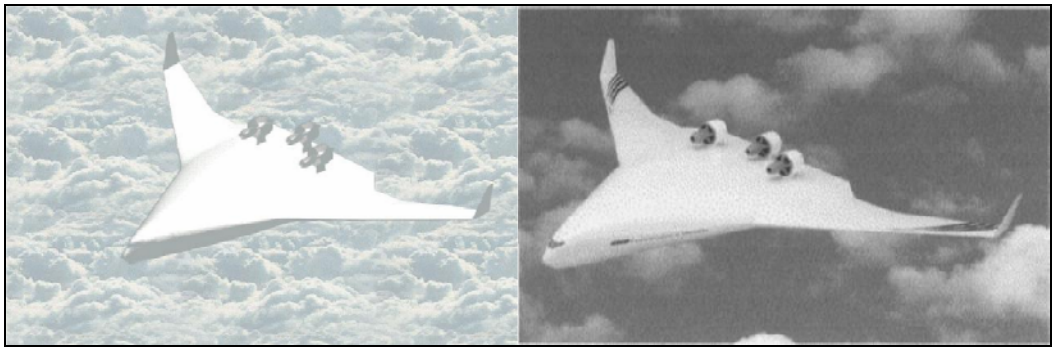

Fig. 1.15 Cranfield BW-98 BWB Study (Left: Smith 2000, Right: Howe 2001)

The primary design requirements and specifications of the BW-98 project are to design an airliner

with a similar payload and mission performance to the Airbus A380 with 656 seats of accommodation capacity in a three class layout. This alternative cabin layout potentially accommodates a maximum 960 passengers in a single class. Moreover, the design range is 7,650 nautical miles cruising at Mach 0.85 with a payload of 656 passengers and their baggage (Smith 2000).

In regards to the structural design of this BWB configuration, the centre wing-body module is planned to have aluminium alloy and traditional structure member parts such as frames and stringers. An alternative configuration using composite material is also being considered. The first flat and vaulted shell structural configurations for the cabin bay were considered, but the vaulted double-skin ribbed shell design is preferred believed to be superior due to the weight saving and the load diffusion. The inner skin carries pressurisation efficiently through hoop-stress and the cabin wall is utilised to balance the weight of the structure above the cabin bay and the vertical component of the hoop-stress. Moreover, the outer skin supports the major part of the bending moment and the shear force due to the aerodynamic loads acting on the configuration (Howe 2001 & Smith 2000).

For the propulsion units on this design, the Rolls-Royce RB529 contra-rotating project engine offers the additional benefit of lifting the core intake clear of the boundary layer. With this conceptual design, the BW-98 offers the opportunity of a far greater level of engine airframe integration with a tip turbine driven remote fan powered by an engine core integrated within the airframe which includes the possibility of thrust vector control (TVC) (Pachidis 2005 & Smith 2000).

1.3.6 Investigation of BWB Design by University of Sheffield, UK

The University of Sheffield has presented a progressive aerodynamic study of a BWB configuration within a European project, MOB which is a computational design engine incorporating multidisciplinary design and optimisation for BWB configuration (Qin et al. 2004). This BWB project investigated an aerodynamic performance of the various BWB aircraft design projects in relation to

their aerodynamic behaviour. With a theoretical view of the ideal aerodynamic performance for the baseline design, viscous flow simulation was applied to investigate the aerodynamic performance of the BWB configuration. Using CFD simulation the BWB wing was mapped to an airfoil optimisation program and the optimised airfoil design was projected back to the BWB wing to investigate further performance improvement.

In this project, technical descriptions and CFD results of the BWB configuration are represented, including aerodynamic advantages and aerodynamics features of BWB configuration. In regards to the aerodynamic features of the BWB configuration, the main advantage of the new BWB design is its lower wetted area to volume ratio and lower interface drag as compared to the conventional aircraft. Indeed, an increase in a maximum L/D of approximately 20 percent over the cylindrical fuselage design aircraft has been estimated for the BWB configuration. Moreover, on the structural performance side, the potential large aerodynamic gain from the BWB concept is obvious structural advantages due to the integration of the wing structure with the thick centre body. With the tailless design concept, this project is considered that stability and control issues are critical in the design process.

This MOB project was designed the baseline BWB geometry with total span including the winglets of less than 80 m and no powerpant sections, as Fig. 1.16.

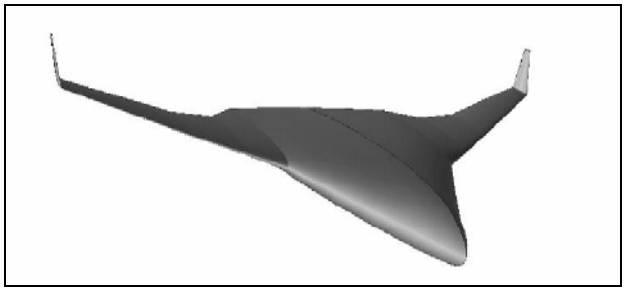

Fig. 1.16 Baseline BWB Geometry of the MOB Project by the University of Sheffield

According to the baseline BWB design, the half mode provided by Delft University used an ICAD parametric model generator program composed of the central body, an inner wing and an outer wing to which a winglet is attached. The design conditions are believed to correspond to the first segment of cruise as Mach 0.85 and 11,500 m altitude, and also the design lift coefficient (C_L) is 0.41 to balance the weight of the aircraft based on the trapezoidal reference area of 842 m^2 (Qin et al. 2004), and Table 1.2 shows the summary of the configuration specification.

Table 1.2 Specifications of the Baseline BWB Model (Qin et al. 2004)

Mach Number	0.85	Aspect Ratio	4.26
Altitude	11,500 m	Sweep Angle (centre)	63.8 deg.
Reynolds Number	5.41×10^6	Sweep Angle (wing)	38 deg.
Design C_L	0.41	C.G. Position	29.3 m
Length of Centre Chord	50.8 m	Centre Body	0 - 13.0 m span
Reference Area	842 m^2	Inner Wing Location	13.0 - 23.5 m span
Wetted Area	3,079 m^2	Outer Wing Location	23.5 - 38.75 m span

According to the wing design, the airfoils for the centre body at 0 m and 13 m spanwise has a front positive camber of $(z/c)_{max}$ = 0.01 at (x/c) = 0.21 which is then reflected at 60 percent chord with $(z/c)_{min}$ = -0.004 at (x/c) =0.81 for the longitudinal stability at the cruise condition. For the winglet design, NACA0012 airfoil was utilised between the relevant root and tip section. In regards to the wing thickness distribution, the spanwise thickness to chord ratio distribution has an average of 17 percent on the centre body with a maximum of 18 percent at about 6 m span. The inner wing blended the thick centre body with the thin outer wing (8 percent) with a large variation in its thickness.

On the aerodynamic performance side, the behaviour of the baseline BWB model was defined as transonic cruise condition. This research project employed both Cranfield high-fidelity implicit multi-block Reynolds-average Navier-Stokes solver, MERLIN, which employs an approximate Riemann solver based on Osher's flux difference splitting for shock and boundary layer capturing,

and the NLR ENFLOW system, which supports aeroelastic deformation and incorporates pitching moment trim. Since using the CFD solver, the aerodynamic performance of the baseline BWB model was calculated and visualised as Fig. 1.17 (Qin et al. 2004).

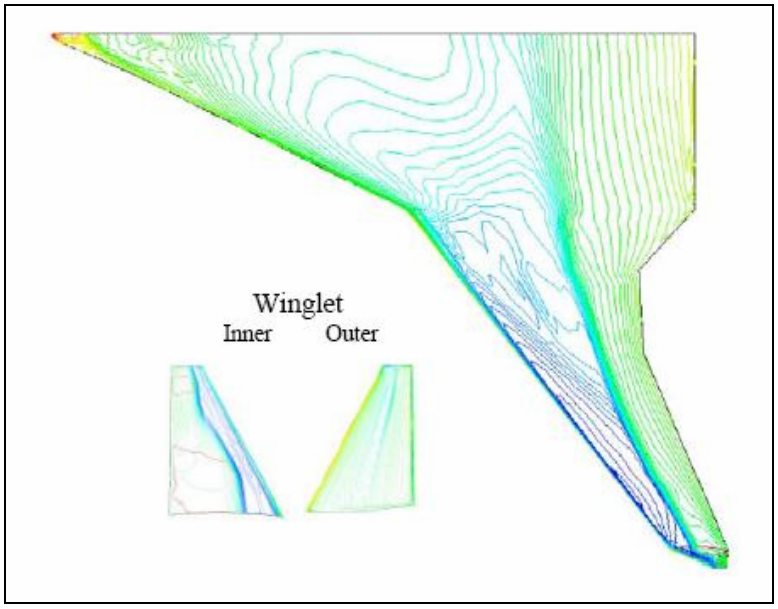

Fig. 1.17 Contour Line of Pressure Coefficient on the Baseline BWB (Angle of Attack 3 deg., Mach number 0.85 (Qin et al. 2004))

From the aerodynamic assessment of the baseline BWB, the span load inboard was shifted in order to off-load the outer wing to reduce the shock strength and the wave drag. The new designs were then implemented in the RANS surface grid models. Through running MERLIN for the new geometries at a series of incidences, the design lift condition can be simulated for each of the new models. The results of MERLIN simulation is shown in Table 1.3 (Qin et al. 2004).

Table 1.3 Navier-Stokes Check of the Euler Optimised BWB (Qin et al. 2004)

	C_L	C_{Dtotal}	$C_{Dpressure}$	$C_{Dfriction}$	C_{Dwave}	L/D	C_m
Initial Reference Geometry	0.4101	0.0286	0.0189	0.0097	0.0010	14.37	-0.03360
Optimised Model	0.4100	0.0260	0.0159	0.0100	0.0002	15.80	0.00401

According to this MOD study, the importance of wave drag, span loading distribution, airfoil section

design and the three dimensional shaping for BWB performance are highlights. In regards to the aerodynamic performance of the BWB configuration, the L/D is similar to conventional aircraft, but the parasite drag is excessively lower than cylindrical body aircraft.

To conclude the current BWB configuration projects, the mainstream aeronautical industries and some institutions have been investigating to prove the flight potential of BWB configuration and to commence producing the novel aircraft concept for next generational airliner. However, many feasible results of BWB features have not been released at this stage, and a lot of BWB projects are studied in fundamental BWB capacity in theory only. In this thesis, flight abilities of BWB configuration, in particular aerodynamic performance, will be presented with theoretical and practical studies using CFD software.

1.3.7 Negative factors of a BWB Configuration Design

Unconventional aircraft configuration with the BWB design have been predicted to pose design challenges in this new class modelling to achieve the BWB projections. The majority of issues involved in the BWB design stage involve the structural capabilities based on the physics analysis of Finite Element Method (FEM), aerodynamic panel-method, and drag and weight prediction, and also a number of problems in aerodynamic performance of the configuration are not understood yet.

In regards to the structural analysis of the BWB concept, the stress level in the box type of pressurised fuselage configuration of the BWB flight vehicle is an order to magnitude higher, because internal pressure primarily results in blending stress instead of skin-membrane stress. Moreover, resulting deformation of aerodynamic surface significantly affects flight performance provided by the lifting body. For example, the pressurised composite conformal multi-lobe tanks of X-33 type space aircraft also suffered from the similar problem (Mukhopadhyay 2005).

Another problem related to the human factor in the wide cabin design model is how to install the windows. The passenger compartment goes into the wing structure area, so it is difficult to set up the windows on the wing surface. Also the outside of the passenger area will be located tank running out into the wings. To solve this problem, a multi-functional liquid crystal display (LCD) screen on the seat for the rear passengers and several windows for the front passengers will be installed.

In regards to the aerodynamic effects of the all delta wing concept, negative aeroelastic behaviours in cruise due to elastic deformations is considered to change in wing twist, aileron reversal of flatter identified which will be overcome by considerable changes in structural arrangement or mass distribution, resulting in weight penalty or unacceptable limitations of the flight envelop. Moreover, the relationship between the engine location and the flight operation is critical to solve the inlet and compressor problems with the turbulence flow off the rear of the wings, because the BWB concept design has the engines raised out of the boundary layer flow when the angle of attack is higher in flight.

1.4 Aims and Objectives

The objective of this research is to prove an aerodynamic performance of the BWB configuration whether the configuration could be better than conventional aircrafts, especially compared with the conventional aircraft Airbus A380-800 modern airliner. This comparative research sets up five specific questions to develop to address and consider the following;

1. Is a BWB aircraft design more aerodynamically efficient than Airbus A380-800?
2. How does the BWB configuration compare overall with large aircraft, especially the A380-800?
3. What are the trade-offs between conventional aircraft and a BWB arrangement?
4. What mission requirements (e.g. payload and range) will a BWB design concept be attractive for?

5. What are the practical issues involved associated with the BWB aircraft configuration that need to be addressed (e.g. airport compatibility and passenger ingress/egress etc.)?

There is anecdotal evidence to suggest that the BWB configuration is an aerodynamically 'clean' aircraft, which relates to the experiment of the Northrop N-9M and the Northrop X-35. According to the results of the both aircrafts, the parasite drag of Northrop N-9M was able to decrease by 20 to 50 per cent, and also, the minimum drag coefficient of the Northrop XB-35 was 0.00113 (e.g. the drag coefficient of Boeing B747 is 0.0255 (Makino 1980)) (Sweetman 1992).

1.5 Research Hypothesis

The BWB configuration has not been utilised for commercial aircraft as yet, because there are a lot of issues to address to produce the new concept aircraft, such as current engineering capacity and mainly marketing potential of the aircraft. However, the BWB concept design aircraft, which does not have fuselage and empennage, potentially could reduce negative factors of conventional aircraft. According to the results from most of the current BWB projects, the BWB configuration achieves higher L/D which is potentially around 30 (Sandilands 2002 et al.). In this research, the BWB configuration will be less than the number of L/D because the wingspan of BWB configuration is shorter than the others to achieve the current airport compatibility. However, the BWB design could achieve approximately 20 of L/D in flight if the BWB arrangement is considered with proper airfoil section and shape.

1.6 Design Methodologies and Processes

This research is a comparative study between BWB configuration and the A380 prototype using Computation Aided Design (CAD) softwares and Computational Fluid Dynamics (CFD) solver. The BWB configuration was designed based on the A380 to prove an aerodynamic performance in flight. A unique point of this research was that the BWB configuration kept the wingspan less than 80 meters and the mission performances were the same as the A380, with 555 passengers, 66.4 tons payload and

15,000 km range.

The BWB design processes are illustrated as in Fig. 1.18. The multidisciplinary design steps were iterated to achieve higher aerodynamic performance than the A380 between the sizing of 2D BWB layout and the CFD analysis using several computational tools. After the CFD results from the BWB model, the preliminary structural analysis was done. The structural factor of the BWB configuration is the significant issue in the project. However, it is not the main issue of this research.

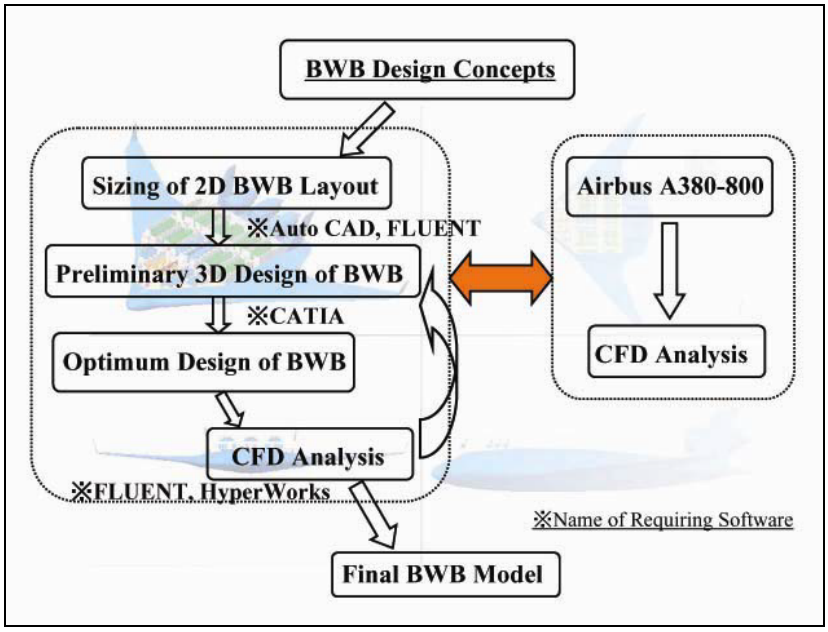

Fig. 1.18 BWB Design Processes

This project was employed using several advanced CAE tools to create and prove the BWB configuration and the A380 prototype (i.e. Dassault Systemes CATIA V5, SolidWorks 2000, AutoCAD 2002, FLUENT 6, HyperWorks 6, MATLAB 6 and XFOIL 9).

1.7 Contribution to Knowledge

Most literature on this subject suggests that the BWB concept has a great potential to be the next generation of air transport without negative flight behaviour. There are however many issues to be addressed before the BWB project become reality. Aviation industries and institutions need to prove

the abilities of the BWB concept and measure whether the aerodynamic performance is attractive and if new structural elements are required. This research will contribute to the body of knowledge by quantifying;

1. The ability of aerodynamic performance of the BWB based on the same specifications as the A380 and comparing CFD results of both aircrafts.
2. How efficient the potential of Take-Off Gross Weight (TOGW) is, using current manufacturing techniques and comparing to the A380.

This research provides a significant contribution to the advancement of the aeronautical research by elucidating the flight performance of the BWB concept simulated with CFD solver. In addition to an absence of literature on this area of research, there are no tangible results of CFD simulation in quantifying the aerodynamic performance of the BWB concept. This research has employed the actual dimension of the BWB model onto CFD simulation and computed the aerodynamic performance recreated in the flight conditions of conventional aircraft.

The research is 'original' in so far as extensive investigation has shown that no previous studies, which keep less than 80 meters wingspan of BWB configuration using CFD solver, have been previously embarked upon. Moreover, the distinction in this thesis of the comparative studies between the commercial aircraft, the A380 prototype, and the new concept of BWB design has not previously been researched.

1.8 Report Structure

The first chapter provides an introduction to the research with the design questions and the current knowledge and status of BWB configuration projects are presented. Moreover, the specifications of the comparative aircraft, Airbus A380, are shown in this chapter. The chapter 2 is described methodologies for BWB configuration design, such as typical aircraft design methodologies and

advanced cabin weight estimation of NASA which is especially for a BWB aircraft configuration. After that, the chapter 3 releases computational approach skills for the BWB configuration analysis, such as computational techniques. A capability of CFD software is examined and shown examples between numerical simulation and wind tunnel experiment results. The following two chapters provide a result of BWB aircraft performance and summary of the findings regarding the subsidiary questions and the main research questions, and conclusions of this research such as suggestions of further areas of research.

Additionally, the utilised data of this research are attached after the main sections. For all questions and CAD models “SI” unit is utilised on this research.

Chapter 2 Aircraft Design Methodologies and Processes

The aircraft design process is the same as all engineering productions with four main processes (Fig. 2.1). Aircraft design, however, has more complex processes and restrictions than for commercial goods, because if aircraft flight fails most of the passengers will be injured or killed.

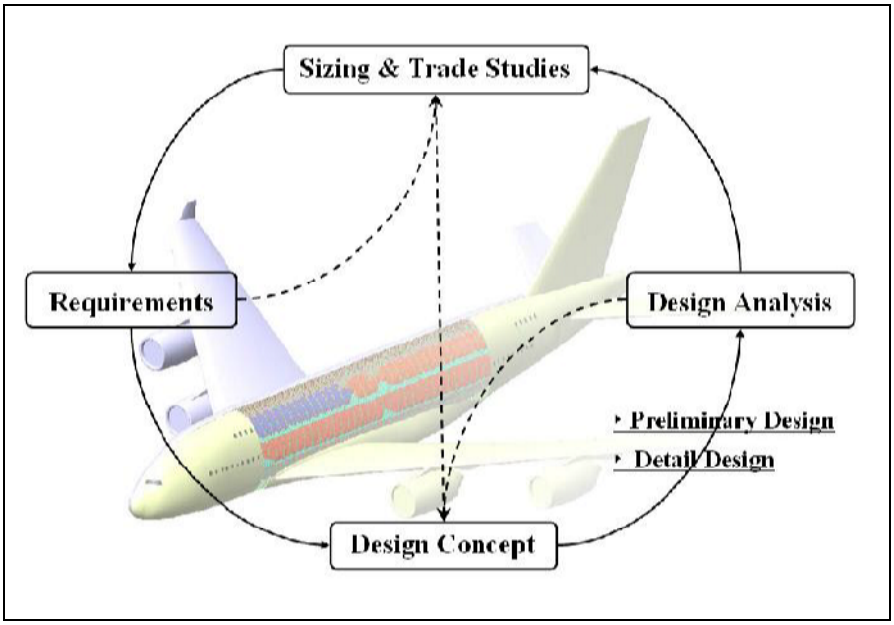

Fig. 2.1 Aircraft Sizing Wheel

In regards to the steps of aircraft design, three design stages are considered when producing an aircraft (i.e. 1. Conceptual Design, 2. Preliminary Design, 3. Detail Design). These steps of aircraft design are described later in more detail.

2.1 Definition of Conceptual Design Process

In this section the basic questions of configuration arrangement, size and weight estimations and flight performance are considered. These parameters are initial descriptions of configuration outline, such as whether the configuration will work or what requirements should be achieved. In addition, the design parameters include the aircraft range and payload, takeoff and landing distances, manoeuvrability and

speed requirement.

The conceptual aircraft design handbook (Raymer 1999) explains that sometimes an aircraft design will begin as an innovative idea rather than as a response to a given requirement. Moreover, it gave an example of the flying wing pioneered by John Northrop which was not conceived in response to a specific Army Air Corps requirement at the time, but instead was the product of one man's idea of a 'better airplane'. Mr. Northrop pursued this idea for years before building a flying wing to suit a particular military requirement.

The conceptual design process considers what kind of technology will be employed or which new methods will have a possibility to be utilised into the design before moving to the preliminary design stage. If a design will be built in the future, especially the near future, it must not exceed used of the current available technologies as well as existing engines and avionics. For the more advanced future aircraft, estimation of technology should be made based on the current technology areas with high potential for future development.

A conceptual sketch can be useful to estimate aerodynamics and weight fractions comparing previous designs. This sketch will illustrate the approximate wing and tail geometries, the body shape, and cockpit, payload and passenger compartment of the internal locations of the major components. This first sketch helps for the weight estimations such as gross weight and fuel weight to design the mission performance. In the initial sketch design, the aircraft design work is done in full scale using CFD tools. Using the aircraft design on CAD software, the layout is analysed and optimised, with consideration for aerodynamics, structural analysis and the installed propulsion systems. After this performance consideration, the performance capabilities are calculated and optimised compared to the requirements.

To conclude, the design is often changed after new ideas and problems arise. Each time the latest design is analysed and redesigned based on the requirements, the sizing draft must be redesigned to consider the new characteristics of configuration such as gross weight, capacity of engine and shape design. Moreover, CFD simulations and wind tunnel tests constantly expose problems requiring further changes to the design.

2.2 Objective of Preliminary Design Phase for Aircraft Configuration

The preliminary design process is normally started when the outline of the conceptual design has been decided. The conceptual design parameters are given to specialists divided to small areas, such as CFD, structures and control systems, to design and analyse their portion of the aircraft. In this stage, computational and practical experiments are initiated to reveal features of aerodynamics, structure, propulsion, and stability control.

Another activity is to check the aircraft model with sufficient accuracy to ensure proper fit between its different parts, because different designers and companies work together to build an aircraft.

The main objective of this design process is to prepare for the detail design stage which is normally called the 'full scale development', and the end of preliminary design period involves a proposal of full scale development. In addition, this preliminary design needs to identify a possibility that the aircraft can be manufactured on time and the cost estimation.

2.3 Description of Detail Aircraft Design Stage

Initially, small components are designed to improve the assemblage of full scale design configuration from flight-mission requirements perspective. For example, during the conceptual design and the preliminary design processes the wing design will be finished and analysed as a whole. Therefore, in this phase the wing design will be broken down into surface materials, flats and spoilers, individual

ribs, spars, each of which mush be separately designed and analysed. Moreover, the production design will determine how the aircraft will be made using the small and simple subassemblies and building up to the final assembly process. Moreover, another important issue of this stage is to test the actual structures and flight performance using a flight simulator. This test is normally collaborated with company and customer test pilots.

2.4 BWB Configuration Design Process

A BWB configuration is a novel aircraft proposed as a commercial airliner, and the concept design is under development and investigation of flight capabilities. In this research, the BWB configuration was designed based on the same flight characteristics of the A380.

This thesis was undertaken to design a BWB aircraft for next generation of airliner and to consider the conceptual design process, in particular aerodynamic performance of BWB configuration to be investigated and optimised using the CFD solver. Based on the Raymer's design process, the conceptual design steps of this research is summarised as Fig. 2.2.

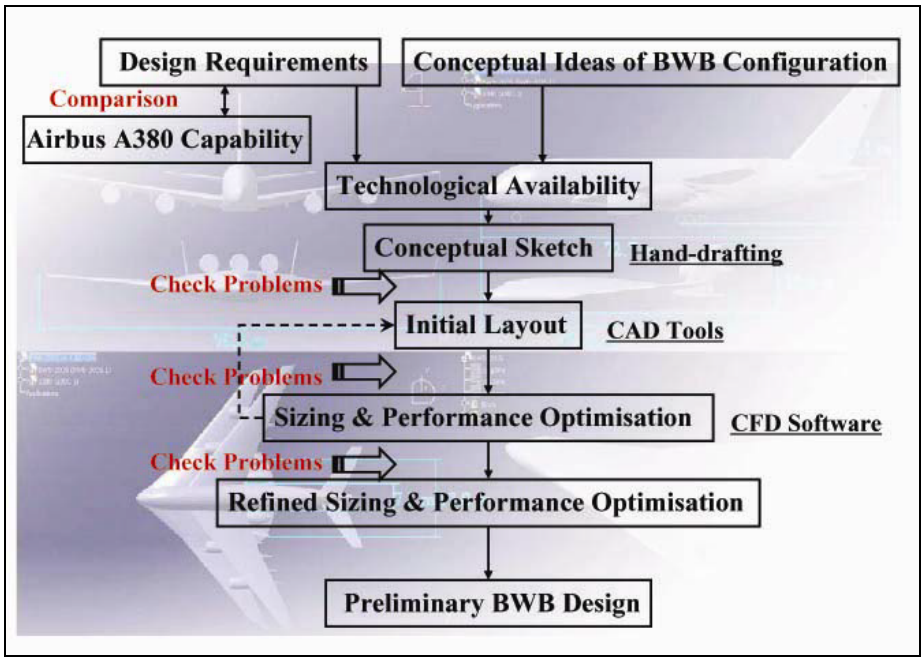

Fig. 2.2 BWB Configuration Design Process based on the Raymer's Design Phase

2.5 Performance Estimation of the BWB Configuration

The performance estimation is significant in the conceptual design phase. For a new concept design of BWB configuration, traditional methodologies for commercial aircraft and new developed methodologies were utilised to calculate the performance of BWB aircraft, such as component weight and aerodynamic performance estimations. In addition, the traditional methodologies may be found in technical books for aircraft conceptual design. Moreover, the new methodologies are often sourced from NASA's laboratories.

2.5.1 Flight Mission Profile of the BWB Aircraft Design

There are many approaches of design procedure in the conceptual design environment. One of the vital parameter is a flight mission profile of aircraft, because it directly relates to a configuration weight and fuel weight. The simple mission profile for commercial aircraft is shown in Fig. 2.3, which was designed based on the flight mission of A380.

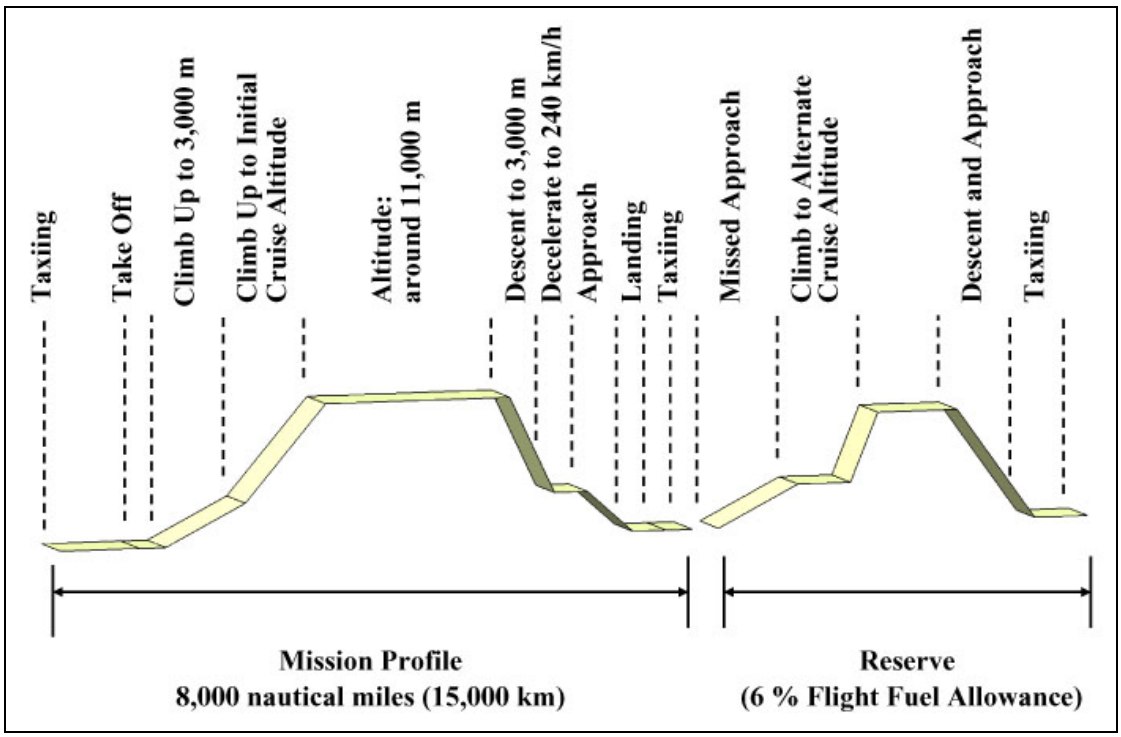

Fig. 2.3 Flight Mission Profile of the BWB Configuration

In regards to the aircraft operating procedure, the Federal Aviation Administration (FAA) and International Civil Aviation Organisation (ICAO) are the specialised agencies whose mandate is to ensure the safe, efficient and orderly assessment of international civil aviation. All aircraft operations follow their rules. For safety issues, aircraft must carry extra fuel in case an airport is closed which means aircraft can fly for an extra 20-30 minutes (FAA 2005a). For example, the A380 carries extra fuel which is 5 percent of total fuel (AIRBUS S.A.S. 2004). This kind of extra fuel is normally called as 'fuel allowance'. In regards to the BWB design process, the fuel allowance required for the BWB was required to be 6 percent of total fuel. Traditionally the fuel allowance of a commercial airliner requires 6 percent of extra fuel from the total fuel weight (Raymer 1999).

According to the BWB flight mission of this research, the flight characteristics of the A380 were referred to the BWB design which can operate at the 8,000 nautical miles (15,000 km) range with non-stop flight.

2.5.2 Weight Estimation

Based on the mission requirements, design take-off gross weight was the first estimation process before breaking down to other component weight estimations. This takeoff weight, $W_{takeoff}$, was assumed to be the design weight which was estimated from the empty weight of the aircraft plus payload weight, crew weight and fuel weight. The empty weight was defined as the total weight of the structures, wings, propulsion systems, landing gear and furnishings without crew, payload and fuel, as the following equation,

$$W_{takeoff} = W_{crew} + W_{payload} + W_{fuel} + W_{empty} . \quad (2.1)$$

In regards to Equation (2.1), the fuel weight and empty weight were uncertain parameters. However, the crew weight and payload weight were assumed using typical crew weight estimation and passenger weight estimations as shown in Table 2.1. For example, Qantas Airways allows that international passengers can carry baggage as 40 kg for first class, 30 kg for business class and 20 kg for economy

class (Qantas 2005), because weight and balance factors are critical to the safe operation of an aircraft. The weight and balance refer to the weight of an aircraft and the location of the centre of gravity. Therefore, air operators have several options approved by airlines to calculate passenger weight, such as weighing each passenger getting on board. The air operators and pilots are required to ensure the aircraft weight and balance remain within approved limits and to ensure issues, such as heavier individuals are accounted for accurately in the total payload weight.

Table 2.1 Typical Numbers of Passenger and Crew Weight Estimations (Qantas 2005 & Raymer 1999)

	Average Weight	**Average Baggage Weight**
Flight Crew	80 kg	10 kg
Flight Attendant	70 kg	10 kg
Passenger (International)	75 kg	20 kg

Equation (2.1) is simplified to assume the fuel and empty weights using fractions of the total takeoff gross weight (TOGW).

$$W_{takeoff} = W_{crew} + W_{payload} + \left(\frac{W_{fuel}}{W_{takeoff}}\right)W_{takeoff} + \left(\frac{W_{empty}}{W_{takeoff}}\right)W_{takeoff}. \tag{2.2}$$

Moreover, this equation is changed gathering the fractions of $W_{takeoff}$ as,

$$W_{takeoff}\left\{1-\left(\frac{W_{fuel}}{W_{takeoff}}\right)-\left(\frac{W_{empty}}{W_{takeoff}}\right)\right\} = W_{crew} + W_{payload}, \tag{2.3}$$

$$W_{takeoff} = \frac{W_{crew} + W_{payload}}{1-\left(\frac{W_{fuel}}{W_{takeoff}}\right)-\left(\frac{W_{empty}}{W_{takeoff}}\right)}. \tag{2.4}$$

In regards to the empty weight fraction, historical trends between empty weight and TOGW are utilised to estimate the parameter in statistical in Table 2.2 (Raymer 1999). In the initial process the parameter of empty weight fraction was useful to describe approximately the configuration weight. To estimate the empty weight fraction the equation is shown based on the designed aircraft as,

$$\frac{W_{empty}}{W_{takeoff}} = A W_{takeoff}{}^{C} K_{VS}, \tag{2.5}$$

where A is the statistical empty weight fraction, C is the negative exponent of the relationship between empty weight and TOGW and K_{VS} is the variable sweep constant (e.g. 1.04 for variable sweep wing, 1.00 for fixed sweep wing). The differences of these parameters come from different types of aircraft based on the trade-off study. Moreover, advanced composite materials, such as aluminium-glass-fibre laminate, are difficult to assess the weight using statistical trend estimation.

Table 2.2 Empty Weight Fraction vs. TOGW (Raymer 1999)

	A	***C***
General Aviation (Twin Engine)	1.51	-0.10
Twin Turboprop	0.96	-0.05
Jet Airliner	1.02	-0.06
Military Cargo/Bomber	0.93	-0.07

In this research, the flight range of the BWB configuration was already decided as the same as the A380 characteristics (8,000 nautical miles: 15,000 km range). Therefore, to assume each mission segment weight, such as warm-up, taxiing, approach and landing segments, the Breguet Range equation was utilised, which was designed considering typical historical values of aircraft for initial sizing. In this simple sizing method, descent process was ignored as it was assumed that the cruise ends with a decent, and that the distance travelled during descent was part of the cruise range.

The Breguet Range equation is related to the aerodynamic (L/D) and propulsion capacity efficiencies (V/c). The cruise range is calculated by integrating the specific range as (Raymer 1999),

$$R = \int_{W_i}^{W_{i-1}} \frac{V}{c} \frac{L}{D} \frac{1}{W} dW. \tag{2.6}$$

If the aircraft is in level flight in the isothermal atmosphere (above approximately 11,000 m) where the speed of sound is constant, which means that the speed and the specific fuel consumption are nearly

constant. The equation is recomputed based on Equation (2.6) as,

$$R = \frac{V}{c}\frac{L}{D}\int_{W_i}^{W_{i-1}} \frac{1}{W} dW = \frac{V}{c}\frac{L}{D} In \frac{W_{i-1}}{W_i} . \tag{2.7}$$

When the altitude is such that *L/D*, *V* and *c* are not constant, the integral may be evaluated numerically. Moreover, the Breguet Range equation was utilised with cruise segment mission weight fractions in the sizing phase. The Breguet Range equation is commonly known as,

$$\frac{W_i}{W_{i-1}} = \exp \frac{-Rc}{V\left(\frac{L}{D}\right)}, \tag{2.8}$$

where, *i* is the mission segment, (W_i/W_{i-1}) is the mission segment weight fraction as in Table 2.3, *R* is the range, *c* is the specific fuel consumption (SFC) and (*L/D*) is the lift-to-drag ratio (Raymer 1999).

Table 2.3 Historical Mission Segment Weight Fractions for Transport Aircraft (Raymer 1999)

	Weight Fraction (W_i/W_{i-1})
Warm-up and Take-Off	0.970
Climb	0.985
Landing	0.995

2.5.3 Fuel Weight Estimation for Commercial Aircraft

Based on the traditional value of commercial aircraft, the equation is designed with 6 percent fuel allowance for reserve and trapped fuel. In addition, the A380 prototype employs 5 percent fuel allowance for flight operation. The total fuel fraction is estimated as in Equation (2.9).

$$\frac{W_{fuel}}{W_{takeoff}} = 1.06 \times \left(1 - \frac{W_x}{W_{takeoff}}\right), \tag{2.9}$$

where W_f is the fuel weight, $W_{takeoff}$ is the TOGW, and *x* is the final mission segment. Moreover, the Equation (2.9) can be simplified using the specific fuel consumption with *T* (the engine thrust) and *d* (the mission segment range) as follow;

$$W_{fuel} = cTd . \tag{2.10}$$

2.5.4 L/D Estimation

In the conceptual design process, the L/D ratio is a significant parameter to analyse an aerodynamic performance (Ikeda et al. 2005b & Makino 1980). Based on the Bernoulli's equation, the ratio is defined as,

$$\frac{L}{D} = \frac{Lift}{Drag} = \frac{\frac{1}{2}\rho V^2 S C_L}{\frac{1}{2}\rho V^2 S C_D} = \frac{C_L}{C_D}, \tag{2.11}$$

where C_L is the lift coefficient and C_D is the drag coefficient. Moreover, the Equation (2.11) can be changed using aircraft specifications when an aircraft is cruising; i.e. the weight is equal to the generated lift of the aircraft.

$$C_L = \frac{W}{\frac{1}{2}\rho V^2 S}, \tag{2.12}$$

$$T = \left\{ C_{D_P} + \left(k + \frac{1+\delta}{\pi AR} \right) C_L{}^2 \right\} \frac{\rho}{2} V^2 S, \tag{2.13}$$

where, W is the TOGW, C_{Dp} is the parasite drag coefficient, k is the aircraft shape factor, δ is the parameter of wing shape, AR is the aspect ratio, ρ is the density, V is the velocity and S is the reference area of the wing. In regards to the aircraft shape factor, the aircraft with high aerodynamic performance is close to 1 and the current aircraft is approximately 0.009-0.012. Moreover, the C_{Dp} of current commercial aircraft is around 0.015-0.025. In Equation (2.13), the C_D is divided into two parameters, which are C_{Dp} and induced drag coefficient C_{DI} as,

$$\begin{cases} C_{D_P} = C_{D\min} + kC_L{}^2 \\ C_{D_I} = \left(\frac{1+\delta}{\pi AR} \right) C_L{}^2 \end{cases}. \tag{2.14}$$

Based on the Equation (2.14), the C_{DI} of the C_D is defined as,

$$C_{D_I} = \left(k + \frac{1+\delta}{\pi AR} \right) C_L{}^2. \tag{2.15}$$

Since the Equations (2.13)-(2.15), T is designed with Aircraft efficiency, e,

$$e = \frac{1}{1 + \delta + k\pi AR}, \tag{2.16}$$

$$T = \left(C_{D_P} + \frac{C_L{}^2}{e\pi AR} + \Delta C_{D_C} \right) \frac{\rho}{2} V^2 S \,, \tag{2.17}$$

and $\Delta C_{Dc} \equiv 0$ when the cruising Mach number is low. For commercial aircraft, the Equation (2.17) can be redesigned as,

$$T = \left(C_{D_P} + \frac{C_L{}^2}{e\pi AR} \right) \frac{\rho}{2} V^2 S \,. \tag{2.18}$$

Thus, the L/D is redefined by Equation (2.11) and Equation (2.18) as,

$$\frac{L}{D} = \frac{\sqrt{\pi}}{2} \frac{b\sqrt{e}}{\sqrt{C_{D_P} S}} \,. \tag{2.19}$$

Since $(L/D)_{max}$, the C_L equals to $(C_{Dp} e\pi AR)^{1/2}$. In addition, AR is the aspect ration between wingspan, b, and reference area, S, defined as (b^2/S).

Another measurement to estimate the L/D is to analyse the relationship between the wetted area of the configuration and wingspan, because the L/D is highly dependant on the configuration arrangement and directly affects the wingspan and wetted area, in particular at subsonic flight. In level flight at subsonic cruise, parasite drag is related to skin friction drag, and as such is directly corresponding to the total surface area of the configuration exposed to the air. The comparison between wetted area and wingspan can be restated as a wetted aspect ratio, which is defined as the square of the wing span divided by the wetted area of configuration, as being similar to the normal AR. For initial design purposes, wetted aspect ratio is utilised to assume L/D based on the initial sketch. For example, two different aircraft concepts, the Boeing B-47 and the AVRO Vulcan, were compared with aspect ratio and wetted aspect ratio (Raymer 1999). The B-47 was 9.4 of aspect ratio and 1.2 of wetted aspect ratio, and the AVOR was 3.0 of aspect ratio and 1.1 of wetted aspect ratio. An interesting result is that the both aircraft achieved exactly the same L/D. For the reliable early estimation of L/D, the wetted aspect ratio is a feasible parameter, which is clearly dependant upon the actual configuration layout. Since the relationship between L/D and wetted aspect ratio considered existing aircrafts, Fig. 2.4 shows L/D

estimation chart (Ikeda et. al 2005).

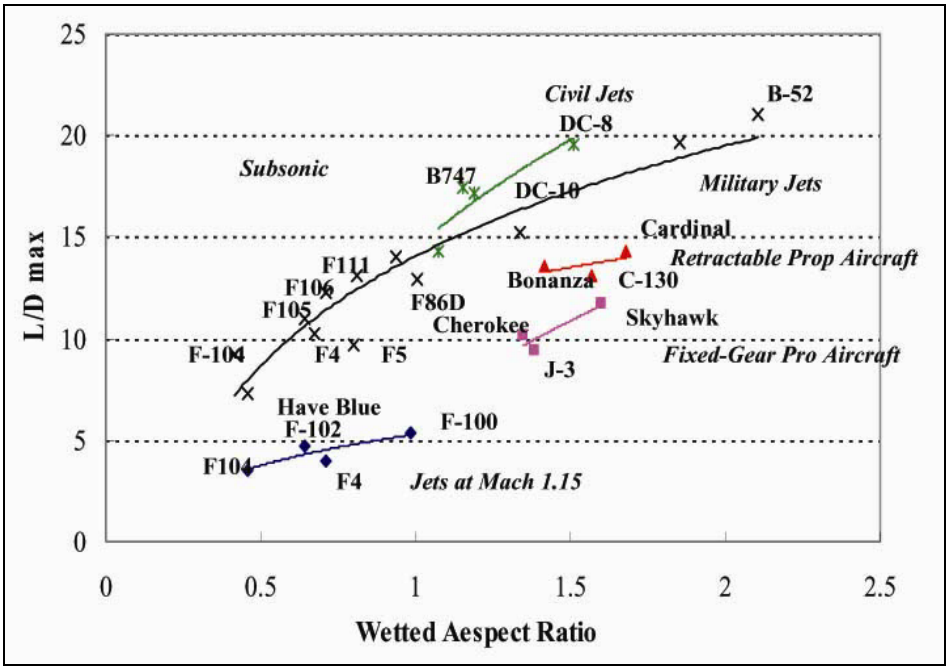

Fig. 2.4 Maximum L/D Trends based on Wetted Aspect Ratio

2.5.5 Thrust-to-Weight Ratio Consideration

The thrust-to-weight (T/W) ratio is an important parameter affecting aircraft performance. A major part of the analytical design activities are done to optimise this parameter form after an initial design sizing. Moreover, the wing loading (W/S) is another important factor directly relating to the T/W, for example, the estimated W/S can be used to calculate the T/W required to attain other performance issues such as the single engine rate of climb. Thus, it is essential that a credible estimate of the T/W and W/S is considered before the initial design sketch is begun.

The T/W is a parameter of engine activity required to perform the flight mission. For example, an aircraft with a higher T/W performs higher acceleration, climbs rapidly and has a higher turn rate. On the other hand, the larger thrust engines will consume more fuel in flight, which means an increase of the TOGW to perform the design mission. The T/W is not a constant, because the weight of aircraft changes during flight as fuel burns. The engine's thrust requirements are considered relative to altitude

and velocity. In addition, the T/W is generally referred at the sea level static setting with standard day conditions at design TOGW and maximum throttle activity.

Table 2.4 shows typical values of T/W for different classes of aircraft (Raymer 1999). This T/W is closely related to maximum speed of aircraft. Moreover, based on the T/W thrust matching is considered to estimate a better initial requirement of T/W. This consideration is referred to selected engine's thrust along with the estimated aircraft drag in cruise (Table 2.5: Raymer 1999). For this thrust matching with L/D estimation from the selected aspect ratio and an estimated wetted area of aircraft, the cruse L/D of jet aircraft may assume to be 86.6 percent of the maximum L/D (Raymer 1999).

Table 2.4 Typical Trends of T/W (Raymer 1999)

Aircraft Type	Typical Installed T/W
Jet Trainer	0.4
Military Cargo	0.25
Jet Transport	0.25-0.4

Table 2.5 Typical Trends of T/W_0 vs. Maximum Mach number (Raymer 1999)

$T/W_0=aM_{max}^C$	a	C
Jet Trainer	0.488	0.728
Military Cargo	0.244	0.341
Jet Transport	0.267	0.363

In regards to the level flight without the acceleration, the thrust is equal to the drag of aircraft, as well as the weight equals the lift. In these flight conditions, the relationship between T/W and L/D is described as,

$$\left(\frac{T}{W}\right)_{cruise} = \frac{1}{\left(\frac{L}{D}\right)_{cruise}}. \tag{2.20}$$

The T/W estimation using Equation (2.20) is only at cruise conditions (Fig. 2.5). For other flight

mission segments, the relationship between T/W and L/D is different from others. For example, the highest weight of aircraft occurs at the beginning of the cruise during operation. The weight of aircraft is decreased as fuel burns during each flight segment, such as take off and climbs to cruise altitude.

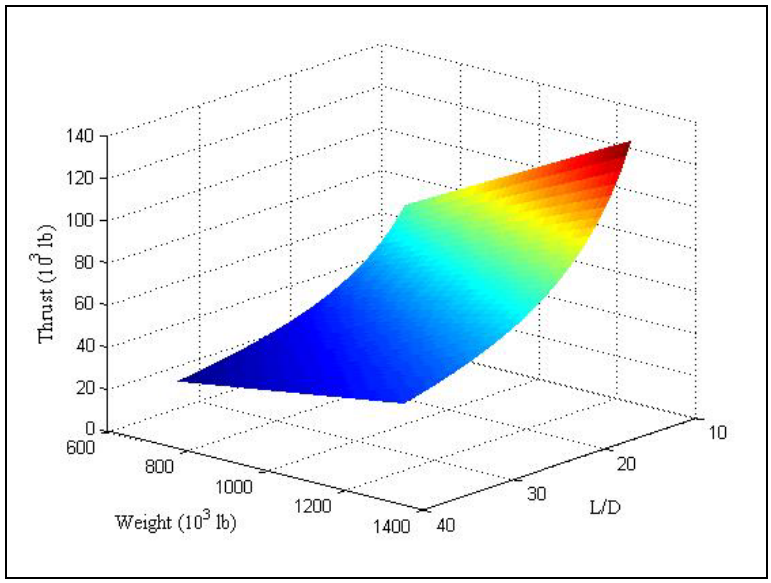

Fig. 2.5 T/W vs. L/D Matching Diagram

The takeoff T/W can be calculated by Equation (2.21) considered with weight fraction (Table 2.3) as,

$$\left(\frac{T}{W}\right)_{takeoff} = \left(\frac{T}{W}\right)_{cruise}\left(\frac{W_{cruise}}{W_{takeoff}}\right)\left(\frac{T_{takeoff}}{T_{cruise}}\right). \tag{2.21}$$

2.6 Aircraft Design Considerations

Aircraft design involves requirements and issues of flight efficiency and safety. The requirements cover all safety-related phases of flight including strength, fatigue, stability and control capability, emergency performance, and emergency design such as fire resistance and evacuation. Some of the major contents to estimate aircraft performance are shown as follows.

2.6.1 Airfoil Section Series

The airfoil shape directly relates to the aerodynamic performance of aircraft, such as L/D and noise

emission. Moreover, airfoil characteristics are strongly affected by the Reynolds number at every operating condition. Therefore, the airfoil must be chosen considering conditions and the activities whether the flow will be laminar or turbulent, or whether flow separations will occur. For example, typical aircraft operate at a Reynolds number of about ten million.

There are varieties of airfoil families the most known is the NACA airfoil series which was designed by the National Advisory Committee on Aeronautics (NACA). These different types of airfoil can be distinguished by camber, leading edge radius and thickness. Other airfoil series includes the H_Quabeck series, Eppler series and DAE series available for wing design.

2.6.2 Aspect Ratio

Aspect ratio (simply, AR in equation) is an aerodynamic parameter which is simply defined as the span squared divided by the wing area. If a wing is designed with a high aspect ratio this means that the L/D ratio will be increased, and the strength of the tip vortex will be reduced. Another effect of aspect ratio is to consider the stalling angle that changes the calculations. Later in the design phase, the aspect ratio is always varied with the weight of aircraft. For example, jet aircrafts have a strong trend of aspect ratio decrease with increasing Mach number due to L/D becoming relatively less important at higher velocity. For high speed aircraft lower aspect ratio is required to save weight (Amano 2001).

2.6.3 Wing Sweep

Swept back wing layout is useful to reduce negative factors for transonic and supersonic flow, because the phenomenon of shock wave on a swept wing can be easily controlled by the actual velocity of the air flow passing over the wing, as well as to shift an aircraft's centre of gravity for the aerodynamic balance. Moreover, wing sweep potentially improves stability, because it has a natural dihedral effect. With the swept wing layout, zero or negative dihedral of such a wing is frequently required to avoid unnecessary stability. In any case, current commercial aircraft are designed with swept wing

configuration as standard (Raymer 1999).

2.6.4 Wing Loading

Wing loading, which is defined as the weight of aircraft divided by the reference area of the wing, is a measurement of how much total weight is supported by how large the wing is, and normally refers to the take-off wing loading. The wing loading is the biggest determinate of speed, and also impacts upon the TOGW of aircraft, landing distances and stall speed. In the design process, the wing loading is considered with the design lift coefficient and drag coefficient impacting through its effect upon wetted area and wing span. After determining the parameter, the wing loading and the T/W are optimised together using aerodynamic, weight and propulsion data which are calculated from the initial design layout. For BWB configuration of the new concept design, the wing loading will be different from the typical commercial aircraft. However, this result of wing load is feasible to compare configuration performance between the initial deign and evaluated design. For example, the wing load will be lower when the configuration is optimised properly, which means that the wing provides better lift than the previous model.

2.6.5 Function of Winglets

Winglets are vertical extensions of wingtips that improve aircraft's fuel efficiency and cruise range reducing the drag associated with vortices at the wing-tips as the aircraft moves through air. With reducing this negative factor, fuel consumption becomes more economic and range is extended. The winglets are designed to generate negative pressure on the upper surface and positive pressure on the lower surface in flight. This pressure difference creates lift across the upper surface and the aircraft is able to fly efficiently. Fig. 2.6 shows alternative winglet design, and the pressure distributions of different winglet types are shown in Fig. 2.7 (Houghton 2003).

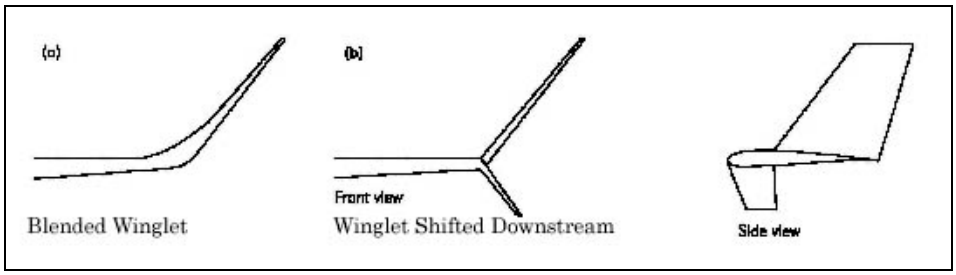

Fig. 2.6 Alternative Winglet Design (Houghton 2003).

According to the NASA Langley report (NASA 2005), the Boeing B747 with winglets could reduce a 4 percent drag in flight. Moreover, the DC-10 model tested in a wind tunnel demonstrated that winglets on the model reduced overall drag by 5 percent compared to the model without the devices.

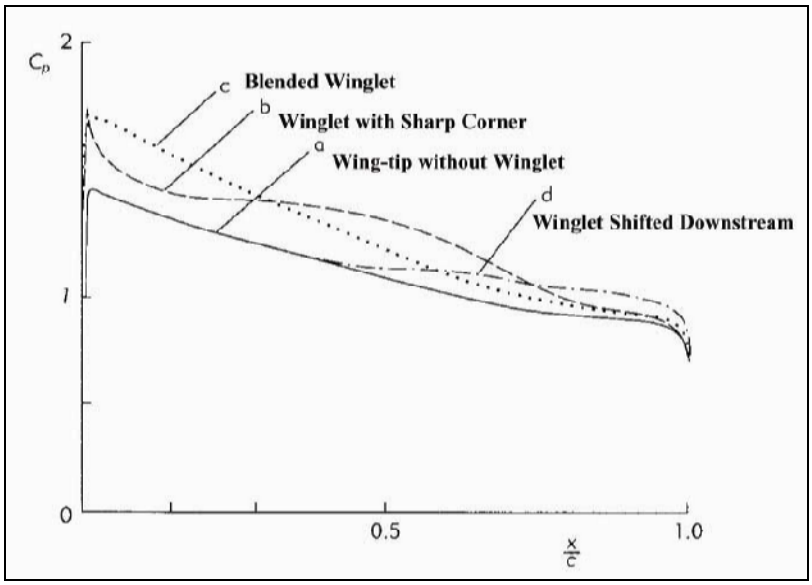

Fig. 2.7 Streamwise Pressure Distributions over the Upper of the Main Wing close to the Wing-tip for Different Winglet Configuration (Houghton 2003).

2.6.6 Passenger Compartment

For cabin design, passenger compartments (Fig. 2.8) are considered to design a cabin space for passenger activity during flight. There is typical passenger compartment data in Table 2.6, for example, doors and entry aisles are required to occupy 1.0-1.5 m of cabin length each (Raymer 1999). In addition, the A380 is designed with wider layout of passenger compartment required as shown in Table 2.6 (AIRBUS S.A.S 2004).

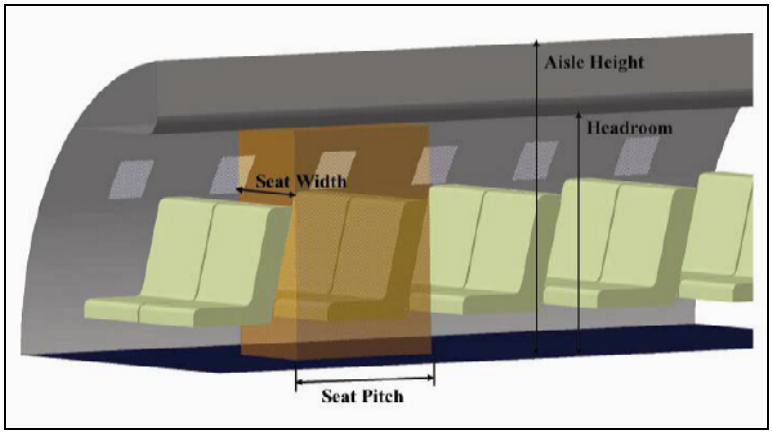

Fig. 2.8 Simple Definitions of Cabin Layout for Commercial Aircraft

Table 2.6 Typical Compartment Data and the A380 Passenger Allowance

	First Class	Business Class	Economy Class	High Density/ Small Aircraft
Seat Pitch (m)	0.97-1.0	-----	0.86-0.91	0.76-0.81
Seat Width (m)	0.51-0.71	-----	0.43-0.56	0.41-0.46
Headroom (m)	>1.65	>1.65	>1.65	-----
Aisle Width (m)	0.51-0.71	0.5-0.6	0.46-0.51	>0.30
Aisle Height (m)	>1.93	>1.93	>1.93	>1.52

A380-800	First Class	Business Class	Economy Class
Seat Width (m)	0.725	0.685	0.535
Aisle Width (m)	0.97	0.58	0.51

In the BWB cabin layout, the passenger compartment has been arranged similar to the passenger allowance of the A380. The passenger cabin design is important for passengers to have a spacious and comfortable space with a high enough ceiling. For passenger's comfort, cabin illumination and warm colours of noise absorbing panels of such functions emphasises the modern advancements of commercial aircraft.

2.7 Component Weights Estimation

The estimation of aircraft weight is a significant part in the conceptual design process, especially the BWB configuration as a new concept design, because the aircraft weight directly relates to the flight

performance. Conventional aircraft are approximately composed from 20 component sections including avionic systems and amenity equipments (Aircraft Aerodynamics and Design Group 2004, and Raymer 1999). For BWB weight estimation, methodologies of the traditional weight estimation for commercial aircraft design, NASA's Laboratory results (Brandley 2004) and data of existing components have been utilised. In addition, the wing design of BWB configuration is shown how to estimate the weights of such non-cylindrical fuselage design using the traditional methodologies later.

3.7.1 Aircraft Structural Load Factor

A structural design process is required to consider all safety and performance requirements. The safety margin is described with the design load factor (Willems et al. 1981). In aircraft design the load factor is an aerodynamic load factor which includes how much the loading of aircraft undergoes during manoeuvres as a multiple of the standard acceleration due to gravity ($g = 9.8\ ms^{-2}$). Fig. 2.9 shows the relationship between aircraft velocity and the load factor (Amano 2001).

Table 2.7 Typical Aircraft Load Factor Lists (Torikai 1999)

Aircraft Type	Load Factor (N)	
	Positive	Negative
Utility Category	4.4	-1.76
Normal Category	3.17-3.8	-1.52- -1.26
Transport Category	2.5-3.8	-1.0

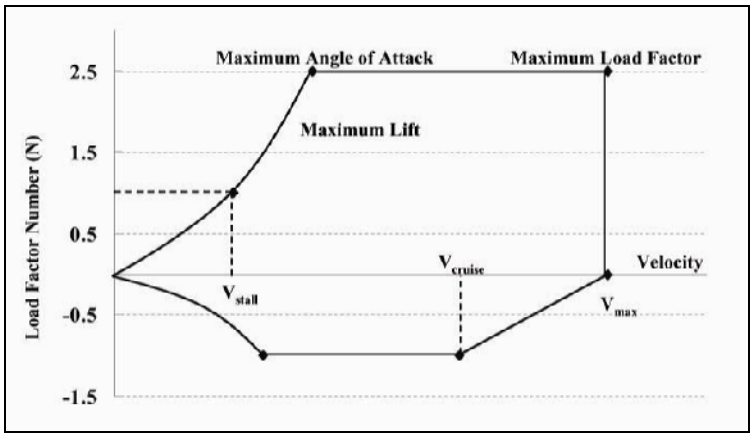

Fig. 2.9 Aircraft Velocity-Load Factor Diagram

The typical load factors of aircraft are shown in Table 2.7 (Torikai 1999). These values are decided by the Federal Aviation Administration (FAA) for safety flight operation of every kind of aircraft, and the regulations are referred to Federal Aviation Regulations (FAR) of Part 25 in FAA as 'Airworthiness Standard: Normal, Utility, Acrobatic, and Commuter Category Aircraft' (FAA 2005a & Kroo 2005).

For commercial aircraft design, weight estimation is considered with load factors and aircraft specifications to improve flight performance keeping within flight safety guidelines. This requires achieving the FAR Part 25 with ultimate load factor, which is a 1.5 times higher value of limit load factor. Moreover, commercial aircraft is considered design with of other load factors such as for gust load factor during flight (Torikai 1999).

3.7.2 Fuselage

The fuselage section of commercial aircraft is manufactured with semi-monocoque structures using frame, stringer and aluminium skin. In recent years modern airliner are manufactured with composite structures such as carbon fibre frameworks. When estimating the fuselage weight, the gross wetted area of fuselage is considered with the pressure bending load parameter, defined as,

$$W_{fuse} = S_{fuse} \times \left(1.051 + 7.617 \times 10^{-3} P B\right), \tag{2.24}$$

where S_{fuse} is the gross wetted area of fuselage, P is the maximum pressure differential and B is the fuselage width (Aircraft Aerodynamics and Design Group 2004).

3.7.3 Wing

The wing estimation is considered with traditional structure of a wing section, such as skin, spar and stringers et al, employing the fully-stressed bending weight of the wing box. Moreover, the BWB configuration has been estimated the wing weight with Equation (2.25) with existing aircraft. The equation of weight estimation for the wing component is defined as,

$$W_{wing} = 4.22 \times S_{gw} + 1.642 \times 10^{-6} \frac{N_{ult} b^3 \sqrt{W_{takeoff}\ W_{ZFW}} (1 + 2\lambda)}{\left(\frac{t}{c}\right)_{avg} \cos^2 \Lambda_{ea} S_{gw} (1 + \lambda)}, \quad (2.25)$$

where N_{ult} is the ultimate load factor, b is the wing span, W_{ZFW} is the zero fuel weight of aircraft, $(t/c)_{avg}$ is the average airfoil thickness, λ is the taper ratio of wing, Λ_{ea} is the swept angle of structure axis and S_{gw} is the gross wing area (Aircraft Aerodynamics and Design Group 2004).

2.7.4 Horizontal Tail

The conventional aircraft is installed with a horizontal tail wing with elevator to control the pitching moment of aircraft during flight. However, BWB concept design is no longer compounded with horizontal tail. The function of horizontal tail may be replaced with wing flap, aileron and leading-edge device, as demonstrated in the B-2 Spirit Bomber.

2.7.5 Vertical Tail and Rudder

The vertical tail is designed with a torsion box and rudder to steer itself toward the mission destination. The tail weight with rudder will be estimated by Equation (3.26).

$$W_{vert} = 4.19 \times S_{vert} + 2.4 \times 10^{-5} \frac{N_{ult} b_{vert}{}^3 \left(8 + 0.44 \frac{W_{takeoff}}{S_{gw}}\right)}{\left(\frac{t}{c}\right)_{avg} \cos^2 \Lambda_{ea}}, \quad (2.26)$$

where S_{vert} is the area of vertical tail with rudder section, b_{vert} is the tail length, $(t/c)_{avg}$ is the average airfoil thickness of tail's airfoil section and Λ_{ea} is the swept angle of tail's structure axis (Aircraft Aerodynamics and Design Group 2004).

2.7.6 Landing Gear

Aircraft require landing gear for ground operation. For example, five landing gears are installed in the A380 airliner. The weight of landing gear includes structure, actuating systems and the rolling

assembly consisting of wheels, brakes and tyres, and is closely related to the total TOGW of aircraft (Aircraft Aerodynamics and Design Group 2004).

$$W_{gear} = 0.04 \times W_{takeoff} \tag{2.27}$$

2.7.7 Surface Controls

For commercial aircraft, surface controls are the control systems associated with surface actuation with fully powered control of engines. The weight of the surface controls is related to the area of horizontal and vertical tails (Aircraft Aerodynamics and Design Group 2004). Therefore, this weight of the BWB configuration is estimated with only the area of vertical tail, S_{vert}, with the parameter of fully powered controls function as,

$$W_{sc} = 3.5 \times S_{vert}. \tag{2.28}$$

2.7.8 Propulsion System

A jet propulsion system is constructed with an engine section (e.g. fan, compressor, combustor, turbines and contra-rotation et al.) and structural section (e.g. nacelle and pylon et al.). When estimating the total propulsion weight, W_{pro}, dry engine weight, W_{deng}, which excludes nacelle and pylon weights, is normally utilised as Equation (2.29) (Aircraft Aerodynamics and Design Group 2004). Moreover, the propulsion weight may be at least estimated using existing jet engines of aircraft if new propulsion systems are required to your design.

$$W_{pro} = 1.6 \times W_{deng} \tag{2.29}$$

2.7.9 Auxiliary Power Unit (APU)

The APU system is a relatively self-contained generator to start engines, and to provide electric power during ground operations as well as during flight. The APU weight, W_{apu}, is directly related to the seat numbers as defined in Equation (2.30) (Aircraft Aerodynamics and Design Group 2004).

$$W_{apu} = 3.175 \times N_{seats} \tag{2.30}$$

2.7.10 Hydraulics and Pneumatics

Aircraft employ hydraulics and pneumatics for electrical control systems. The weight of hydraulics and pneumatics, W_{hp}, is estimated with the reference area of aircraft (Aircraft Aerodynamics and Design Group 2004), as shown as,

$$W_{hp} = 0.295 \times S_{ref} . \tag{2.31}$$

2.7.11 Electrical Equipment

The electrical equipments of commercial aircraft are usually installed for passenger's comfort during flight. Therefore, the equation is designed as,

$$W_{elecp} = 5.9 \times N_{seats} , \tag{2.32}$$

where W_{elecp} is the weight of electrical equipment and N_{seats} is the number of seats (Aircraft Aerodynamics and Design Group 2004).

2.7.12 Avionic Equipments

The avionic equipment is the on-boarded electrics to control aircraft operation, such as communication and navigation systems, autopilots and electrical management systems. The avionic installed equipments are similar systems in each aircraft category. For example, the weight of instruments and navigational equipment may be assumed as 545 kg for long range aircraft. The electrics of avionic equipment are estimated to be 680 kg of the system weight for overseas operations (Aircraft Aerodynamics and Design Group 2004).

2.7.13 Furnishing

The furnishing is installed into aircraft cabins for passenger comfort. Most of this equipment consists

of occupied by passenger seats. Therefore, the furnishing weight is directly related to the number of passengers. The equation of furnishing weight, W_{furni}, is defined (Aircraft Aerodynamics and Design Group 2004) as,

$$W_{furni} = 35.65 \times N_{seats}. \tag{2.33}$$

2.7.14 Air Conditioner and Anti-icing Systems

This system is installed for air circulation in the cabin area and for passenger comfort. This equipment weight also depends upon the number of passengers. This weight, $W_{air\ con}$, may be calculated (Aircraft Aerodynamics and Design Group 2004) as,

$$W_{air\ con} = 6.8 \times N_{seats}. \tag{2.34}$$

2.7.15 BWB Cabin Design Using NASA's Methodology

NASA's methodology was presented by Dr. Bradley to develop the capability of BWB concept design using Finite Element Analysis (FEA) in 2004. In regards to the fuselage structure of BWB transport at NASA, the pressurised cabin was designed considering with bending, share and torsion from aerodynamics loads. In the comparison between conventional circular fuselage and non-conventional fuselage, it was predicted that the non-conventional fuselage shape requires higher structural strength because of large bending stresses on the skin.

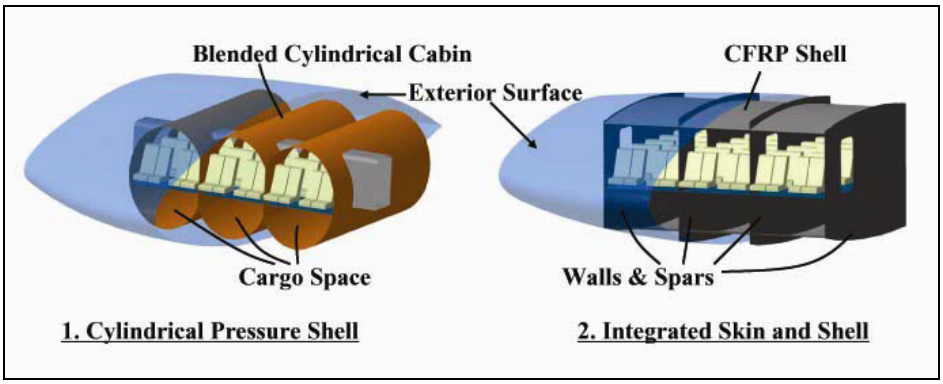

Fig. 2.10 Structural Cabin Design Concept

The first BWB design consisted of inner cylindrical shells for the internal pressure and the outer skin for bending, and utilised approximately 12.7 cm (5 inches) thickness sandwich structural shell with a deep skin/stringer concept (Fig. 2.10 No.1). After optimising the NASA design based on cost and weight, the skin/stringer concept with 12.7-15.24 cm (5-6 inches) deep stringers was redesigned to take the inner pressure concept without the bending shells (Fig. 2.10 No.2). According to the skin design, the internal ribs had Y-braces to reduce the bending force from internal pressure.

Since the internal pressure was on all sections, NASA presupposed that the depth of the stringers would be a function of the cabin size and the maximum aerodynamic loads of TOGW. Thus, a weight estimation of the entire pressurised cabin may be defined in the following equation;

$$W_{cabin} = a \times \left(W_{takeoff}\right)^{b} \left(S_{cabin}\right)^{c}, \tag{2.35}$$

where a, b and c are constants and S_{cabin} is the area of cabin (Bradley 2004).

With the cabin design using FEA, the weight of the pressurised cabin section of BWB concept was explained with various values of TOGW. This TOGW involves the thickness of ribs and spars of the centre body, aerodynamic load, and the element of thickness of cabin skin. The materials used in the wing and centre body were composed of carbon fibre reinforced plastic (CFRP) laminates with a Young's modules of $E=1\times10^{7}$ pis, Poisson's ratio $\nu = 0.4$, 0.056 lbin.$^{-3}$ density and allowable tensile stress of approximately 50,000 pis (Bradley 2004).

With the relationship between cabin weight, size and TOGW, the weight estimation is defined with the linearised Equation (2.35) as,

$$\int W_{cabin} dW = \int a \; dW + b \int W_{takeoff} dW + c \int S_{cabin} dW \,, \tag{2.36}$$

using the method of least squares fitting,

$$\Pi = \sum_{i=1}^{n} \left[\int W_{cabin} dW - \int a \; dW - b \int W_{takeoff} dW - c \int S_{cabin} dW \right]^{2} = Minimum \,, \tag{2.37}$$

results in the parameters as,

$$\frac{\partial \Pi}{\partial a} = 0, \qquad \frac{\partial \Pi}{\partial b} = 0, \qquad \frac{\partial \Pi}{\partial c} = 0 . \tag{2.38}$$

The Equation (2.38) was solved by FEA simulation to obtain the coefficients. Thus, Equation (2.35) is redescribed from regression analysis as,

$$W_{cabin} = 0.31642 \times W_{takeoff}{}^{0.16655} S_{cabin}{}^{1.06116} . \tag{2.39}$$

Moreover, the weight of centre body was scaled to match data supplied by the Boeing Company to estimate the credible actual weight of BWB pressurised cabin. The final equation of cabin weight is defined with a scale factor, K_s, (Bradley 2004) as,

$$W_{cabin} = K_s \times \left(0.31642 \times W_{takeoff}{}^{0.16655} S_{cabin}{}^{1.06116}\right). \tag{2.40}$$

Chapter 3 Computational Approach for Aircraft Design

In recent years the computational approach has been used as a significant function to create, analyse and optimise production in industrial and institution sectors. This numerical process also provides numerous advantages, such as saving time and cost during the conceptual design phase (Torenbeek 1991). In the future these computational techniques will also improve the current manufacture process speed and quality of production in industrial fields which directly relate to cost diminution and time curtailment.

3.1 Computational Techniques Using CAD and CFD Softwares

In this research, several softwares were utilised to analyse the aerodynamic performance of a BWB configuration and the A380 model. These CAE softwares were Dassault Systemes CATIA V5, Fluent software package (FLUENT 6, Gambit 2 and TGrid 3), HyperMesh in HyperWorks V6 (Altair Engineering) and SolidWorks 2002 (SolidWorks Corporation), and a general process and the own CAE approach of this project are shown in Fig. 3.1.

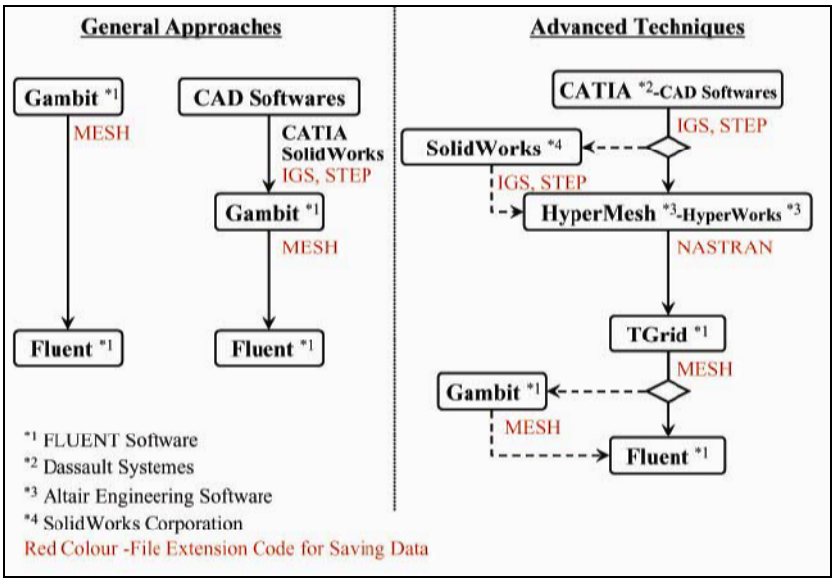

Fig. 3.1 Computational Modelling Approach

Computational process for CFD analysis is mainly divided into three phases as follows;

1st Step: Model is designed on CAD softwares, such as CATIA V5, SolidWorks 2002 and Pro/Engineer 2002. In this research CATIA V5 was utilised.

2nd Step: The CAD Model is imported from CATIA V5 into Pre-processing Softwares, such as Gambit 2, HyperMesh and TGrid 3, to create meshing surface and meshed volume of boundary area.

3rd Step: The Meshed Volume design is imported from the Pre-processing software into FLUENT 6 to analyse aerodynamic performance of the configuration.

In this research, the advanced computational approach (Fig. 3.1) was normally utilised to demonstrate CFD simulations, because this process was effective to work with complex geometry, such as aerial and automotive vehicles which have twisted or shaped edge surfaces.

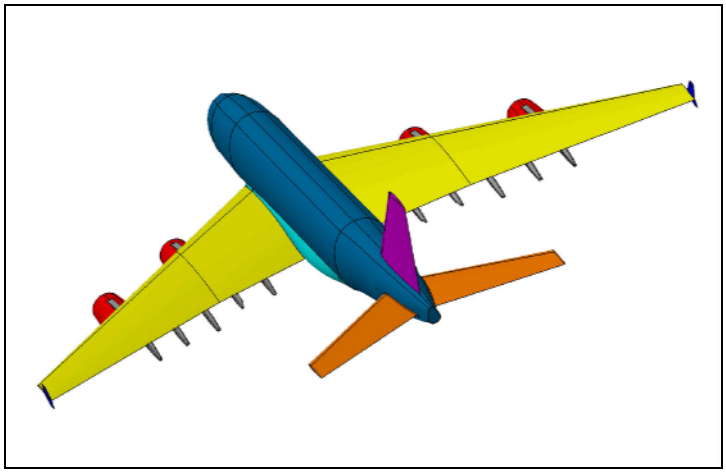

Fig. 3.2 A380 Aircraft Design on CATIA V5 for CFD Simulation

In the first step, a model (e.g. Fig. 3.2) is designed on CATIA V5 saved with IGS or STEP file extension to import this data file onto pre-processing software, such as Gambit 2 and HyperMesh. In addition, before exporting a CATIA V5 design file sometime the model is transferred to a SolidWorks 2002 environment simplify the geometry shape, and SolidWorks 2002 can create a tight surface

configuration, because the value of tolerance is different between CATIA V5 and SolidWorks 2002 (CATIA V5: Sensitive < SolidWorks 2002: Rough) and SolidWorks 2002 has an automatic trimming function. This extra process is effective when generating a meshing surface on geometry in the next step. Moreover, the CATIA V5 or SolidWorks 2002 model should be a single surface model or one volume model.

Secondly, this project employs HyperMesh (e.g. Fig. 3.3) and TGrid 3 programs to generate a meshing surface and a meshed volume of the boundary area. The first step of this stage is to modify and simplify the configuration shape for a meshing process based on the CATIA V5 model. Normally CAD geometry has many non-essential edges and twisted surfaces, which easily makes difficulties when generating a meshing surface on the geometry during prepossessing phase. On the HyperMesh program, the model is simplified by deleting unnecessary edges, creating a new support line for complex and big surfaces and filled gaps in (Fig. 3.3 Right Image).

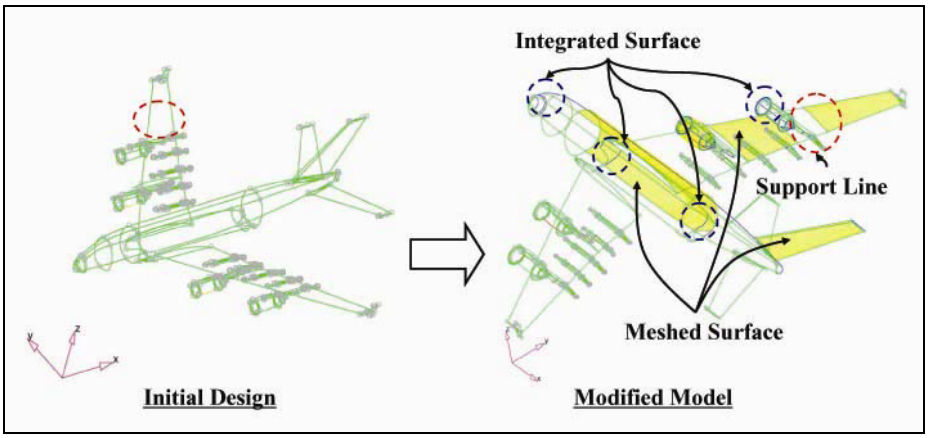

Fig. 3.3 Design Process on HyperMesh

The redesigned and simplified model is then moved onto the next step of creating a meshed surface and making volume mesh for the boundary area. In this process, meshing quality, such as element skewness, element type and bias intensity, are taken into account to create a mesh on the boundary surfaces. This key point of meshing quality is especially focused on element skewness in this process,

which is kept to less than 0.9. The reason why this mesh quality directly relates to CFD results, for example, is that a rough quality of meshed surface makes inequalities and asperity on geometry. However, a difficulty in generating a meshing surface is to take into account a balance between skewness size and processing hour for CFD simulation, because a finer meshed geometry takes much more time in processing, but it will produce better results. With these considerations in the preprocessing period, a model is produced with a meshed surface as a shell image on HyperWorks V6 (Fig. 3.4, 3.5).

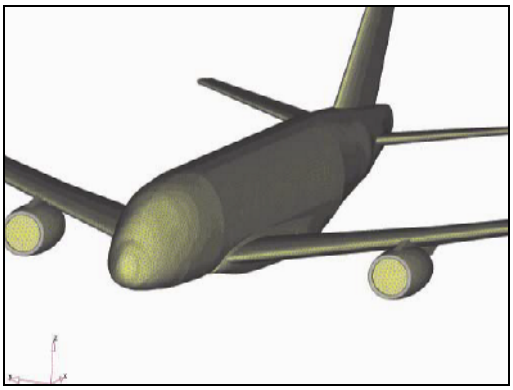

Fig. 3.4 Meshed Aircraft Model on HyperWorks V6

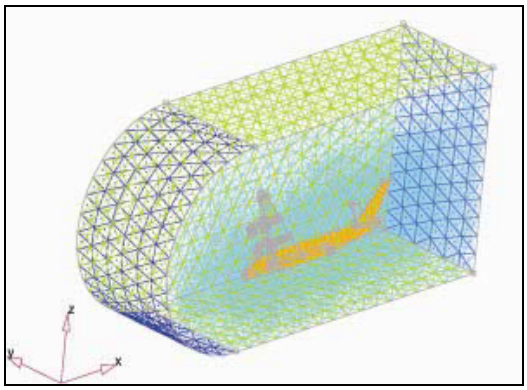

Fig. 3.5 Meshed Boundary Area with Aircraft Model

In Fig. 3.5, the half model of the aircraft is utilised for CFD simulation, because the configuration was symmetric, and this procedure could save file size and use less element number. This has the great advantage of faster and more economic processing time of CFD calculation as against CFD simulation employed for the whole aircraft model.

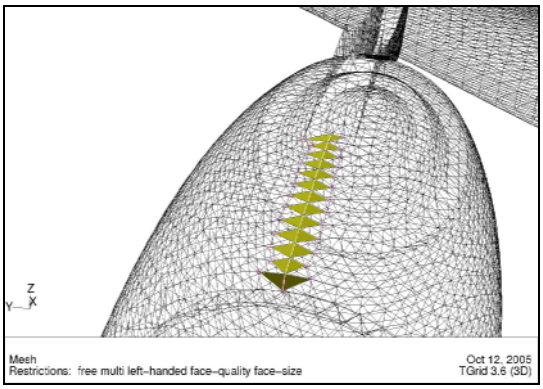

Fig. 3.6 Connection Errors on Engine

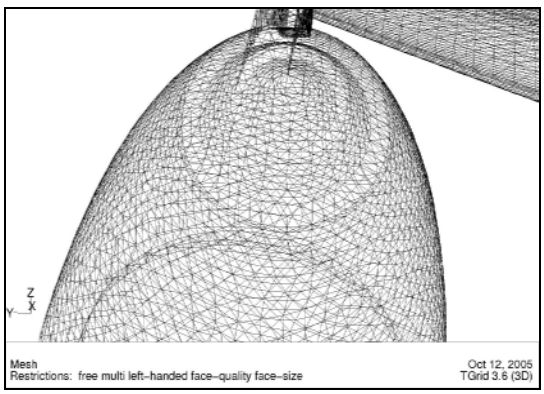

Fig. 3.7 Modified Engine Design on TGrid 3

After the meshed shell model (Fig. 3.5) on HyperWorks V6 is created, the model is imported to the TGrid 3 platform to generate a volume mesh of boundary area. According to the feature of TGrid 3, any connection error (Fig. 3.6: on Yellow colour) can be checked, such as nodes' connection error, duplicated surface or element shape error. Here the meshed model can also be modified in the modification function of the TGrid. In addition, the TGrid 3 has an auto-tolerance and skewness improvement function, although complex connection errors should sometimes be modified manually. This is because the configuration outline is easily too radically changed by the automatic improvement function. After connection errors have been fixed on the meshed boundary area, the model may move onto the next step to generate a volume mesh around the boundary area.

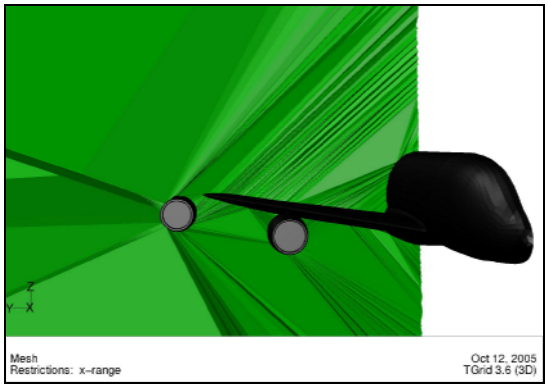

Fig. 3.8 Partly Connected STL on TGrid

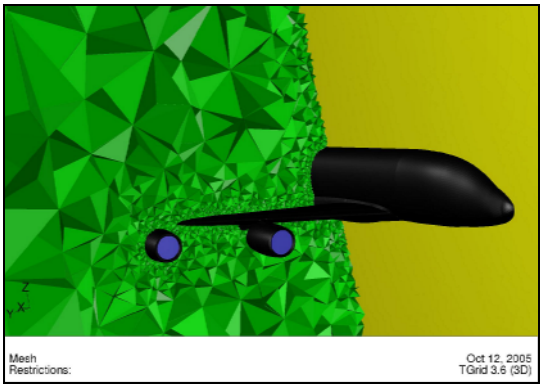

Fig. 3.9 Fully Connected Mesh on TGrid

Two stereolithographies (STL) used TGrid 3, Fig. 3.8 and Fig. 3.9, are shown with filled face model on the aircraft, side wall and the boundary area of 33-70 m. Fig. 3.8 was created with initialised volume mesh in the pre-wrapping process on TGrid 3. Fig. 3.8 was not connected to each node and had unorganised STL. To solve this connection error on TGrid 3, the STL needs to be initialised and refined with several tens iterations. After several tens iterations, the STL became as Fig. 3.9, which was a well organised and functional model.

Finally, the volume meshed geometry may import onto Fluent software by saving the file with MESH

extension for CFD simulation. This activity is the final part of CFD simulation, but before running CFD simulation several condition settings are required to calculate and obtain aerodynamic performance configuration accurately. The procedure of Fluent is shown in Fig. 3.10. Normally, the processes on the Fluent platform are similar to Fig. 3.5, because each condition setting always relates to the before and after process settings.

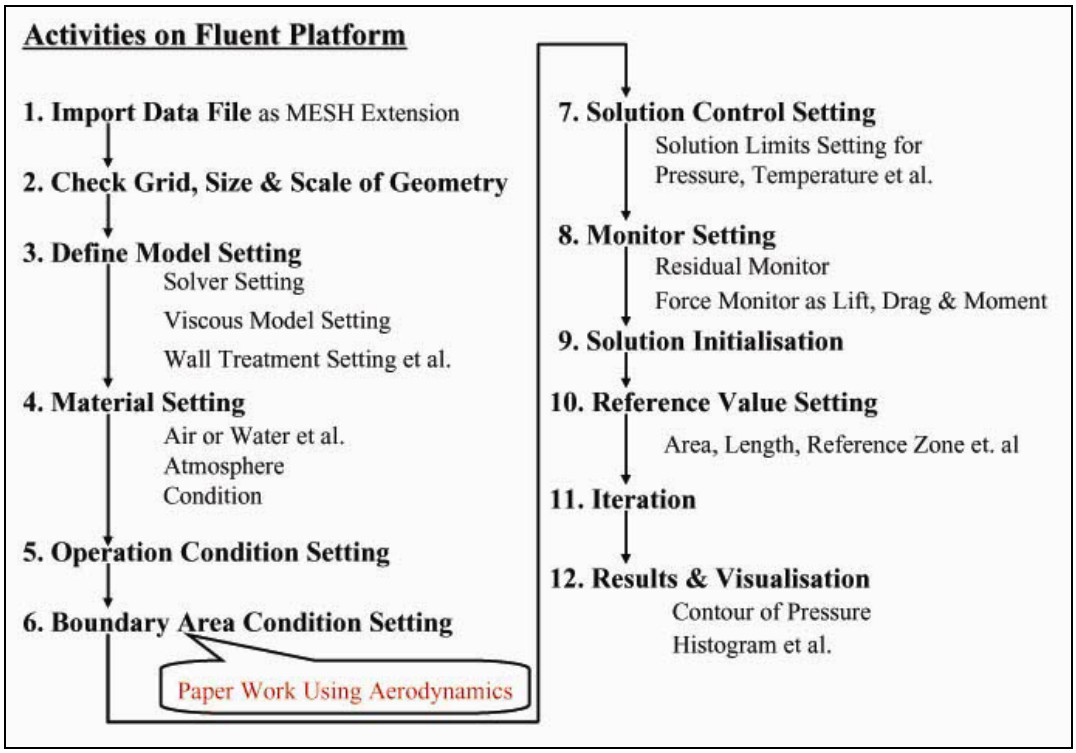

Fig. 3.10 General Activities on Fluent Platform

For example, Fig. 3.11 is a sample of boundary area conditions and a view of CFD simulation. This illustration utilised a whole aircraft model and rectangular box as the outside boundary surface. However, a half model is utilised for symmetric configuration in CFD simulation. In addition, it is better to employ a whole model if turbulence flows strongly affect aerodynamics performance of configuration and need to be considered in FLUENT 6, such as with a racing car or an unsymmetrical vehicle.

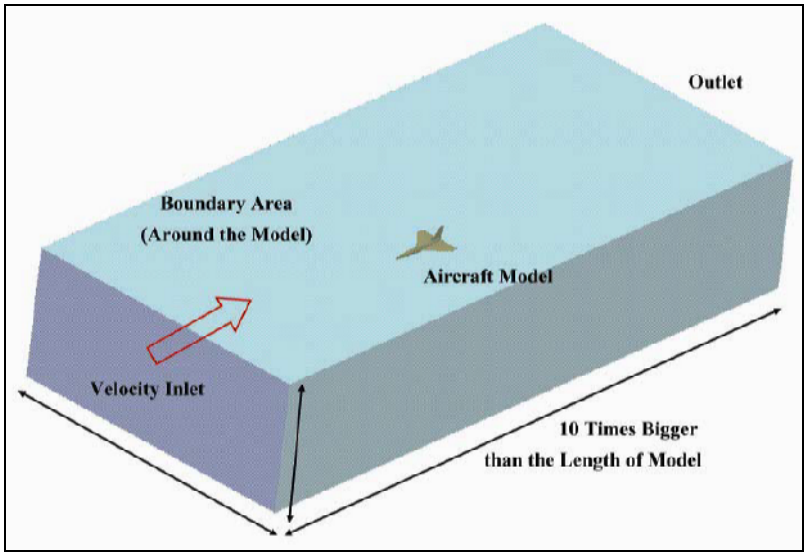

Fig. 3.11 Sample CFD Design Model & Setting Conditions

For the activity processes between 3 and 7 mentioned in Fig. 3.10, aerodynamics and computational methodologies are taken into account to produce a similar space condition as in atmospheric conditions. These methodologies and computational techniques will be explained later in section 3.2.

After running CFD simulation on FLUENT 6, aerodynamics results are obtained as shown in Fig. 3.12 and Fig. 3.13. In regards to the CFD simulation of this A380 model, the processing time taken was approximately 2 days and with 500 times iterations done based on the Realisable k-ε model.

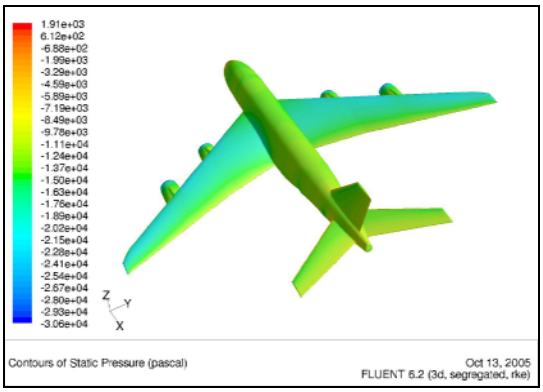

Fig. 3.12 Contours of Static Pressure

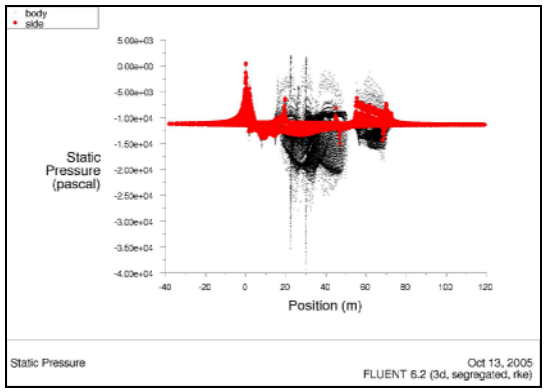

Fig. 3.13 Data Plot of Static Pressure

3.2 Numerical Methods for Aerodynamic Analysis of BWB Configuration

Advanced CFD analysis is a well established technique for aerodynamic analysis in automotive and aerial vehicle industries. For especially a new concept design such as the BWB configuration of this research, CFD analysis plays a significant part to demonstrate aerodynamic performance of the model, as well as for the design optimisation process. The strength of CFD is its ability to inexpensively produce a small number of simulations leading to understanding necessary for design, and can produce data using actual flight operating conditions. Moreover, the CFD application is well suited to provide air flows detail with the use of a stereograph.

In life, the majority of air flows are turbulent, such as air flows from an air conditioner and air flow around a car. The way to discriminate between turbulent and laminar flows is represented by the Reynolds number. For a generalised example, a Reynolds number well above 1,000 is a turbulent flow, and a Reynolds number below 100 is not. A Reynolds number of flow measurement is defined as,

$$\mathrm{Re} = \frac{\rho L V}{\mu} \quad or \quad \frac{LV}{\nu}, \tag{3.1}$$

where *Re* means Reynolds number, ρ is the density, L is the length, μ is the dynamic viscosity and v is the kinematic viscosity. The Reynolds number is the appearance of the dimensionless equation which represents the ratio of the inertial to the viscous term.

Turbulent flow is represented by the Navier-Stokes and Euler equation. In the CFD application, both equations are employed to simulate aerodynamic performance accurately as actual air flow for turbulent flow. In this research Fluent Version 6.2 was utilised to analyse the aerodynamic performance of the BWB configuration.

In Fluent CFD solver several viscous design models exist; Spalart-Allmaras (SA), Standard k-ε, Re-Normalisation-Group (RNG) k-ε, Realisable k-ε, Standard k-ω, Shear-Stress-Transport (SST) k-ω, v^2-f^2 model, Reynolds Stress Model (RSM), Detached Eddy Simulation (DES) and Large Eddy

Simulation (LES) models (Fluent Inc. 2003). Moreover, CFD progresses are always contingent on several constraints, not only in the field of external aerodynamics. A number of other considerations, computational capabilities (i.e. allocatable RAM size, total amount of CPU and expected response time for calculations) have to be taken into considerations. Together with finite element method (FEM), this is a significant procedure to create high quality meshes of geometry using either structured or unstructured/hybrid meshes for CFD modelling. During this preprocessing work, Gambit, TGrid and HyperMesh are likely to be utilised for meshing of geometry.

According to the numerical techniques required to measure turbulence flows, turbulent streams are manoeuvred by the Boussinesq hypothesis (Aumann 2001). In turbulence models, the Boussinesq approach is employed to compute turbulent parameters. This classical approach is related to the Reynolds stresses and the mean flow strain through the turbulent viscosity concept (Briganti 2004 & Wei et al. 1994). With literature of view of CFD simulation, the SA and the Realisable k-ε turbulence models of Fluent package's viscous models were employed to analyse an aerodynamic performance of the configuration in this research. A more detailed description of numerical and computational methodologies will be shown in the next section.

3.2.1 Two Dimensional Method with the Spalart-Allumaras Turbulence Model in Fluent

The Spalart-Allumaras (SA) model is a relatively simple, one equation model that solves a modelled transport equation for the turbulent kinetic viscosity. The SA turbulence model was designed specifically for aerospace applications involving wall-boundary flows, and has been shown to give good results for boundary layers subjected to adverse pressure gradients. Moreover, the SA model is effective for low Reynolds number simulation requiring the viscous affected regions of the boundary layer to be resolved properly (Fluent Inc. 2003).

A simple understandable example of 2D flow phenomenon is a 2D incompressible flow of Newtonian

fluid, which considers mass and momentum equations as,

$$\rho\overline{u_j}\frac{\partial\overline{u_i}}{\partial x_j} = -\frac{\partial\overline{p}}{\partial x_i} + \frac{\partial}{\partial x_j}\left(\mu\frac{\partial\overline{u_i}}{\partial x_j} - \rho\overline{u_i'u_j'}\right), \tag{3.2}$$

where ρ is the fluid density, p is the pressure, μ is the dynamic viscosity, u is the velocity and i and j are flow directions. The Reynolds-Averaged Navier-Stokes equation governs equations for the problem computation (e.g. momentum balance) with the continuity equation based on Equation (3.2). Subsequently, the Boussinesq hypothesis is employed to compute the turbulence viscosity relating to the Reynolds stresses and the mean flow strain through the turbulence viscosity concept. This classical approach is described as,

$$-\rho\overline{u_i'u_j'} = \mu_t\left(\frac{\partial\overline{u_i}}{\partial x_j} + \frac{\partial\overline{u_j}}{\partial x_i}\right) - \frac{2}{3}\rho\delta_{ij}k\,, \tag{3.3}$$

where μ_t is the turbulent kinetic viscosity, δ_{ij} is the Kroenecker Delta and k is the turbulent kinetic energy (Briganti et al. 2004). The turbulent kinetic energy, k, is defined as,

$$k = \frac{1}{2}\overline{u_i'u_j'}. \tag{3.4}$$

In many cases, models based on the Boussinesq hypothesis perform well. The advantage of this approach is reasonably low computational processing time associated with the computation of μ_t. With this considerable condition, the transport viscosity (or the-eddy-viscosity-like term), $\tilde{\nu}$, is equal to the turbulent kinetic viscosity in the near-wall region. The transport viscosity equation is explained as,

$$\frac{\partial}{\partial t}\left(\rho\tilde{\nu}\right) + \frac{\partial}{\partial x_i}\left(\rho\tilde{\nu}u_i\right) = \frac{1}{\sigma_{\tilde{\nu}}}\left[\frac{\partial}{\partial x_i}\left\{\left(\mu+\rho\tilde{\nu}\right)\frac{\partial\tilde{\nu}}{\partial x_j}\right\} + C_{d2}\rho\left(\frac{\partial\tilde{\nu}}{\partial x_j}\right)^2\right] + G_\nu - Y_\nu + S_{\tilde{\nu}}\,, \tag{3.5}$$

where G_ν is the production of turbulent viscosity and Y_ν is the destruction of turbulent viscosity, which occurs in the near-wall region due to wall blocking and viscous damping (Oki et al. 2003). Furthermore, $\sigma_{\tilde{\nu}}$ and C_{d2} are constants, ν is the molecular kinetic viscosity and $S_{\tilde{\nu}}$ is a user-defined source term.

For the turbulent viscosity modelling, the viscosity, μ_t, is simplified as,

$$\mu_t = \rho\tilde{\nu} f_{\nu 1}, \tag{3.6}$$

where the viscous damping function, f_{v1}, is given by,

$$f_{\nu 1} = \frac{X^3}{X^3 - C_{\nu 1}{}^3}, \tag{3.7}$$

and where X is the ration of kinetic viscosity as,

$$X \equiv \frac{\tilde{\nu}}{\nu}. \tag{3.8}$$

With Equation (3.5), the turbulent production term, G_v, is described as,

$$G_\nu = C_{b1}\rho\tilde{S}\tilde{\nu}, \tag{3.9}$$

where

$$\tilde{S} \equiv S + \frac{\tilde{\nu}}{k^2 d^2} f_{\nu 2} \quad , \quad f_{\nu 2} = 1 - \frac{X}{1 + X f_{\nu 1}}, \tag{3.10}$$

where C_{b1} and k are constants, d is the distance from wall, and S is a scale measure of the deformation tensor. Furthermore, in the turbulent destruction modelling the destruction term is modelled as,

$$Y_\nu = C_{\omega 1}\rho f_\omega \left(\frac{\tilde{\nu}}{d}\right), \tag{3.11}$$

and

$$f_\omega = g\left(\frac{1 + C_{\omega 3}{}^6}{g^6 + C_{\omega 3}{}^6}\right)^{\frac{1}{6}} \quad , \quad g = r - C_{\omega 2}\left(r^6 - r\right) \quad , \quad r \equiv \frac{\tilde{\nu}}{\tilde{S}k^2 d^2}, \tag{3.12}$$

where $C_{\omega 1}$, $C_{\omega 2}$ and $C_{\omega 3}$ are constants, and $\tilde{S}$ is given by Equation (3.10). The modelling constants and the turbulent kinetic energy, k, are defined with the sea level atmosphere conditions as (Fluent Inc. 2003 & Oki et al. 2003),

$$C_{b1} = 0.1355, \quad C_{b2} = 0.622, \quad \sigma_{\tilde{\nu}} = \frac{2}{3}, \quad C_{\nu 1} = 7.1$$
$$C_{\omega 1} = 2.7566, \quad C_{\omega 2} = 0.3, \quad C_{\omega 3} = 2.0, \quad k = 0.4187.$$

According to the wall boundary conditions, the modified turbulent kinetic viscosity is set to zero at walls. For example, in some cases the wall shear stress is obtained from the laminar stress relationship

when the mesh is fine enough to resolve the laminar sublayer and the centroid of the wall-adjacent cell falls within the logarithmic region of the boundary layer and the law of the wall is employed if the mesh quality is too coarse to settle the laminar sublayer (Fluent Inc. 2003).

3.2.2 Three Dimensional Approach with the Realisable k-ε Turbulence Model in Fluent

The fidelity of CFD predictions for turbulent flow, in particular 3D simulation, is highly dependent upon the quality of the turbulence modelling whose salient flow features include 3D boundary layers with strong streamline curvature, separation and strong vortices. In Fluent solver three turbulence models are recommended for transport simulations, which are the Realisable k-ε turbulence model, LES model and RSM. With the consideration of PC capability in this research, the Realisable k-ε model was suitable to employ for 3D turbulent simulation. For example, the RSM model consumes approximately 40 percent more computational processing time and 20 percent higher RAM resources required when compared to the Realisable k-ε model in Fluent (Lanfrit 2005).

The Realisable k-ε model is one of the k-ε models in Fluent solver. The term of 'Realisable' means that the model satisfies certain mathematical constraints on the normal stresses and is consistent with the physics of turbulent flows (Fluent Inc. 2003). This turbulence model encompasses the Boussinesq approach and the eddy viscosity definition for normal stress in an incompressible strained mean flow. In the turbulent viscosity model, the turbulent eddy viscosity, μ_t, is defined with the kinetic energy (k) and the dissipation rate (ε) as,

$$\mu_t = \rho C_\mu \frac{k^2}{\varepsilon}, \tag{3.13}$$

where $C\mu$ is constant. Based on Equation (3.3) and Equation (3.13), the normal Reynolds stress is explained as,

$$\overline{u^2} = \frac{2}{3}k - 2\nu_t \frac{\partial U}{\partial x}. \tag{3.14}$$

In addition, the normal stress is always defined with a positive quantity in the Realisable model (Shih et al. 1995). If it becomes a negative, this means that the model has 'non-realisable' turbulent flow and the Schwarz's inequality (Cauchy-Schwarz inequality) for shear stresses can be violated (Fluent Inc. 2003 & Li et al. 2004). When the strain is large enough to satisfy, the relationship between these parameters becomes as,

$$\frac{k}{\varepsilon}\frac{\partial U}{\partial C_\mu}\frac{1}{3C_\mu} \approx 3.7. \tag{3.15}$$

The model coefficient, Cμ, is related to the mean strain rate. For example, Cμ is approximately 0.09 in the inertial sublayer of a flat boundary layer with Sk/ε = 3.3, and if it is around 0.05 in a homogeneous shear flow the (Sk/ε) becomes 6.0 (Fluent Inc. 2003).

Subsequently, the modelled transport equations for k and ε in the Realisable k-ε model are,

$$\frac{\partial}{\partial t}(\rho k) + \frac{\partial}{\partial x_i}(\rho k u_j) = \frac{\partial}{\partial x_j}\left[\left(\mu + \frac{\partial \varepsilon}{\sigma_k}\right)\frac{\partial \varepsilon}{\partial x_j}\right] + G_k + G_b - \rho c - Y_M + S_k, \tag{3.16}$$

and

$$\frac{\partial}{\partial t}(\rho \varepsilon) + \frac{\partial}{\partial x_j}(\rho \varepsilon u_j) = \frac{\partial}{\partial x_j}\left[\left(\mu + \frac{\mu_t}{\sigma_\varepsilon}\right)\frac{\partial \varepsilon}{\partial x_j}\right] + \rho C_1 S_\varepsilon - \rho C_2 \frac{\varepsilon^2}{k + \sqrt{\nu\varepsilon}} + C_{1\varepsilon}\frac{\varepsilon}{k}C_{3\varepsilon}G_b + S_\varepsilon, \tag{3.17}$$

where

$$C_1 = \max\left[0.43, \frac{\eta}{\eta + 5}\right], \qquad \eta = S\frac{k}{\varepsilon}, \qquad S = \sqrt{2S_{ij}S_{ij}}.$$

According to Equation (3.16) and Equation (3.17), G_k is the generation of turbulent kinetic energy due to the mean velocity gradient, G_b is the generation of turbulent kinetic energy due to buoyancy, Y_M is the contribution of the fluctuating dilation in compressible turbulence to the overall dissipation rate, and C_2 and $C_{1\varepsilon}$ are constants. Moreover, σ_k and σ_ε represent the turbulent Prandtl numbers for k and ε. S_k and S_ε are user defined source terms (Fluent Inc. 2003).

With Equation (3.13) and Equation (3.17), the turbulence model coefficients, C_μ and C_2, are given with considerations, such as rotation, separation and flow angle as follows,

$$C_\mu = \frac{1}{A_0 + A_S \dfrac{kU}{\varepsilon}}, \tag{3.18}$$

$$C_2 = \frac{\sqrt{1 - 9C_\mu{}^2\left(\dfrac{kS}{\varepsilon}\right)}}{C_0 + 6\dfrac{kS}{\varepsilon}\dfrac{k\Omega}{\varepsilon}}, \tag{3.19}$$

where

$$U = \sqrt{S_{ij}S_{ij} + \widetilde{\Omega}_{ij}\widetilde{\Omega}_{ij}}\,, \tag{3.20}$$

and

$$\widetilde{\Omega}_{ij} = \Omega_{ij} - 2\varepsilon_{ijk}\omega_k, \qquad \Omega_{ij} = \overline{\Omega}_{ij} - \varepsilon_{ijk}\omega_k, \tag{3.21}$$

where $\widetilde{\Omega}_{ij}$ is the mean rate of rotation tensor and ω_k is the angular velocity (Fluent Inc. 2003 & Shih et al. 1995). In Equation (3.18) the model constants A_0 and A_s are calculated as,

$$A_0 = 4.04, \qquad A_S = \sqrt{6}\cos\phi,$$

where

$$\phi = \frac{1}{3}\cos^{-1}\left(\sqrt{6}W\right), \qquad W = \frac{S_{ij}S_{jk}S_{ki}}{\widetilde{S}^3}, \qquad \widetilde{S} = \sqrt{S_{ij}S_{ij}}, \qquad S_{ij} = \frac{1}{2}\left(\frac{\partial u_j}{\partial x_i} + \frac{\partial u_i}{\partial x_j}\right).$$

With these equations, C_μ is a function of the mean strain and rotation rates, the angular velocity of system rotation and the turbulence fields (k and ε).

The coefficients of model constants are assumed as their standard values.

$$C_\mu = 0.09, \qquad C_{\varepsilon 1} = 1.44, \qquad C_{\varepsilon 2} = 1.92, \qquad \sigma_k = 1.0, \qquad \sigma_\varepsilon = 1.2$$

With Equation (3.16), the production of turbulent kinetic energy term, G_k, is utilised identifiably for all k-ε models, which is defined with the Boussinesq hypothesis as,

$$G_k = -\rho\overline{u_i'u_j'}\frac{\partial u_j}{\partial x_i} = \mu_t S^2, \tag{3.22}$$

where S is the modulus of the mean rate of strain tensor (Fluent Inc. 2003).

For a CFD simulation with high Mach number flow, dilation dissipation affects turbulent flows, which is normally neglected in the modelling of incompressible flows. The dilation dissipation term, Y_M, is modelled to consider the decrease in spreading rate with increasing Mach number for compressible mixing and other free shear layers, as follow,

$$Y_M = 2\rho\varepsilon M_t^2, \tag{3.23}$$

where M_t is the turbulent Mach number which is defined as,

$$M_t = \sqrt{\frac{k}{a^2}}, \tag{3.24}$$

where a is the speed of sound (i.e. $\equiv\sqrt{\gamma RT}$).

To conclude, the advantage of the Realisable k-ε turbulence model shows that it is possible to achieve good results in terms of integral values, such as drag coefficient, which are within 2-5 percent different to experimental data (Lanfrit 2005). Due to its implementation it is very stable and fast converging. Therefore, it is suited for CFD simulations allowing huge numbers of calculations in a relatively small processing time (Kucukgokoglan 2000 & Lanfrit 2005).

3.3 Valuation between Numerical Simulation and Experimental Results

CFD simulation is a useful tool to analyse model-air interactions playing with fluid in the understanding turbulent flow features. Fig. 3.14 shows that the relationship between progressing time and accuracy of 2D and 3D analyses in Fluent with viscous model ranking.

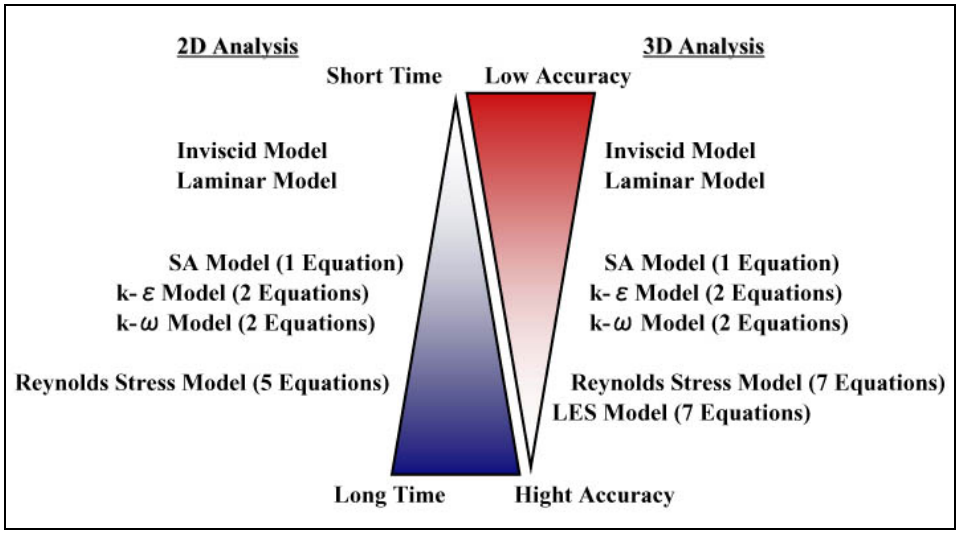

Fig. 3.14 Relationship Diagram between Processing Time and Accuracy in Fluent

In regards to CFD processing time and accuracy in Fluent, better accurate CFD results take longer processing time employing with two, five or seven equations in each turbulence model. High capable PC facilities can reduce processing time and play with higher accurate viscus model in CFD application. Therefore, balance between the processing time and accuracy is considered for CFD simulations each time.

CFD results should be evaluated how it validities comparing to physical flow data. Therefore, CFD results should be validated against wind tunnel measurements, because an experiment of the wind tunnel has the advantage of dealing with 'real' fluid and can produce global data. In this section, some validation tests between CFD simulation and wind tunnel results are applied and shown as follows.

Alinghi boat racing team (Alinghi 2005) was employed FLUENT application for flow simulation of high performance racing yachts. The engagement of the Ecole Polytechnique Fédérale de Lausanne (EPFL), as Official Science Advisor of the Alinghi Challenge for the 2003 America's cup, utilised the Reynolds-Average Navier-Stokes (RANS) equations to analyse complex flow behaviour as fluid-structure interaction with mast and sails. By calculating the pathlines, fluid activities as pressure and forces on the boat were examined

(Fig. 3.15), and with the numerical flow simulation the bulb-keel-winglet configurations were designed with the least drag. In addition, the EPFL remarked that the recent availability low-cost desktop workstations are able to perform sizable flow simulations comfortably (Cowles et al. 2002).

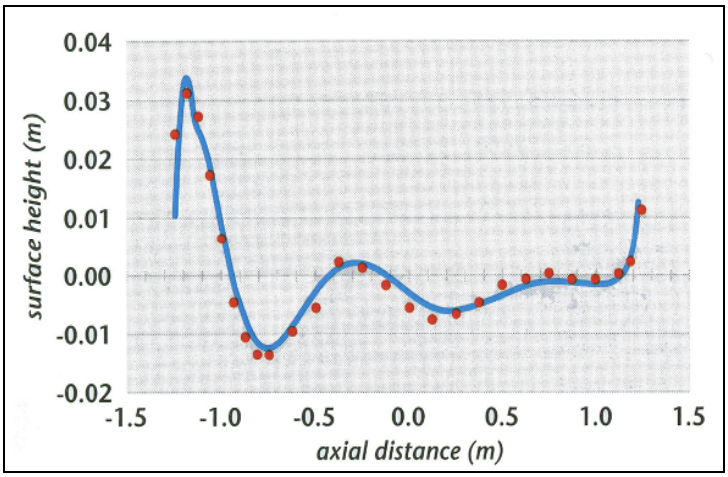

Fig. 3.15 Comparison of CFD results (Blue Line) and Experimental values (Red Circles) of the Waterline on the Surface of a 2.5 m Wigley Hull (Cowles et al. 2002)

Instituto Nacional de Tecnica Aerospacial (INTA, Spain) has participated in European aeronautical projects used FLUENT software, as the C-WAKE European project to characterise and control vortex wakes (INTA 2005). The C-WAKE project focused on estimating the optimum fluid separation between aircraft in-flight conditions and taking-off conditions on airport runway as well as improving the aircraft design for new configuration that generate reduced vortex wakes and reduction in aircraft separation. The CFD results were compared with experimental data extracted from wind tunnel tests (Fig. 3.16). With validating the CFD results used Fluent, Mr. Mongo stated that Fluent simulations have currently been run to research high lift systems that allows an increase of 15-20 percent in the aerodynamic efficiency of supersonic aircraft flying with low speed (Monge 2002)

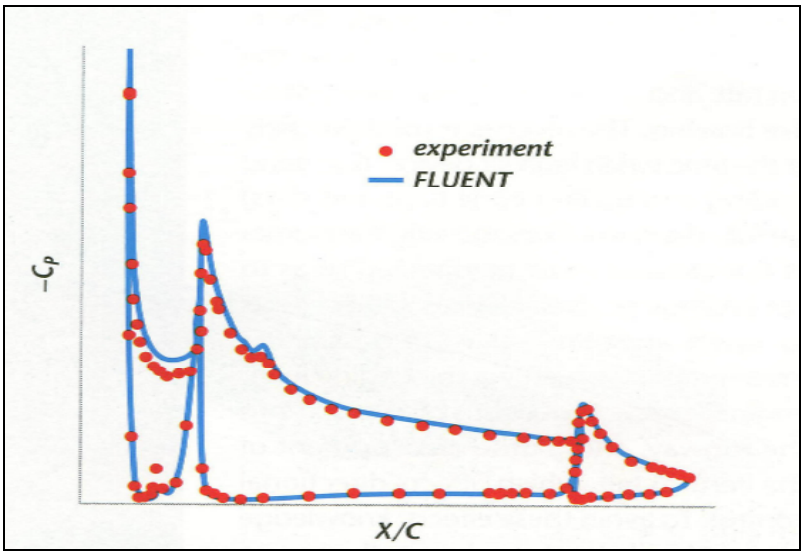

Fig. 3.16 Surface Pressure Distribution for 2D Airfoil Design with Slat plus Flap (Monge 2002)

The k-ε model was employed to solve turbulent dispersion problems (Leung et al. 2005). The case CFD study was to prove turbulent dispersion around a building, especially for a demonstration of accidental leakage of gaseous contaminant considered with the human health effects. In this project three different models, CFD statistical model, the k-ε model and experimental data, were compared by time dependency (Fig. 3.17). With the comparison in Fig. 3.17, the result of k-ε model was better than the CFD-statistical model, and its model was obtained a reasonable agreement with the measurements. Moreover, the CFD-statistical model was able to save the computational processing time approximately one third times faster than the k-ε model, but the results of the k-ε model was more reasonable (Leung et al. 2005).

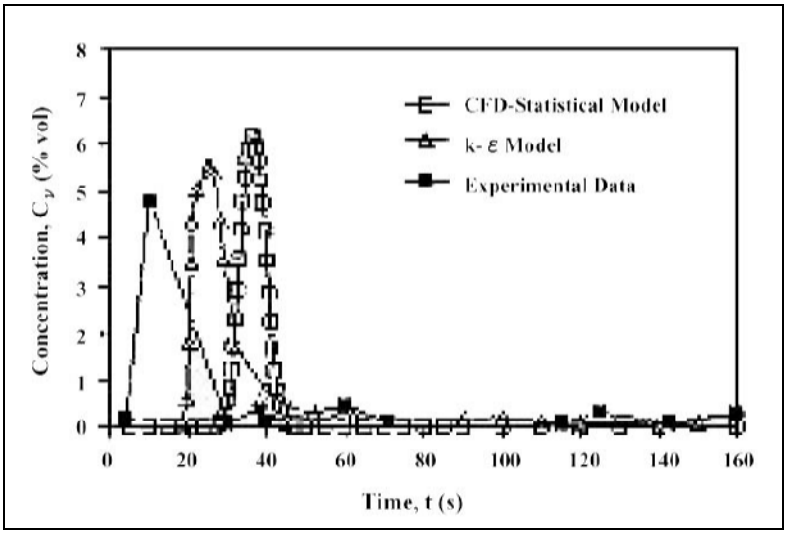

Fig. 3.17 Comparison of the k-ε Model and Experimental Data (Leung et al. 2005)

Dr. Kim (2005) agrees that the Large Eddy Simulation (LES) model is more accurate, robust, and efficient than other viscous models in Fluent. The LES of the RANS based models has been the major workhorses for industrial applications. For example, the 3D flow past a circular cylinder was demonstrated using LES model at a sub-critical Reynolds number of 1.4 $\times 10^5$. The summary of comparison between computational simulation and experimental results are shown in Table 4.1 (Kim 2005 & Kim et al. 2005). With the results, the LES model was able to computed being very close to the experimental results. Moreover, the LES model has a good agreement with turbulence flows, and it reveals the air flow features by animation and visualisation on Fluent.

Table 3.1 Comparison of Fluent's LES Model and Experiment Results (Kim 2005)

	CFD Results	Experiment Results	
	LES (Fluent)	Lower Value	Higher Value
Mean Drag Coefficient	1.16	1.15	1.35
Fluctuating Drag Coefficient	0.15	0.15	0.18
Fluctuating Lift Coefficient	0.59	0.50	0.60
Mean Base Pressure Coefficient	1.20	1.05	1.21
Strouhal Number	0.204	0.18	0.21

To conclude regarding the CFD simulation using FLUENT software, the LES model was informed as the best solution to simulate turbulent flows. However, the PC capacity requires being higher if a heavy calculation predicts for CFD simulation. With consideration of PC environment, the two equations turbulence models as k-ε and k-ω models may be substituted to run CFD simulation with reasonably well performance in Fluent. In addition, for external turbulent studies the k-ε model is feasible to demonstrate flow activities, because the model is possible to treat near wall region.

Chapter 4 Results and Discussions

This research has focussed on the comparative study between the A380 prototype and a BWB configuration has been investigated in aerodynamic performance and aircraft capability. This has included the Airbus A380 aircraft analysed in flight performance compared to the BWB design. The BWB model was designed based on Raymer's methodologies (Raymer 1999) and the existing equations (Chapter 2). All of the BWB design requirements have been considered and achieved, meeting the safety requirements of ICAO and FAA regulations. In particular, the BWB configuration has been carefully designed to ensure a less than 80 m wingspan to meet the current airport compatibility issues, and to also accommodate 555 passengers with a three class layout.

4.1 Aerodynamic Analysis of the A380 Prototype

Aerodynamic performances of the A380 were investigated using traditional equations (Chapter 2) and CAE softwares. The specifications of the A380 were referenced in Table 1.1 based on the 'A380 Facility Planning Manual Maintenance Facility Planning MFP' (AIRBUS S.A.S 2004). The A380 aircraft was simply designed using CATIA V5, and then this model was analysed in aerodynamic performance in FLUENT CFD code.

4.1.1 Airbus A380 Modelling

In this research the first A380 model was design on AutoCAD 2004 to analyse aerodynamic performances (Fig. 4.1). However, for CFD analysis the data extensions of AutoCAD 2004 are currently no longer available. Therefore, AutoCAD 2004 was utilised to only calculate a dimension for configuration arrangements in this research. According to utilities of AutoCAD 2004, the measurement features are superior, but the other features are not as user friendly as CATIA V5 or SolidWorks to create a 3D geometry, because a design plane and a User Coordinate System (UCS) must be always

specified to design a 3D geometry in AutoCAD environment saving as IGS (IGES) and STEP extensions.

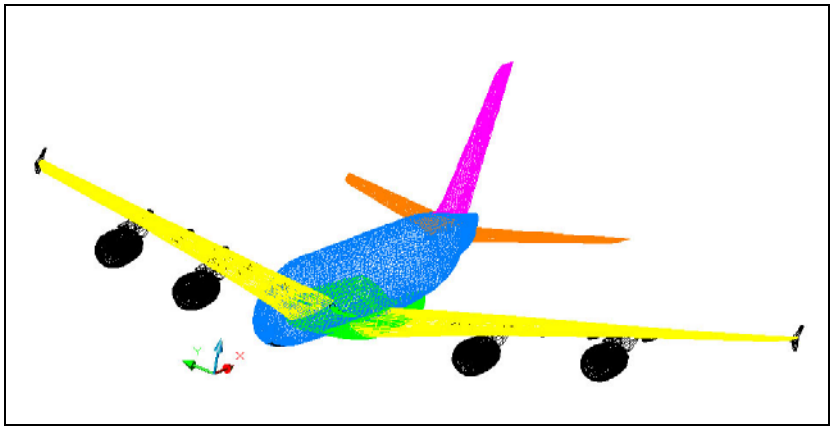

Fig. 4.1 Airbus A380 Design Using AutoCAD

Fig. 4.2 shows the A380 model which was designed on CATIA V5. The Modelling features of CATIA V5 performance well to create a 3D geometry, and the CATIA model can also directly export data file onto CFD environment.

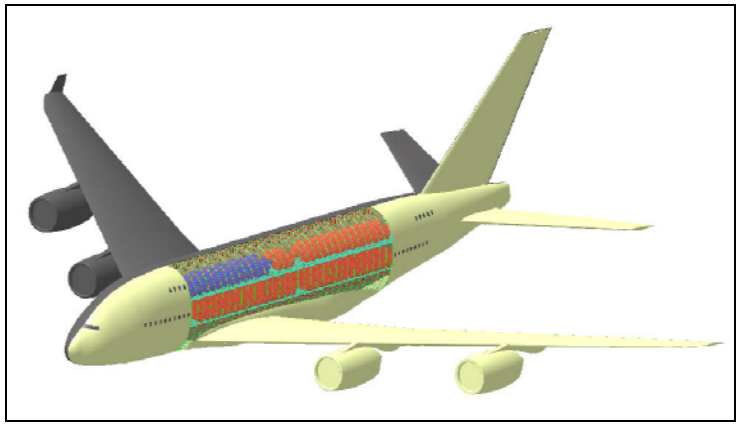

Fig. 4.2 Airbus A380 CATIA Model

In addition, when comparing software performances between AutoCAD 2004 and CATIA V5, CATIA V5 can be used conveniently to design geometry and significantly using the CATIA V5 can save modelling time. For example, the A380 CATIA model (Fig. 4.2) was designed in 5 days but the A380 AutoCAD design (Fig. 4.1) took 30 days using the same data of the A380 specifications.

4.1.2 Aerodynamic Analysis of the A380 Configuration

Based on the Bernoulli's equations (Equation (2.11) - Equation (2.19)) and Table 1.1, the L/D ratio was calculated in cruise as follows.

When an aircraft is in level flight, the weight is equal to the generated lift of the aircraft, and the aircraft efficiency of the A380 was assumed to be 0.95, and the parasite drag ratio was chosen as 0.025 (Amano 2001). The L/D ratio was assumed using Equation (2.19) as:

$$\frac{L}{D} = \frac{\sqrt{\pi}}{2}\frac{b\sqrt{e}}{\sqrt{C_{D_P}S}} = \frac{\sqrt{\pi}}{2}\frac{79.8\sqrt{0.95}}{\sqrt{0.025\times 845}} = 14.594\,.$$

However, the L/D ratio of A380 was chosen as 13.74 of maximum L/D ratio (Buescher 2001), because this assumption took into consideration other aerodynamic features of theA380, such as fuselage and tails.

The A380 CATIA model aerodynamic features (Fig. 4.2) were simulated and computed in Fluent. In regards to flight conditions, typical flight conditions of conventional aircraft and the flight mission profile of the A380 were referred to, such as flying at 11 km altitude at Mach number 0.85. With these parameters using Fluent, the aerodynamic features of the A380 are shown in Fig. 4.3 with contours of static pressure.

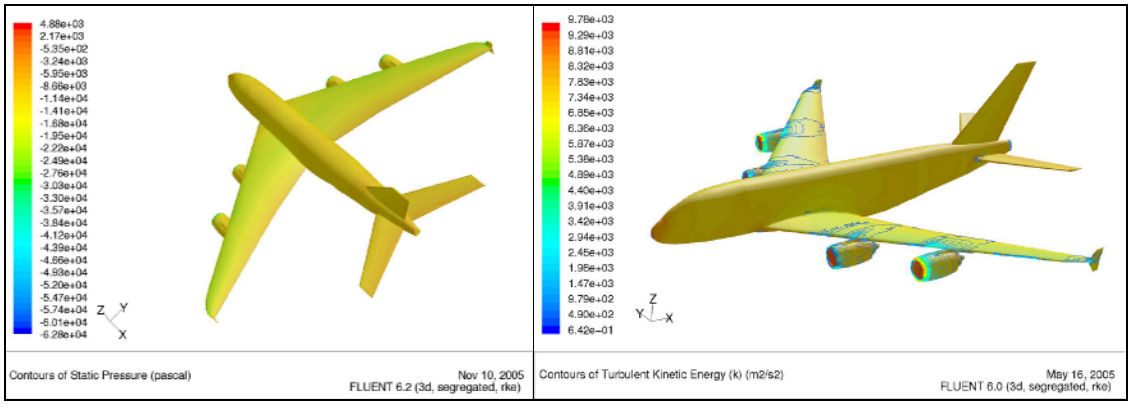

Fig. 4.3 Contours of Static Pressure of the A380 (Right: With Contours of Turbulent Kinetic Energy)

According to the aerodynamic specifications of the A380 CATIA model in Table 4.1, the L/D value of CFD results were different from the published results of 13.74 of the L/D ratio (Buescher 2001). This reason for this is that there is no airfoil data for the A380 to design of the wing section, because it has not been presented by the company as it is a confidential issue at Airbus.

Table 4.1 CFD Results of the A380 CATIA Model

	Momentum Coefficient C_M	**Lift Coefficient C_L**	**Drag Coefficient C_D**	**L/D**
Airbus A380 CATIA Model	0.99070	0.28764	0.05351	**5.38**

The C_L and C_D of the A380 CATIA model has not displayed the same aerodynamic performance of the actual A380, because the airfoil sections of the A380 CATIA model were not designed as equal to the A380 airliner. Therefore, the C_L value of the A380 CATIA model is not compatible, but its C_D may be substituted for aerodynamic parameter of the actual A380 to compare the aerodynamic performance of BWB design, because the wetted area of the A380 CATIA model is similar to the actual A380. In addition, the Boeing B747-400 (the current mainstream airliner) was referred when analysing the C_D value of the A380 CATIA model. The C_D of the B747 is 0.0255 in flight (Makino 1984), and the fuselage space of the A380 is approximately 1.5 times larger than the B747 (AirlinesGate 2000 & Stößel 2005) and the C_D value of aircraft is directly related to its wetted area in flight (Chapter 2 Section 2.5.4). With the aerodynamic parameters between the actual A380 and its CATIA model, the C_D value of the actual A380 may assume the value of its CATIA model.

4.2 BWB Configuration Design for Conventional Aircraft

A BWB configuration has been researched using CAE softwares based on typical aircraft design methodologies (Fig. 2.2) in this design project. With the BWB design processes several advantages and disadvantages of BWB concept design have been encountered, and design methodologies for BWB aircraft were shown in this section.

4.2.1 Monotonous Parameters of BWB Configuration Design

The priority considerations of a BWB configuration design were that 555 passengers can accommodated on while achieving flight comfort and meeting safety standards with a 66.4 tonnes payload, 8,000 nautical miles (15,000 km) range and the cruising speed of Mach 0.85, which are the same as the A380 specifications.

4.2.2 Initial Sketch of BWB Configuration

The initial sketch of the BWB model was illustrated with four components, such as wing with winglet, fuselage, engines and tails, considered within the limited of the wing span length of less than 80 m. The preliminary hand draft was a rough indication of what the design may look like for a BWB configuration concept. Based on the initial configuration sketch, the first-order sizing has provided the information needed to develop an initial design that takes into consideration with an important arrangement details including passenger compartments, engines and tails. Before moving onto a sizing phase, the BWB model has included arranged cabin layout, engines' location and tails, and the sweep angle of wing and wing edge configuration required for aerodynamic features. At the same time, airfoil selections were developed with consideration of aerodynamic performance using XFOIL and FLUENT of 2D CFD code to achieve a higher L/D ratio during flight.

4.2.3 BWB Cabin Layout

The priority issue of this BWB design was to accommodate 555 passengers while achieving flight safety and passenger comfort during flight operation. To provide the cabin space for 555 passengers, wide cabin layout (single cabin layout) and double cabin layout were styles considered for the passengers' accommodation in the first sizing phase. However, a single cabin layout was chosen because of the aerodynamic efficiency (i.e. less parasite drag since the less configuration thickness).

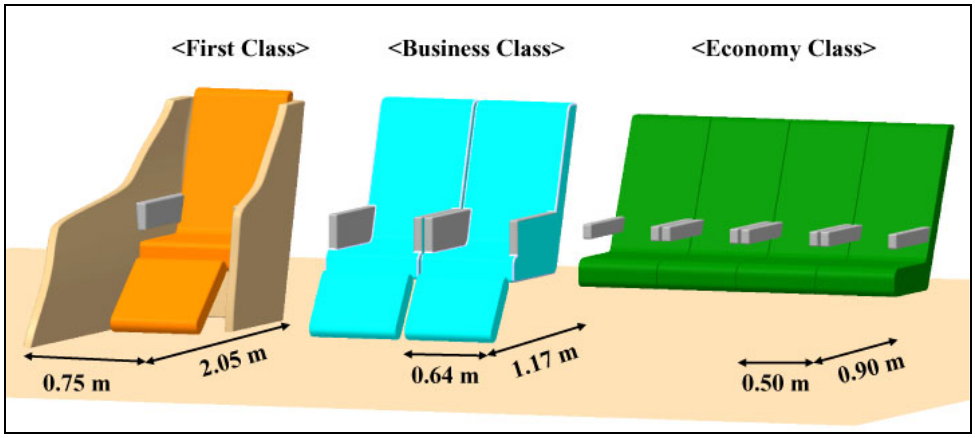

Fig. 4.4 Comparison of Three Class Seat Size

Fig. 4.4 shows seat design specifications according to travel classes of the BWB design. Each class seat was designed larger than the standard compartment, and these dimensions were similar to the A380 passenger allowance (Table 2.6). These seats of the BWB design were designed with longer seat pitch for passenger comfort during flight. Based on the BWB compartment, cabin layout was designed with three travel class arrangements with aisles and to meet evacuation requirements allowing all passengers to evacuate through only half the available exits in less than 90 seconds (FAA 2005a & National Transportation Safety 2000). For passenger evacuation procedure, the main aisles of the BWB design have been designed with approximately 1.6 m width, which is three times wider than typical conventional aircraft (Table 2.6). The reason for the wider aisle arrangement is that the BWB configuration consists of several passenger modules on one floor, so the main aisles are wide enough for the evacuating passengers crawling from each module in evacuation. The first plane figure and cabin layout of the BWB model were shown in Fig. 4.5 and Fig. 4.6.

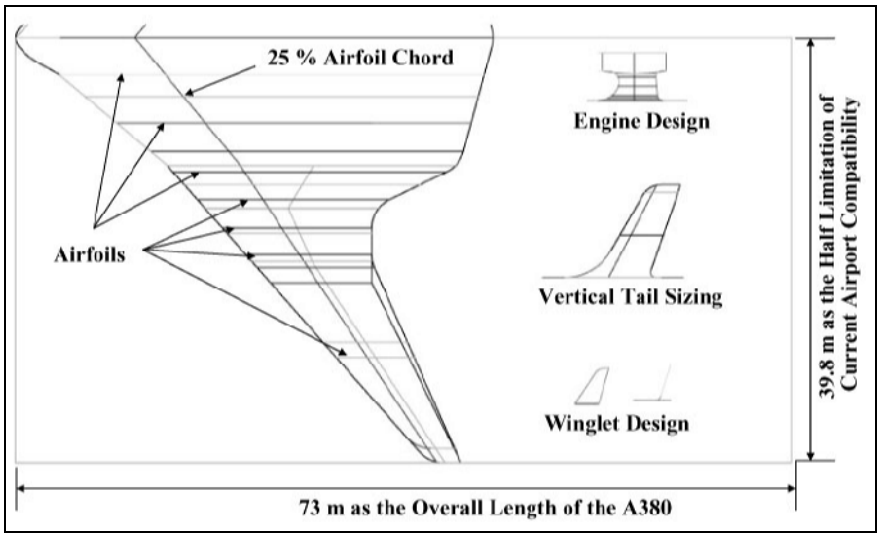

Fig. 4.5 2D Initial BWB Layout Planning

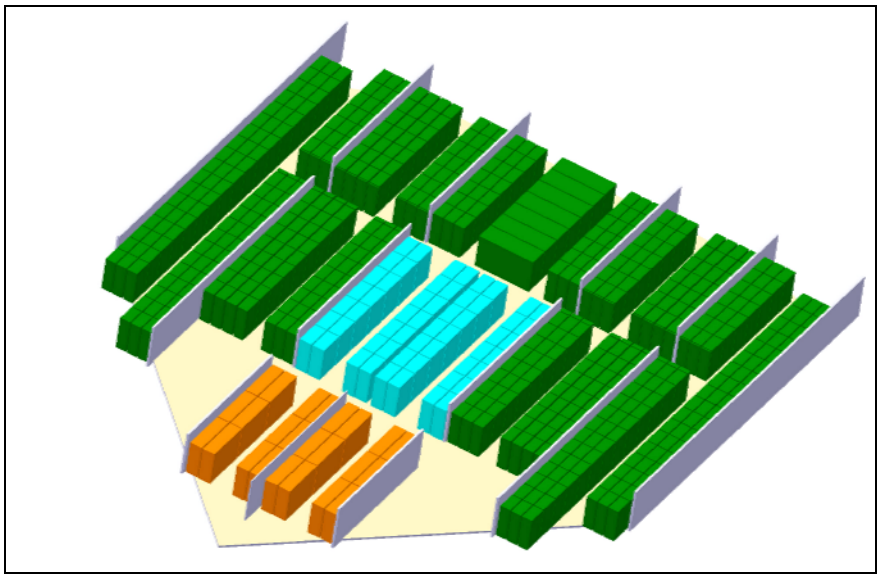

Fig. 4.6 Single Cabin Layout Sizing
(Orange: First Class, Blue: Business Class, Green: Economy Class)

The BWB 2D layout (Fig. 4.5) includes the passenger compartment arrangement. For an accommodation of 555 passengers with the three class seat arrangements, a cabin area of the BWB design needed at least 398 m^2 including aisles area (Table 4.2).

Table 4.2 Cabin Layout Parameters of BWB Design

	First Class	Business Class	Economy Class	Aisle
Area (m^2)	33.82	71.84	196.65	95.00

With these considerations, the cabin layout was optimised as within Fig. 4.7. This cabin layout was arranged to include 2 pilots, 24 first class seats (2 extra seats), 98 business class seats (2 extra seats) and 439 economy class seats (2 extra seats), and 19 toilets (29 passengers/toilet) and 6 doors (2 emergency exits). Moreover, the cabin arrangement of the BWB configuration as a flying wing concept was directly influenced the external shape with factors, such as airfoil thickness and sweep angle of the wing, which will be described in the further section.

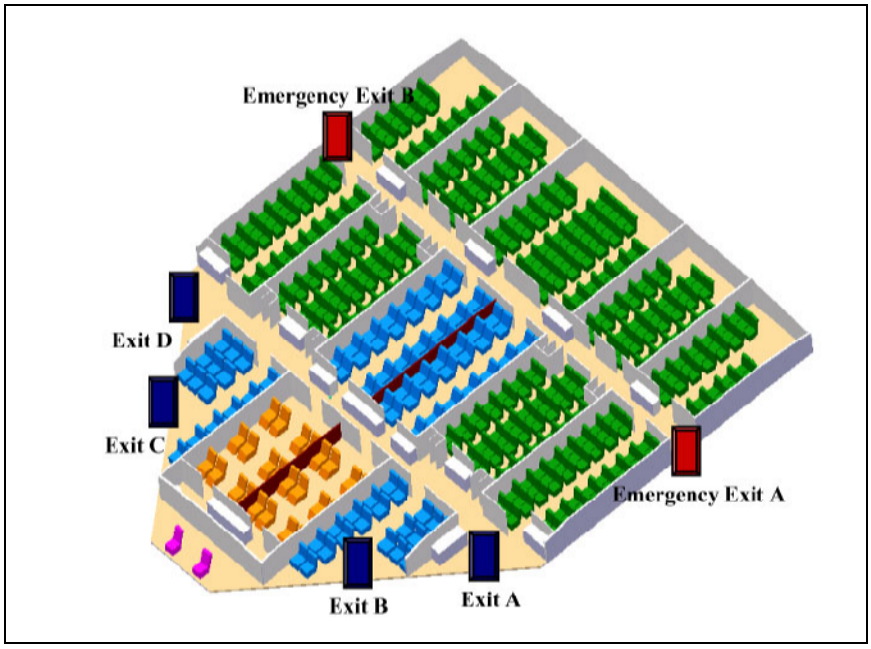

Fig. 4.7 Optimised Three Class Cabin Arrangement of BWB Model
(Purple: Cockpit (2 Pilots), Orange: First Class, Blue: Business Class, Green: Economy Class)

In regards to the evacuation procedure for BWB configuration with FAA regulation (FAA 2005a & National Transportation Safety 2000), Fig. 4.8 shows one of predicted evacuation procedures of the BWB configuration where only half the exits are available. In Fig. 4.8 the passenger, who is sitting at the location of the smile icon in the far distance from the exit, is approximately 30 m from the emergency exit A (Fig. 4.7), and will take 21 seconds to evacuate the aircraft without passenger hold-ups. According to passenger walking speed, an average walking speed of an adult may be

assumed to be 1.43 m/s (eHow 2005). However, in actual evacuation, passenger hold-ups will occur and passengers' walking speed will be slower than the average speed. Therefore, with considering these cases, the passenger who sits at the location of the smile mark will likely take up to 80 seconds to reach the evacuation point (Appendix 3).

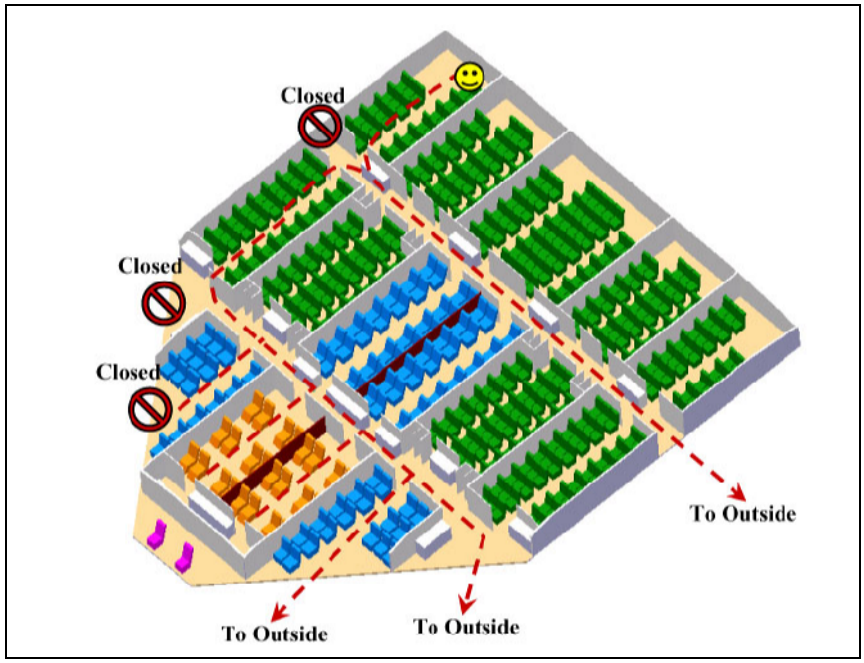

Fig. 4.8 Prediction of Passenger Evacuation of BWB Model

With these cabin design requirements of the BWB model, the 2D layout was optimised as in Fig. 4.9. Compared to the initial sizing (Fig. 4.5) and the optimised layout (Fig. 4.9) of BWB design, the area of cabin was reduced and the amenity equipment and facilities also taken into consideration. The specifications of the optimised BWB cabin layout are shown in Fig. 4.10. According to Fig. 4.9, the top half plane design is the optimised 2D BWB layout and the bottom half design is the initial BWB design. With the optimisation of the cabin arrangement, the body length of the optimised BWB body design became 1 m smaller than the initial design.

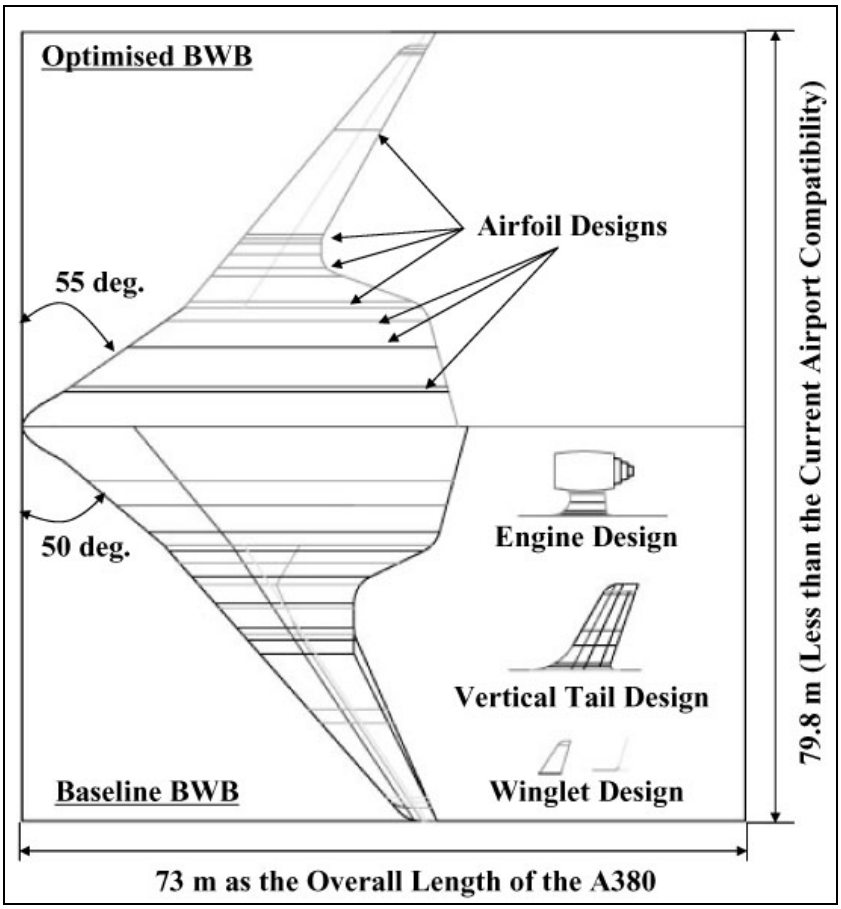

Fig. 4.9 Optimised 2D BWB Layout (Top) and Baseline 2D Profile (Bottom)

Fig. 4.10 Specifications of the BWB Cabin Design

4.2.4 Swept Wing Consideration of the BWB Design

At transonic speeds the sweep wing reduces drag, and because the phenomenon of shock wave is controlled (i.e. the airflow above the wing will be supersonic and this supersonic flow has to be shocked to subsonic flow before the trailing edge). Moreover, this design produces a lower profile drag and a lower root bending momentum. In regards to a swept wing of a conventional airliner, an average angle of the swept wing is around 30 (Raymer 1999). The Airbus A380 has been designed with a swept wing with 33.5 degrees of the swept angle (Table 1.1). For this BWB design, the swept wing has been calculated according to aircraft momentum and the centre of gravity, resulting in the swept angle of the wing set at 33.5 degrees, as the same as the A380 specification.

4.2.5 L/D Estimation of the BWB Configuration

The relationship between L/D and wetted aspect ratio based on Fig. 2.4, Fig. 4.11 shows a possible L/D assumption of BWB concept configuration (Blue Circle Area: L/D ratio = 20-30 and Wetted Aspect ratio = 2.5-4.5). This assumption was drawn from research in the field, suggesting that such as the minimum drag coefficient of BWB concept configuration of XB-35 is approximately 50 percent lower than from the mainstream conventional aircraft of the B747 (Chapter 2).

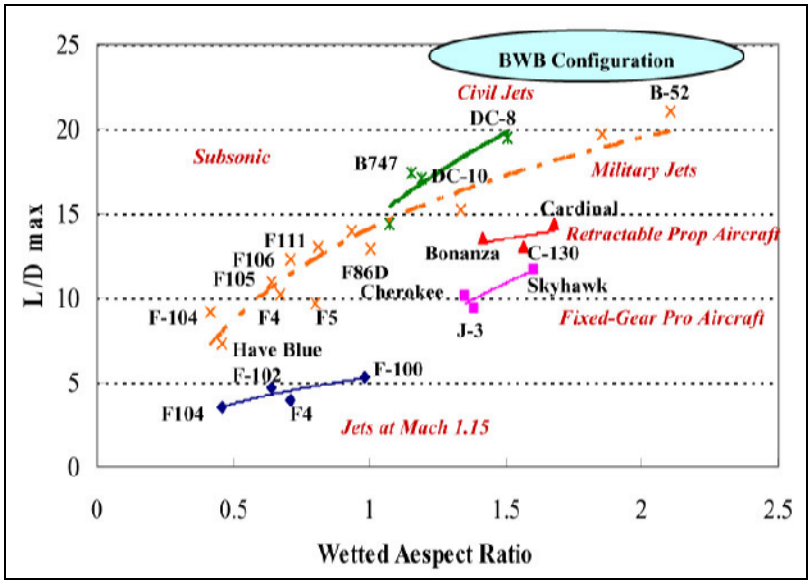

Fig. 4.11 L/D Trends with Wetted Aspect Ratio

In the initial BWB design phase, 30 of the maximum and 20 of the minimum L/D assumptions were utilised to estimate component weights of the BWB configuration along with the NASA and traditional methodologies based on the wetted aspect ratio.

4.2.6 Airfoil Selection

In the conceptual airfoil design, an existing airfoil series was referred to, and the XFOIL code, which is an interactive program for the design and analysis of subsonic isolated airfoils (Chapter 1 Section 1.5), was utilised for 2D airfoil selection. In this research, NACA (Trapp et al. 2005), H_Quabeck and Eppler airfoil series were analysed for the BWB wing design. The airfoil selection process was focused on the airfoil component achieving higher L/D ratio in level flight within the design requirements (i.e. cabin space for 555 passengers and 66.4 tonnes payload).

An airfoil which can achieve approximately 0.4 of lift coefficient with zero angle of attack (in level flight) has been set for the airfoil selection of BWB configuration in 2D design phase (Chapter 2 Section 2.6.1). Fig. 4.12 and Fig. 4.13 show the comparison of 4 different airfoil series using XFOIL program.

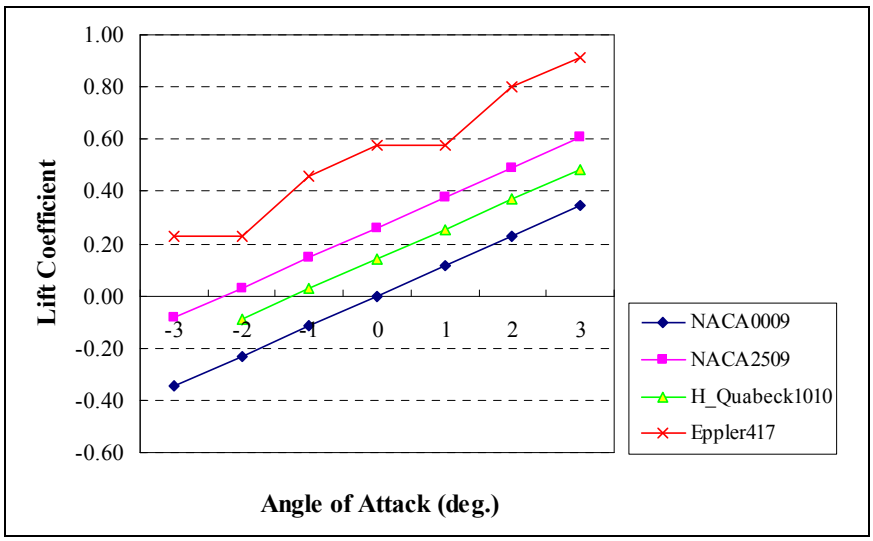

Fig. 4.12 Comparison of Lift Coefficient Using XFOIL (M = 0.85, Re = 2.83×10^8)

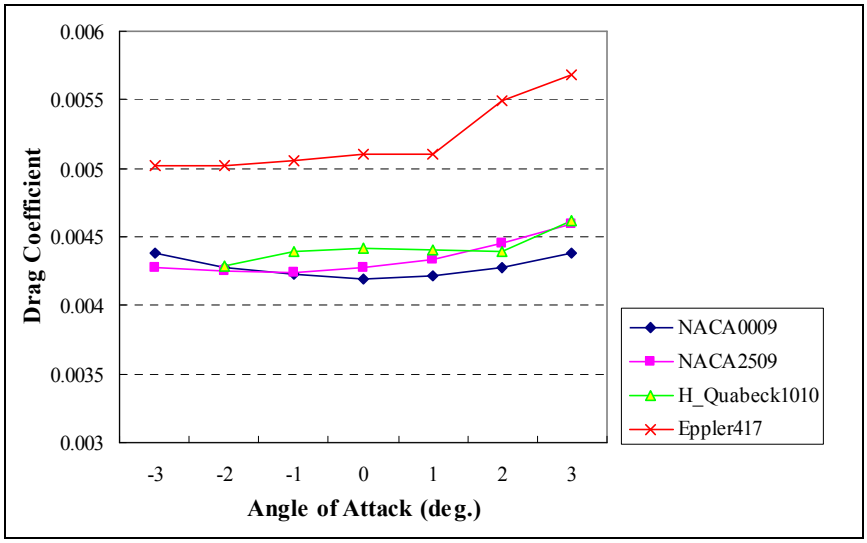

Fig. 4.13 Comparison of Drag Coefficient Using XFOIL (M = 0.85, Re = 2.83×10^8)

First of all, the NACA series was utilised to analyse the aerodynamic features for the baseline airfoil selection of the BWB design, as well as H_Quabeck and Eppler airfoil series have analysed for the wing section. The results of the NACA airfoil series, and H_Quabeck and Eppler airfoil series were shown in Fig. 4.13 to compare looking at aerodynamic features for a wing design of BWB configuration. In the H_Quabeck airfoil series, Dr. H. Quabeck in Germany has designed airfoil profiles (normally known as H_Quabeck or HQ profile) for sailplanes and winglet (Quabeck 2005). The Eppler airfoil series are designed by Professor R. Eppler for subsonic aircraft (Hepperle 2005).

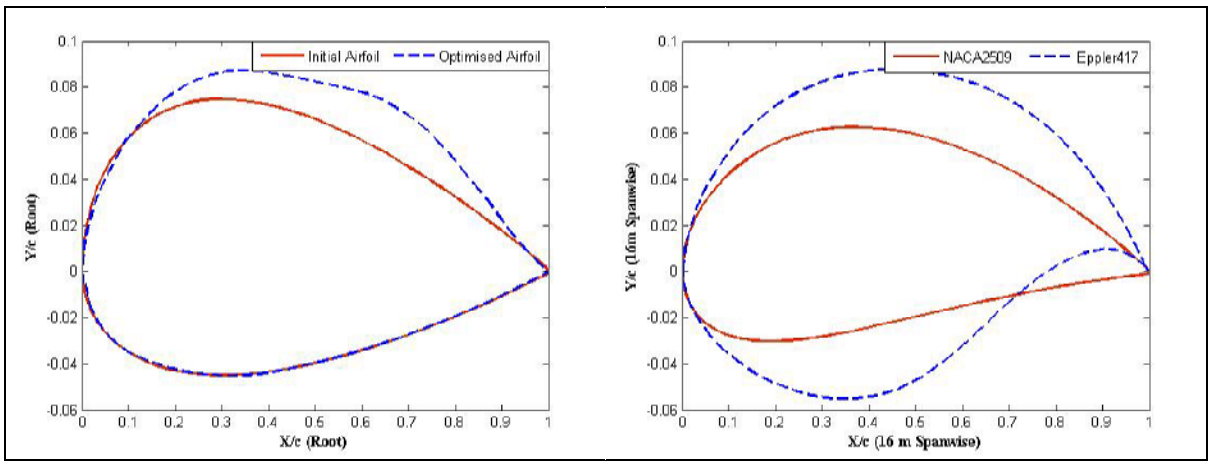

Fig. 4.14 Airfoil Shape Modification of the Main Sections for the BWB
(Left: Root Section, Right: 16 m Spanwise Section)

In regards to an airfoil selection for the root section of the BWB (Fig. 4.14 Left), the initial airfoil design was referred to as NACA0015 and NACA0009. The thickness of the initial airfoil was enough for the cabin compartment at the location of maximum thickness. However, for the whole cabin compartment, the initial airfoil was not feasible to achieve passengers' comfort. The initial airfoil was redesigned with consideration of cabin space, as well as improving aerodynamic performance. Also, the location of the maximum thickness was moved to the airfoil chord, approximately 15 percent backward. An airfoil at the 16 m spanwise of the BWB (Fig. 4.14 Right), NACA2509 was initially chosen and analysed according to the aerodynamic features. To improve aerodynamic features on the wing in flight, Eppler417 was selected for the wing of the BWB configuration.

Aerodynamic features of the selected airfoils were calculated using Fluent 2D solver (Fig. 4.15 and Fig. 4.16) with the actual scale of the BWB configuration.

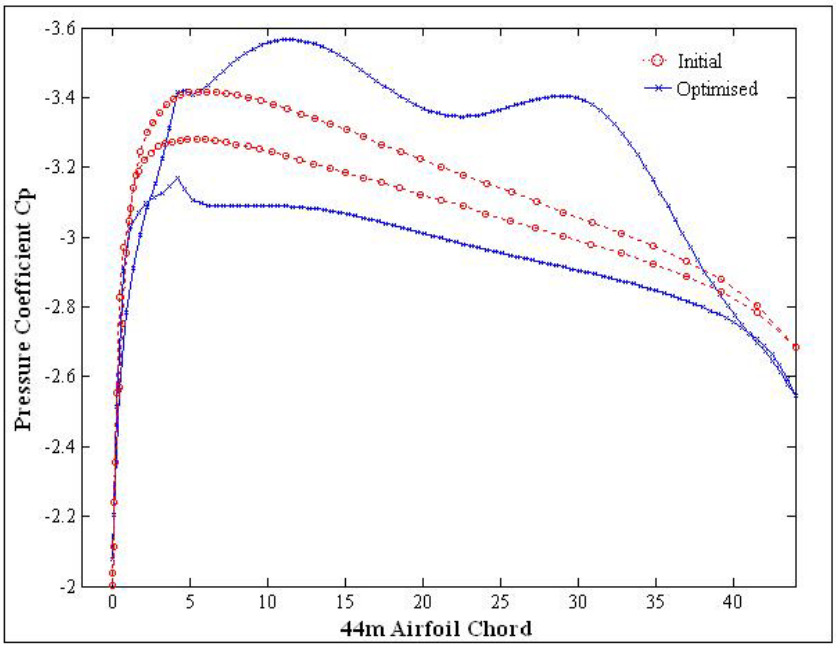

Fig. 4.15 Comparison of the Wing Surface Pressure Coefficient Distribution at the Root Section ($M = 0.85$, $Re = 2.83 \times 10^8$)

In Fig. 4.16, the comparison of pressure contour between the initial and the optimised airfoils at the central wing section are shown. These pressure distributions of Fig. 4.16 are presented in Fig. 4.15.

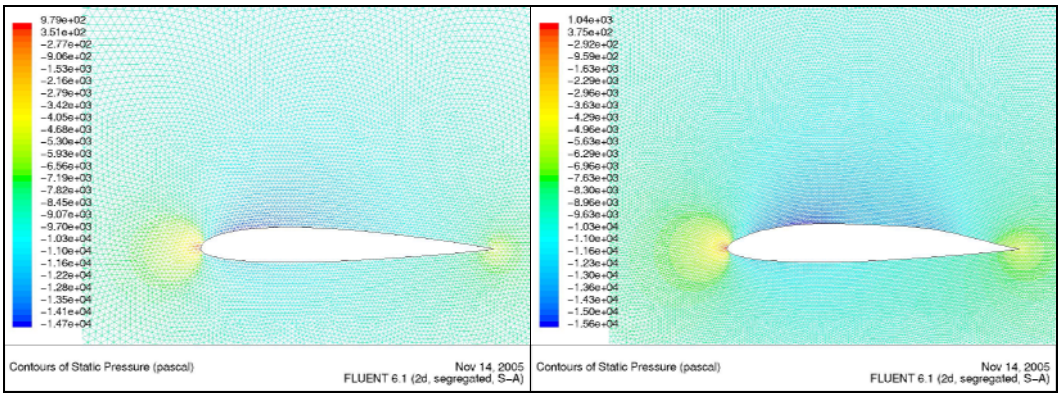

Fig. 4.16 Contours of Static Pressure of the Central Wing Section
(Left: Initial Airfoil, Right: Optimised Airfoil)

In Fig. 4.17 the location of minimum pressure coefficient of the optimised airfoil was moved onto the airfoil chord of 10 m, and this feature led to move the centre of gravity of the whole BWB configuration backward.

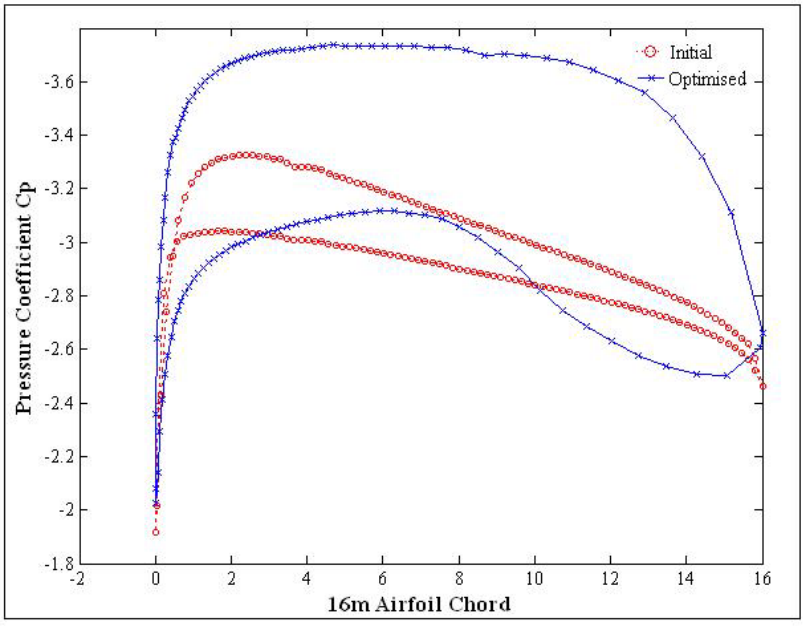

Fig. 4.17 Comparison of the Wing Surface Pressure Coefficient Distribution at the 16 m Spanwise
($M = 0.85$, $Re = 1.03 \times 10^8$)

In Fig. 4.18, the comparison of pressure contour between the baseline and Eppler417 airfoils at the 16 m spanwise was shown. These pressure distributions of Fig. 4.18 show in Fig. 4.17.

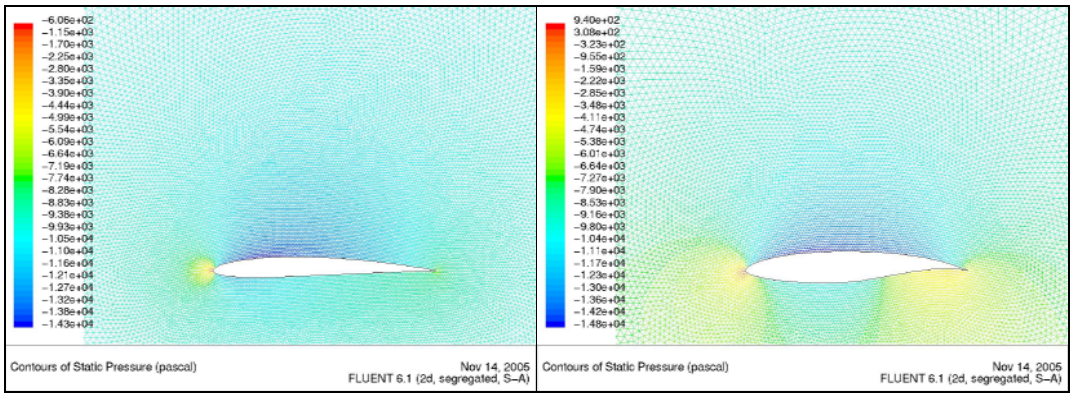

Fig. 4.18 Contours of Static Pressure of the 16 m Spanwise Wing Section
(Left: NACA2509, Right: Eppler417)

The baseline airfoils (NACA0015+0009 and NACA2509) changed to improve the aerodynamics and the selected airfoils (Optimised and Eppler417) generated a higher L/D in cruise in Table 4.3, as well as higher momentum coefficient on 25 percent of airfoil chord.

Table 4.3 CFD Results of Four Selected Airfoils

Airfoil	**Momentum Coefficient C_M**	**Lift Coefficient C_L**	**Drag Coefficient C_D**	**L/D**
NACA0015+0009	0.72080	0.04785	0.0021188	22.58
Optimised	2.38030	0.22297	0.0067673	32.95
NACA2509	0.96943	0.24103	0.0069122	34.87
Eppler417	2.62730	0.56871	0.0097022	58.62

4.2.7 Component Weights Estimation of the BWB Configuration

After deciding on a BWB configuration profile with assumption made of the aerodynamic features, the next phase was to analyse and estimate component weights of the BWB configuration.

With the typical transport trends (Raymer 1999) and the A380 specifications, a T/W of the BWB design was estimated to be 0.23, which is lower than the typical aircraft trend (Table 2.4: T/W = 0.25-0.4) and it is the same as the A380 performance (Table 1.1: 0.23 is the average of the T/W ratio of the A380).

For weight estimations of wing, tails and propulsion, weight trends of aircraft components were analysed and obtained from relationships based on existing aircraft. The BWB configuration design also includes the current aircraft technology assembly in each part, such as rib, stringer and spar cap with skin for wing structure. With Equation (2.25) and the aircraft database (AIRLINERS.NET 2005), an inclination of wing weight was estimated as Fig. 4.19 depending on the wing area. The equation for the wing weight estimation was defined as,

$$W_{wing} = 3.8297 \times S_{wing}^{1.0156}. \tag{4.1}$$

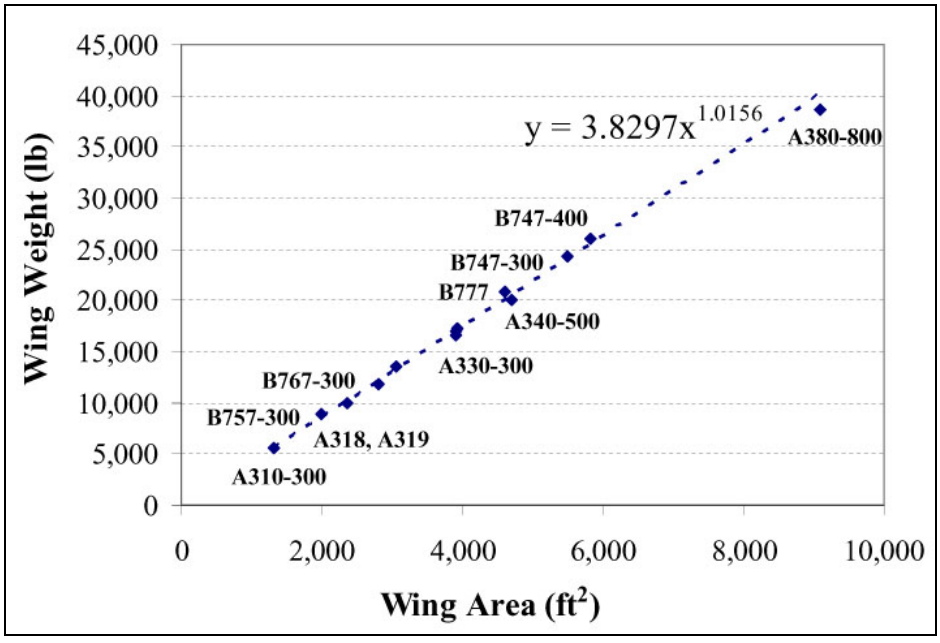

Fig. 4.19 Comparative Wing Weight Trends

For vertical tails of the BWB configuration, the design of Boeing B737-800 (Boeing Company 2005b) was referred to estimate a tail weight. With Equation (2.26), the tail weight was calculated with the

vertical wing area of 294.76 ft^2, and the ultimate load factor was assumed to be 4.0, with the span length of 26.25 ft, and the TOGW of 174,200 lbs, and the main wing area as 1,344 ft^2, the mean chord as 13.12 ft and the swept angle at 25 percent chord at 30 degrees (AIRLINERS.NET 2005 & Boeing Company 2005b) as,

$$W_{vert} = 4.19 \times S_{vert} + 2.4 \times 10^{-5} \frac{N_{ult} b_{vert}{}^3 \left(8 + 0.44 \frac{W_{takeoff}}{S_{gw}} \right)}{\left(\frac{t}{c} \right)_{avg} \cos^2 \Lambda_{ea}}$$

$$= 4.19 \times 294.76 + 2.4 \times 10^{-5} \frac{4.0 \times 26.25^3 \left(8.0 + 0.44 \frac{174{,}200}{1{,}344} \right)}{14.4 \times 0.8866^2}$$

$$= 779.44 \quad lbs \quad \left(= 353.49 \quad kg \right).$$

The vertical tail weight was recalculated with the vertical fin, and the total weight of the vertical tail estimated to be 565.58 kg (1,247.11 lbs). For the BWB configuration, two tails were installed and this weight was assumed to be 1,131.17 kg (2,494.23 lbs).

Fig. 4.20 shows total engine weight (Red Line) and dry weight (Blue Line) estimations between engine thrust and weight. With Equation (2.29), the weight of propulsion systems was estimated including the nacelle and pylon as 1.6 times heavier than the dry engine weight. With the existing engines (Bluefox9 2005), the weight of propulsion system was assumed as,

$$W_{deng} = 0.3114 \times T^{0.9433}, \tag{4.2}$$

since Equation (2.29) the weight of propulsion system was summarised as,

$$W_{pro} = 1.6 \times W_{deng} = 0.4982 \times T^{0.9433}. \tag{4.3}$$

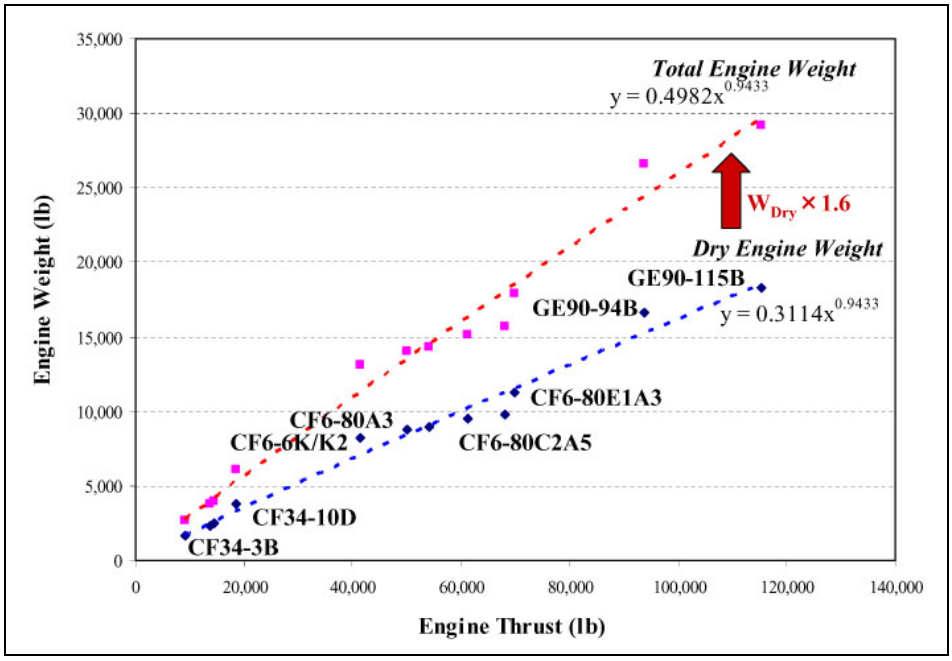

Fig. 4.20 Engine Weight Estimation (Red: Total Engine Weight, Blue: Dry Engine Weight)

Several component weights of BWB configuration were estimated for international operation and with 555 passengers, as Table 4.4 based on the existing methodologies (Chapter 2 Section 2.7.8).

Table 4.4 Component Weight Estimations of BWB Design

	Weight	
Component Name	**kg**	**lb**
Instruments & Navigational Equipment	544.22	1,200.00
Hydraulics & Pneumatics	4,997.56	11,019.61
Electronics	1,004.54	2,215.00
Furnishings	25,572.79	56,388.00
Air Conditioning & Anti-Ice	3,775.51	8,325.00
Operating Items Less Crew	7,789.57	17,176.00
Flight Crew and Attendants	1,301.59	2,870.00
Payload (Passenger Baggage)	6,575.96	14,500.00
APU	1,761.90	3,885.00

To estimate an overall weight of the BWB configuration, a SFC of the BWB configuration was referred to Trent 900 (Appendix 2) and the SFC was defined as 0.557 lb/hr/lb ($=1.547\times10^{-4}$ s^{-1}) (Purdue School of Aeronautics and Astronautics 2005). When compared to several existing aircraft

engines (Bluefox9 2005), the SFC of Trent 900 is more effective with higher thrust performance.

For engine number of the BWB configuration model, a three engines configuration was chosen. Sine the equation of total engine weight estimation in Fig. 4.20, the three engines configuration was feasible for the BWB design as installed on the aft upper body, with the weight estimation of three engines configuration approximately 2 percent lighter than the four engines model (When the engine requirement is 290,000 lbs overall thrust; 1. the weight of three engines configuration was estimated as 25,120 lbs thrust per engine, 2. the weight of four engines model was assumed to be 19,150 lbs thrust per engine).

With the equations (Equation (2.24)-Equation (2.40)), the overall weight of the BWB configuration was estimated. In this weight estimation phase, overall weight was changed depending on the engine performance. Therefore, a relationship between engine thrust requirement and TOGW (Fig. 4.21) was considered with the traditional equations. When estimating component weights of aircraft, L/D of aerodynamic features is a significant parameter and 21.43 of the L/D ratio was utilised, which was a CFD result of the final optimised BWB model calculated by Fluent.

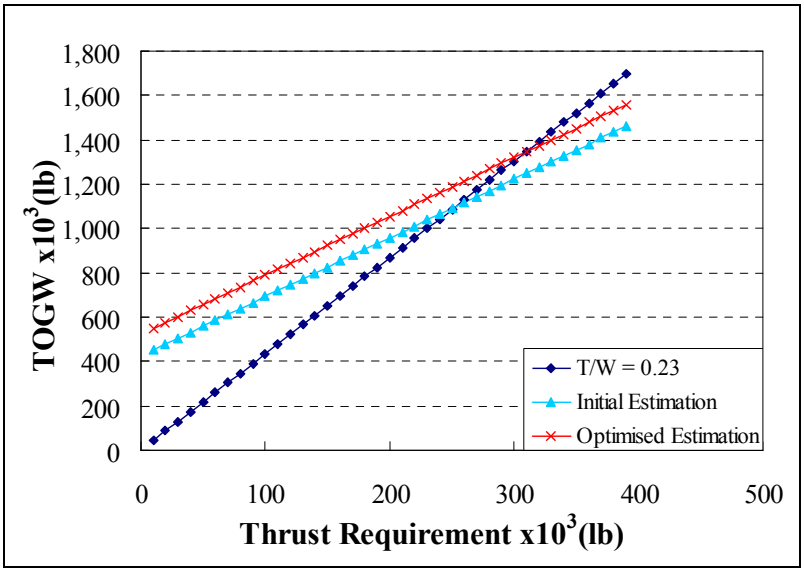

Fig. 4.21 Thrust Requirement vs. TOGW Diagram

In Fig. 4.21, these lines lead to a cross section based on 0.23 of the T/W with TOGW of aircraft in cruise. With the cross point of the T/W and the optimised estimation, the minimum configuration weight of the BWB design was estimated to be 236,193.01 kg (520,805.58 lbs) excluding the fuel weight and the weight of the propulsion system. With the traditional equations, the equation of the optimised trend based on engine thrust requirement and TOGW is described as,

$$\begin{aligned} W_{takeoff} &= W_{const.} + 0.04 \times W_{takeoff} + W_{pro} + W_{fuel} \\ &= W_{const.} + 0.04 \times W_{takeoff} + W_{pro} + 1.06 \times W_{fuel} \\ &= 520{,}805.58 + 0.04 \times W_{takeoff} + W_{pro} + 1.06 \times W_{fuel} \end{aligned}, \tag{4.4}$$

and this equation was redescribed based on the $W_{takeoff}$ as,

$$W_{takeoff} = 520{,}805.58 + 1.04 \times W_{pro} + 1.1 \times W_{fuel}, \tag{4.5}$$

The weight of the propulsion system (Fig. 4.20) and the fuel weight estimation with SFC, c, the endurance, d, and the thrust, T, for jet engine (Raymer 1999), is described as,

$$W_{pro} = 0.4982 \times T^{0.9433}, \tag{4.6}$$

$$W_{fuel} = cdT, \tag{4.7}$$

The c of SFC of the BWB design was calculated as the average rate of overall operation of Trent 900, because the BWB configuration requires the same flight mission of A380 such as 8,000 nautical miles (15,000 km) range at Mach 0.85 (Table 1.1). With Equation (4.7), the average SFC of Trent 900 with the A380 flight profile was calculated as,

$$c = \frac{W_{fuel}}{dT \times time} = \frac{64{,}937.25}{284{,}004 \times 60{,}300} = 3.7956 \times 10^{-5} \quad 1/lb, \tag{4.8}$$

where the fuel weight excluding the 5 percent reserved fuel is 295 tonnes (64,937.25 lbs), the required engine thrust is 76,500 lb thrust each and the assumed operation time is 16.75 hours (60,300 seconds) (Table 1.1). Therefore, with the equations between Equation (4.5) and Equation (4.8) the $W_{takeoff}$ was obtained as,

$$W_{takeoff} = 520{,}805.58 + 0.5181 \times T^{0.9433} + 2.2887 \times T. \tag{4.9}$$

Also, the T/W is 0.23 in cruise and the relationship between thrust and TOGW is explained as,

$$W_{takeoff} = \frac{1}{0.23} \times T \,. \tag{4.10}$$

In addition, to improve the weight estimation with the conceptual sizing methodologies, the thrust, *T*, of Equation (4.9) was divided by each flight segment such as takeoff, climb, cruise and descent flight segments. Based on the (T/W), each flight mission segment was described as,

$$\left(\frac{T}{W}\right)_{takeoff} = \left(\frac{T}{W}\right)_{cruise}\left(\frac{W_{cruise}}{W_{takeoff}}\right)\left(\frac{T_{takeoff}}{T_{cruise}}\right), \tag{4.11}$$

$$\left(\frac{T}{W}\right)_{climb} = \frac{1}{\left(\frac{L}{D}\right)_{climb}} + \frac{V_{vertical}}{V_{horizontal}}, \tag{4.12}$$

$$\left(\frac{T}{W}\right)_{cruise} = \frac{1}{\left(\frac{L}{D}\right)_{cruise}}, \tag{4.13}$$

$$V_{horizontal}\left(\frac{T}{W}\right)_{descent} - V_{vertical} = \frac{\rho V^3 C_{D_0}}{2\left(\frac{W}{S}\right)} + \frac{2K}{\rho V}\left(\frac{W}{S}\right), \tag{4.14}$$

With the flight segment profile (Fig. 2.3), the equations between Equation (4.11) and Equation (4.14) were utilised to estimate a fuel weight excluding a reverse fuel weight. The fuel weight, W_{fuel}, was recalculated with the each flight mission segment as,

$$W_{fuel} = W_{f-takeoff} + W_{f-climb} + W_{f-cruise} + W_{f-descent}\,, \tag{4.15}$$

with Equation (2.10) and the Breguet Range equation (Equation (2.8)), the fuel weight estimation was redesigned as,

$$W_{fuel} = c \times \left(0.17919 \times W_{takeoff} + 0.18192 \times W_{climb} + 0.04666 \times W_{cruise} + 0.05 \times W_{descent}\right), \tag{4.16}$$

where *c* is the SFC, $W_{f\text{-}takeoff}$ is the fuel weight of takeoff segment, $W_{f\text{-}climb}$ is the fuel weight of climb segment, $W_{f\text{-}cruise}$ is the weight of cruise segment and $W_{f\text{-}descent}$ is the fuel weight of the descent segment.

With the above calculations for the BWB weight estimation and Table 4.4, the overall weight of the

BWB configuration model was obtained as Table 4.5.

Table 4.5 Weight Estimation of the BWB Configuration

	Weight	
Component Name	**kg**	**lb**
Wing	34,280	75,580
Cabin	93,130	205,360
Vertical Tail & Rudder	710	1,560
Landing Gear	18,530	40,860
Surface Controls	940	2,060
Propulsion Systems	35,290	77,810
Instruments & Navigational Equipment	540	1,200
Hydraulics & Pneumatics	5,000	11,020
Electronics	1,000	2,220
Furnishings	25,570	56,390
Air Conditioning & Anti-Ice	3,780	8,330
Operating Items Less Crew	7,790	17,180
Flight Crew	1,300	2,870
Payload (Passenger Baggage)	6,580	14,500
APU	1,760	3,890
Fuel Weight	191,940	423,220
Total Components Weight	**428,140 kg**	**944,050 lbs**

The BWB model achieved a 24 percent lighter weight than the A380. The most effective factor in reducing the overall weight was that the BWB configuration has achieved higher L/D ratio in flight, and required less engines thrust. Compared to the fuel weight of the A380 (Table 1.1), the fuel weight of the BWB is far less with 40 percent less fuel required for the same flight mission profile.

With the Breguet Range equation (Equation (2.8)) and Equation (4.16), the payload/range diagram of the BWB design and the A380 are provided in Fig. 4.22 (when estimating the weight of the BWB design and the A380, the fuel allowance of the A380 was 5 percent of the total weight and the fuel allowance of the BWB design was 6 percent of the total weight).

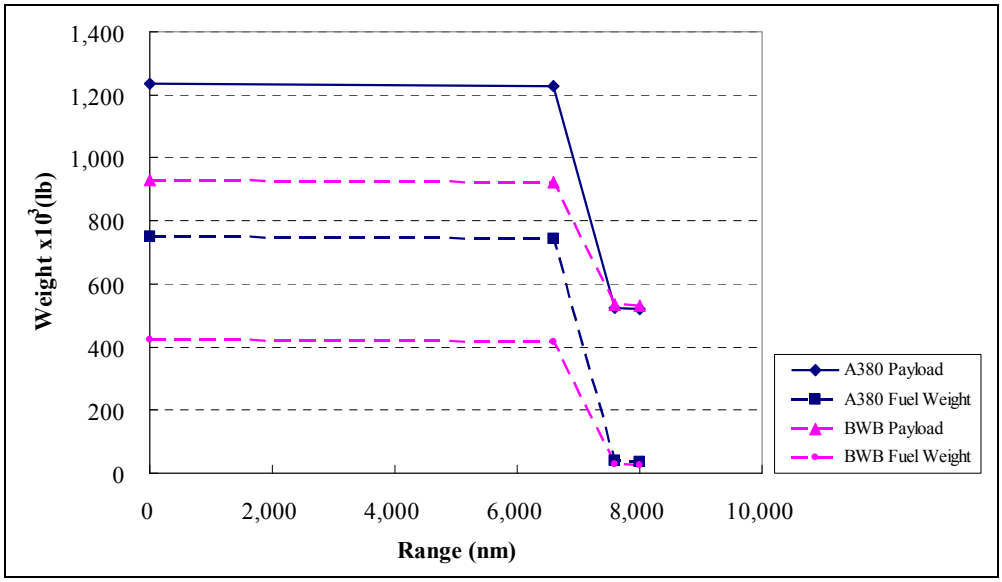

Fig. 4.22 Payload/Range Diagram

Fig. 4.22 shows an interesting result of the payload trends of the BWB against the A380. With Table 1.1 (the characteristics of the A380) and Table 4.5 (Estimated Component Weights of the BWB), the weight of the BWB design is similar to the A380's weight including the payload at the end of the flight mission segment which is approximately 256 tonnes (518,200 lbs).

In regards to the weight estimation of the wing and cabin designs of the BWB, the NASA estimation methodology (Equation (2.40)), the existing equation (Equation (2.25)) and the wing weight trend of the existing aircraft (Fig. 4.19) were utilised to assume these component weights. The detailed descriptions of these weight estimations are shown as below.

To estimate the cabin weight of the BWB, Equation (2.40) was utilised and redefined based on the 450 passengers' BWB pressurised cabin (Bradley 2004),

$$W_{cabin} = 5.698865 \times \left(0.31642 \times W_{takeoff}{}^{0.16655} S_{cabin}{}^{1.06116}\right), \tag{4.17}$$

where K_s is 5.698865 (Bradley 2004). For the 555 passengers' BWB pressurised cabin, Equation (4.17) was redefined with the scale factor, K_s, which was calculated to be 7.0267 for 555 passengers

and 24 m width cabin design as,

$$W_{cabin} = 7.0267 \times \left(0.31642 \times W_{takeoff}^{\ 0.16655} S_{cabin}^{\ 1.06116}\right) = 2.223388 \times W_{takeoff}^{\ 0.16655} S_{cabin}^{\ 1.06116} \quad (4.18)$$

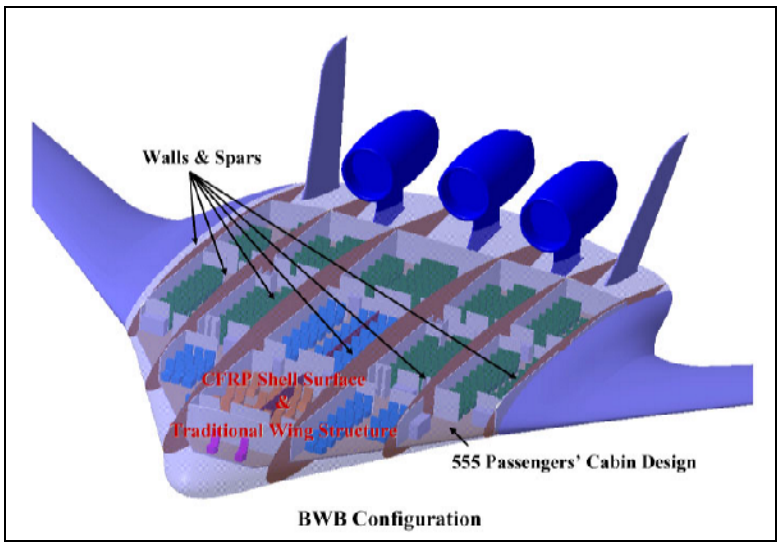

Fig. 4.23 Structural BWB Design Concept

Fig. 4.23 shows the image of structural BWB design concept based on the structural methodology of Fig. 2.10. This structural design was chosen to utilise the CFRP shell pressured surface and the traditional wing structure methodology integrated to surround the cabin area (Fig. 4.23: Area of Transparent Blue Colour).

In regards to the weight estimation of the A380, the weight of each flight mission segment was estimated using the Breguet Range equation (Equation (2.8)) and the several parameters (Table 1.1) with 5 percent fuel allowance. With these parameters based on the maximum TOGW of the A380, the weight estimation is 560 tonnes (1,235,000 lbs), the empty weight of the A380 is 234.36 tonnes (519,000 lbs) and the fuel weight was assumed to be 324.73 tonnes (716,000 lbs) including the 5 percent of fuel allowance.

The summarised characteristics of the A380 and the optimised BWB model are shown in Table 4.6. Fig. 4.24 also shows a list of TOGW of the major BWB aircraft projects and details for the A380 (aerosite 2005, aircrash.org 1996 & Brzezinski et al. 2003).

Table 4.6 Characteristics of the A380 vs. the Optimised BWB Model

	A380-800	**Optimised BWB**
Overall Length (m)	73.00	44.86
Cabin Length (m)	50.70	27.40
Fuselage Width (m)	7.10	24.00
Height (m)	24.10	13.20
Wingspan (m)	79.80	79.80
Wing Area (m^2)	845.00	1,575.60
Aspect Ratio	7.50	4.00
Max. Payload (tonnes)	560.00	428.10
Fuel Weight (litre)	360.90	191.90
Payload (tonnes)	66.40	66.40
Requiring Engines Thrust (lb Thrust)	305,000	290,000
L/D Ratio	13.97	21.43

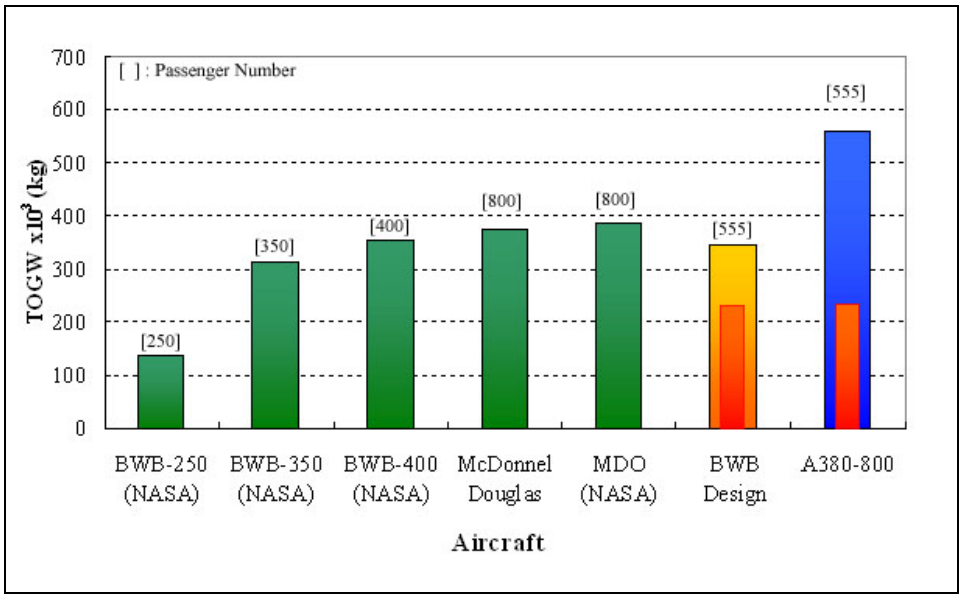

Fig. 4.24 Lists of Aircraft TOGW vs. Number of Passengers
(Orange Bar: Project BWB Design, Red Bars: Empty Weight)

4.2.8 Optimisation Techniques for the BWB Configuration

The baseline BWB configuration was designed with the NACA airfoil series with consideration of the specifications of the A380. This wingspan of the baseline BWB was also less than 80 m to be able to operate within current airport compatibility settings and the payload was accommodated from 0 m (central body) to 12 m spanwise on the BWB model. The flight conditions of the optimised BWB configuration were considered corresponding to the baseline characteristics in Table 4.7 and Table 4.8.

Table 4.7 Cruising Condition of the BWB

Mach Number	0.85
Reynolds Number	5.12×10^{8}
Altitude	11,000 m

Table 4.8 Aerodynamic Performance of the BWB Design

	Lift Coefficient C_L	**Drag Coefficient C_D**
CFD Results of the Baseline BWB	0.0953	0.0448
Target Values for Optimised BWB Model	0.1500	0.0750

In regards to Table 4.7, the flight operating conditions are the same as for conventional aircraft, such as the A380-800. Based on the flight mission segment profile of the A380, the BWB models were targeted on achieving 20-30 of L/D ratio in flight which means that the lift coefficient C_L may be 0.15 and the C_D may be 0.075 (Table 4.8). According to the CFD results of the baseline BWB, these values were calculated using Fluent CFD code for cruising conditions (Table 4.7) and the detailed CFD results will be presented in further sections. According to Table 4.8, the difference of aerodynamic features between the baseline BWB configuration and the target value of BWB model was distributed to the following differences; e.g. the baseline BWB model was analysed aerodynamic performance with the engines, tails and winglets using Fluent, but the target value of BWB model was calculated with the wetted aspect ratio and has not considered the drag of engines and vertical tails.

Fig. 4.25 shows multi-view of the initial BWB model designed using CATIA V5. This initial BWB design was a criterion for optimising a BWB model. This baseline BWB design was created based on the 2D AutoCAD sizing (Fig. 4.5), and installation of NACA0015, NACA0009 and NACA2509 for the fuselage airfoil sections and wing sections. The aerodynamic features of the initial BWB achieved 2.127 of L/D ratio in flight (Table 4.8). In this case, the airfoil selection for the BWB configuration was not feasible and it was adjusted and optimised to achieve the target values required for aerodynamic performance.

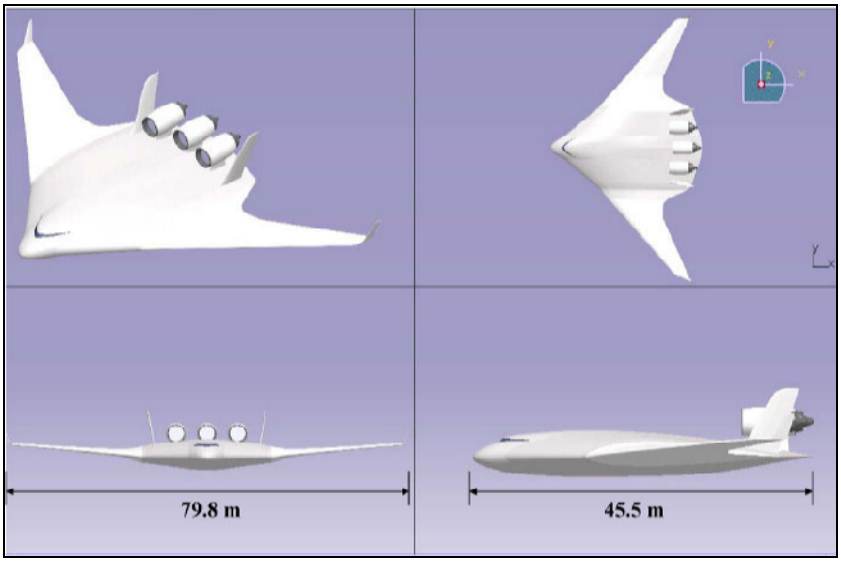

Fig. 4.25 Illustration of the Baseline BWB Model

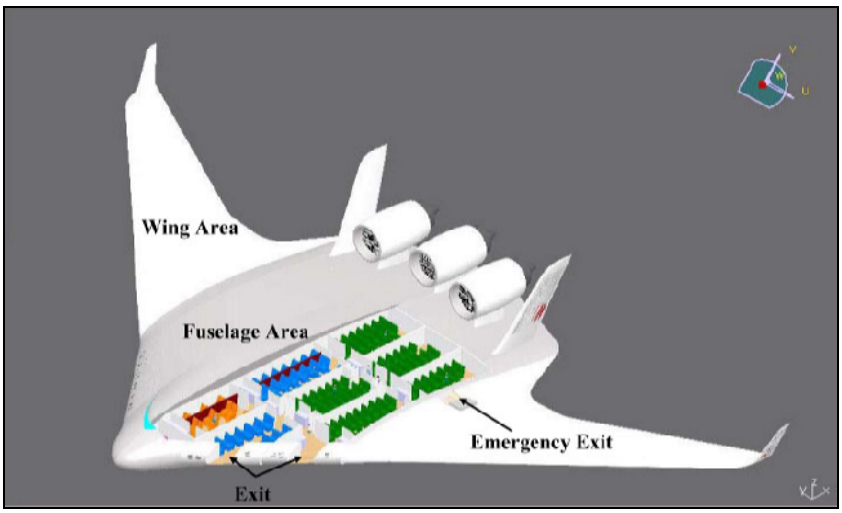

Fig. 4.26 Image of the Baseline BWB with Cain and Exit Doors

The preliminary BWB design (Fig. 4.26) was decided in accordance with comportment arrangement to include the integrated wing body design as flying wing, 3 engines on the aft of upper body, two tails, winglet, passengers' cabin design and the 6 exit doors (2 emergency exits).

With this preliminary BWB arrangement, the baseline BWB model has been adjusted and optimised to improve aerodynamic performance in flight. Therefore, for an evaluation of its aerodynamic performance, a technique of controlling wetted aspect ratio was utilised (Chapter 2 Section 2.5.4). The wetted aspect ratio of the baseline BWB design was 1.81 (Wetted Area = 3,524.85 m^2, Wingspan = 79.8 m). Fig. 4.27 shows the modification of the BWB reference and wetted area and the relationship between the aspect ratio and the wetted aspect ratio compared with the information from the A380 results which were calculated using a simplified model of the A380 based on the preliminary features of the A380 (AIRBUS S.A.S. 2004).

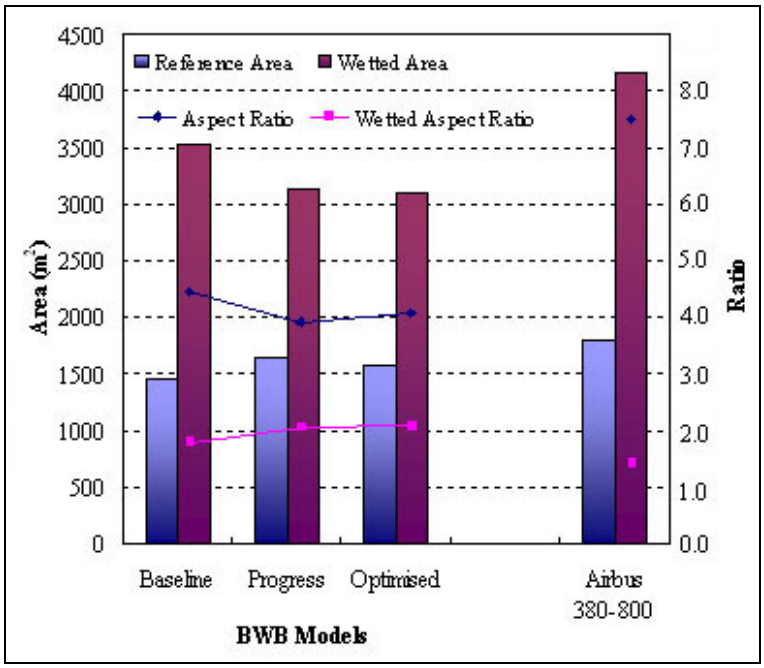

Fig. 4.27 Comparison of the Reference Area vs. Wetted Area, and the Aspect Ratio vs. Wetted Aspect Ratio between BWB Models and the A380

According to the variations of the BWB modifications from the baseline to the optimised BWB

design;

1. the reference area of the optimised model was increased by 8.45 %,
2. the wetted area of the optimised model was successfully reduced by 11.85 %,
3. the aspect ratio of the optimised model became 7.76 % lower,
4. the wetted aspect ratio of the optimised model was improved by a factor of 1.13.

Since the BWB design arrangement of the wetted aspect ratio (Fig. 4.27), the optimised BWB model was changed the external shape as Fig. 4.28.

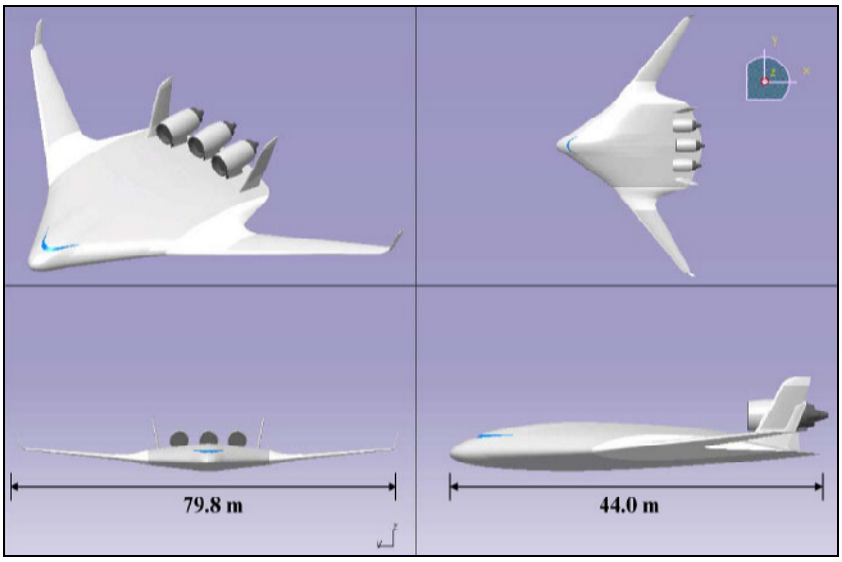

Fig. 4.28 CATIA Design of the Optimised BWB Configuration

The optimised BWB configuration was designed using the trends of wetted aspect ratio and L/D to determine a wing area of the BWB configuration, and the current airport compatibility issue was periodised to decide the length of the wingspan. Since the relationship between aspect ratio and L/D, the wetted and reference area of the BWB were minimised retaining all required components in the wing. Moreover, the wing design of the BWB was considered with typical methodologies of subsonic aircraft, such as swept angle.

Fig. 4.29 reveals the differences between the three aircraft models. These aircraft have been designed with the same flight mission profile.

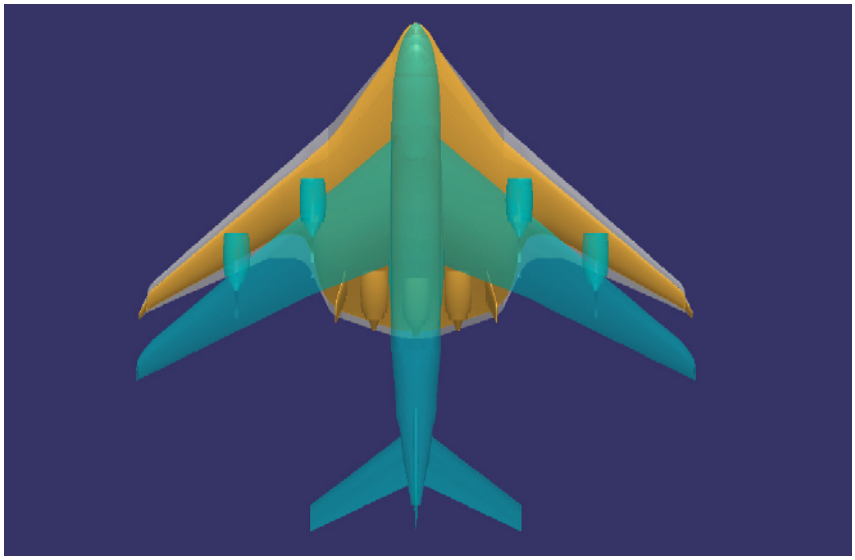

Fig. 4.29 Comparison of the A380 and BWB Configurations for the Same Design Mission
(Green: A380-800, Orange: Optimised BWB Design, Gray: Baseline BWB Design)

When comparing the BWB designs between the initial and the optimised models, the optimised model was redesigned with the thinner width wing and thicker thickness of the cabin dimension than the initial BWB model. In detailed the optimised BWB design (Orange colour in Fig. 4.29) is approximately 40 percent shorter than the A380 (73 m overall length) and its body size (excluding the engines) is approximately 1.5 meter shorter than the baseline BWB model (45.5 m). This downsizing of the aircraft leads to reduced material cost and operates easily at airports. However, the main design parameters of the both airplanes design were the same, such as the wingspan, the number of passengers and the flight mission segment profile.

4.2.9 Aerodynamic Analysis of the BWB Configuration Model

From the conceptual BWB sketches, the BWB models have been optimised and analysed in aerodynamic performance in flight. To evaluate the aerodynamic features of the BWB designs, the FLUENT package was utilised to simulate air flows surrounding the aircraft in similar physical

conditions of the actual cruising aircraft and to compare these three aircraft models in aerodynamic capability within the Realisable k-ε turbulence model in Fluent, which include combining the Boussinesq approach and eddy viscosity methodologies (Chapter 3 Section 3.2.2). In this case, the viscous model was defined with Mach number 0.85 and the Reynolds number of 5.12×10^{8} within atmosphere conditions of 11,000 m altitude.

In regards to the boundary layer conditions for CFD simulation, a half model of the BWB design was utilised, and the BWB model was defined as wall and the engines' intake was defined as an outlet in Fluent, which means that air flow was just through the boundary area of the fans (Fig. 4.30: Red Colour Area).

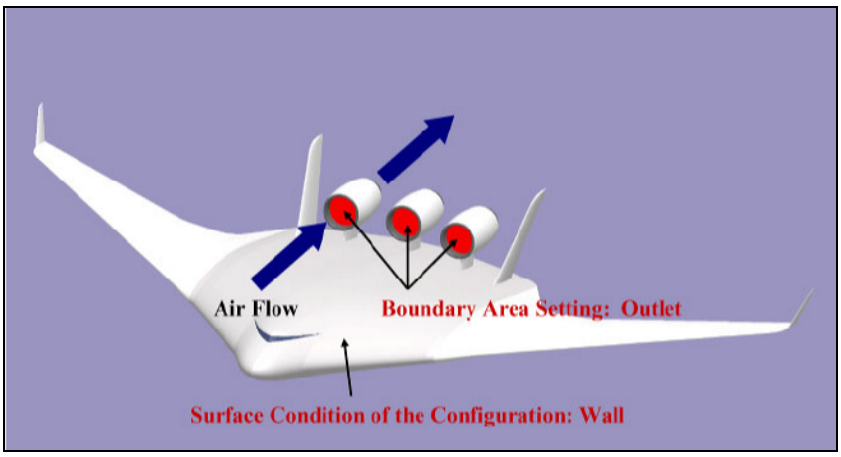

Fig. 4.30 Boundary Area Conditions for CFD Simulation

The baseline BWB model met all design requirements of BWB configuration such as less than 80 meters wingspan, 555 passengers' cabin layout and 66.4 tonnes payload capabilities, and then this model was analysed for aerodynamic features in Fluent. The initial BWB model was simulated in turbulent flow conditions and the aerodynamic features were calculated over a few days (i.e. lift coefficient, drag coefficient and momentum coefficient et al.).

Before the complete BWB models were simulated in Fluent, the BWB designs did not include engines

and were analysed according to aerodynamic capabilities to see whether selected airfoils can generate a lift properly and to see how much C_D provides. Fig. 4.31 shows the CFD results of static pressure on the top and bottom surfaces of the BWB design which was simulated using the Realisable k-ε turbulence model in Fluent. This BWB model was designed with Eppler417. With these contours of the BWB model (Fig. 4.31), the wingspan-wise of this BWB proved to generate lift, as shown the light green area on the top surface which means that the area provides lower pressure than the surrounding area (Bernoulli equation). On the bottom surface, the aft body has a higher pressure area (Orange and yellow colours), and the location of higher pressure occurred at the middle cabin area (Deep green colour). With the CFD results of this BWB, the model was altered and optimised for the pressure distribution to create more lift, and the aerodynamic features were analysed and adjusted to change the pressure distribution and make is smoother on the bottom surface through selecting proper airfoils for the BWB model.

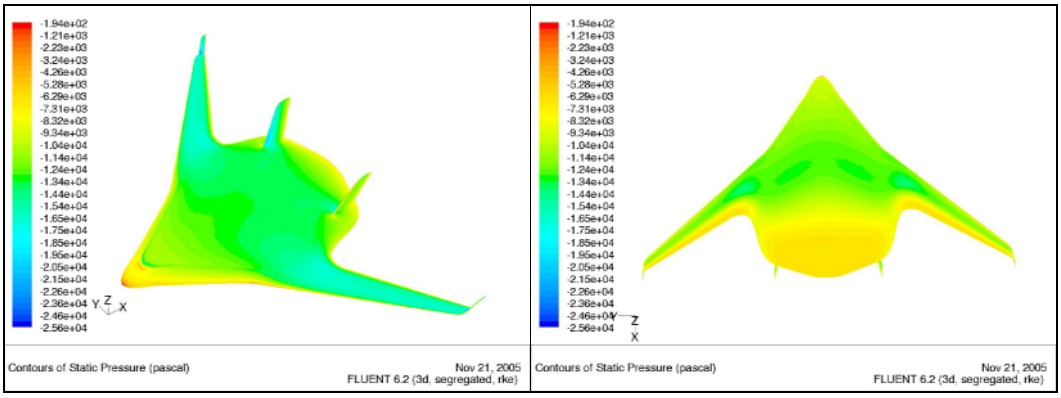

Fig. 4.31 CFD Results of the Progressive BWB (Eppler417) without Engines

The CFD result of the optimised BWB model is shown in Fig. 4.32. This model's airfoil section was redesigned with the optimised NACA airfoil series (Fig. 4.14), and then the redesigned model was computed to simulate airflows around the model. In the CFD results (Fig. 4.32), the upper surface has a lighter blue colour area than the previous model on the wingspan-wise which ensures that the lower pressure area was expanded to generate lift. Furthermore, the orange colour area (Fig. 4.31) on the

bottom surface was now removed and the pressure contours' pattern were changed gently.

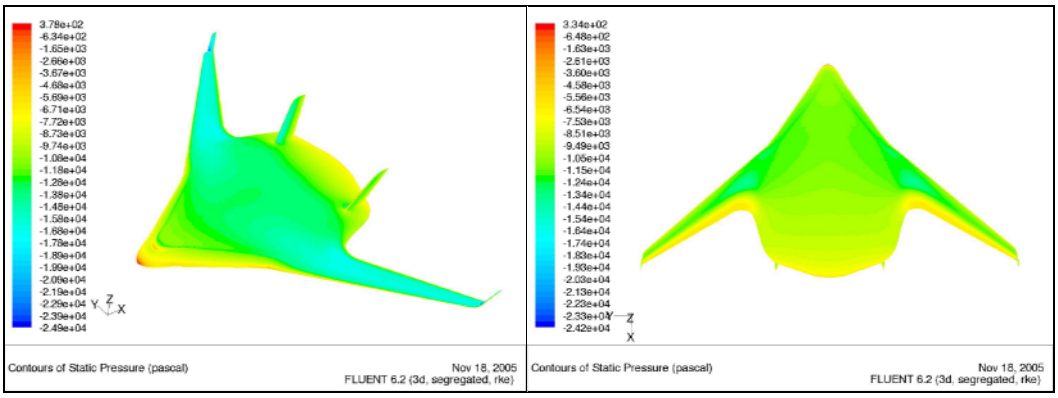

Fig. 4.32 CFD Results of the Progressive BWB (NACA & Eppler Airfoils) without Engines

The CFD results of the BWB models with the different airfoil sections, with the detailed aerodynamic features are presented in Table 4.9. When the two BWB models are compared according to aerodynamic features, the second stage BWB design with altered airfoil sections became more aerodynamically efficient (i.e. the drag was approximately reduced by 30 percent) in flight. Moreover, the second stage BWB design achieved 1.05 times higher L/D ratio than the first BWB model through having changed the airfoil designs during level flight.

Table 4.9 CFD Results of the progressive BWB Models without Engines ( ): Name of Installed Airfoil Series

	Momentum Coefficient C_M	**Lift Coefficient C_L**	**Drag Coefficient C_D**	**L/D**
Progressive BWB 1 (Eppler417)	0.073204	0.21047	0.013267	15.86
Progressive BWB 2 (NACA+Eppler417)	0.067291	0.15513	0.009361	16.57

In the next stage, the draft BWB design had three engines on the aft body added. The baseline complete BWB model (Fig. 4.25) was then analysed according to aerodynamic parameters in Fluent using the Realisable k-ε turbulence model, and the CFD results are shown in Fig. 4.34.

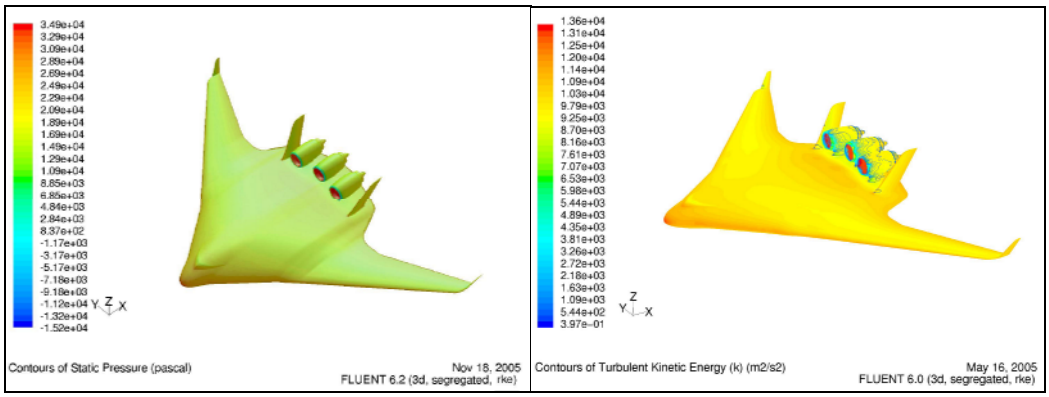

Fig. 4.33 CFD Result of the Baseline BWB Configuration by the Realisable k-ε Model ($M = 0.85$, $Re = 5.12 \times 10^8$)

With the contours of aerodynamic features (Fig. 4.33 Left: Static Pressure, Right: Static Pressure with Lines of Turbulent Kinetic Energy), the initial BWB model was proved to generate lift on the wing, because the upper surface shows a lighter green colour than the surrounding area which means that above the lighter green area has a lower pressure than other area. This CFD results are presented in Table 4.8.

The baseline BWB model was then modified on the wetted aspect ratio to improve aerodynamic performance of the BWB model. In regards to design techniques for aerodynamic improvement, the size of the progressive model was reduced and the wetted area optimised (Fig. 4.27), and then the wetted aspect ratio became 3.89, and the C_L was 0.31778 which is approximately 1.6 times higher than the baseline BWB, and at the same time the C_D was reduced by 80 percent of the total drag. These alterations also resulted in a reduced parasite drag of the aircraft model, because its drag primarily relates to skin-friction drag, and as such is directly proportional to the total surface area of the configuration exposed to the air. Moreover, more suitable airfoils were identified and analysed for the BWB configuration (Chapter 4 Section 4.2.5) and more efficient and better performing airfoils were chosen.

After the CFD results, the initial BWB model was seen to have unfeasible airfoils which were

NACA0009, NACA0015 and NACA2509, because there was not enough data on airfoil design for the BWB configuration. After investigating and considering possible airfoil design for the BWB, a higher performance airfoil was chosen, achieving more than 0.4 of lift coefficient in level flight. The initial BWB model was then redesigned, and the aerodynamic performances were optimised and improved as shown the CFD results in Table 4.10.

Table 4.10 Improvement of Aerodynamic Capabilities of the BWB Configurations

	Initial BWB	**Progressive BWB**	**Optimised BWB**
Lift Coefficient C_L	0.0935	0.1586	0.1577
Drag Coefficient C_D	0.0448	0.009612	0.007359
L/D	2.13	16.53	21.43

In regards to the CFD results from the three different BWB models, the optimised BWB model achieved 21.43 of the L/D ratio which is 10 times higher and with 83.6 percent less drag than the initial model. According to the aerodynamic parameters of the three BWB models, the progressive BWB models achieved approximately 0.158 of the C_L which may lead to the conclusion that a C_L of this shaped BWB model will be limited and the C_D of the optimised BWB obtained lower value than as calculated for the A380 model. When comparing to the B747 of the main stream airliner, the C_D value of the optimised BWB is 3.5 times more effective in level flight. Additionally, the higher L/D ratio may be predicted to provide several advantages including the potential to achieve to reduced noise emission, and to require less engine thrust as well as to being more economical.

The CFD results of the progressive and optimised BWB models, the contours of static pressure and its image with contour lines of lift distributions are shown in Fig. 4.34 and Fig. 4.35. Both BWB aircraft were analysed according to aerodynamic efficiency using Fluent with the same flight conditions. Through Fluent visualisation a pressure distribution was identified.

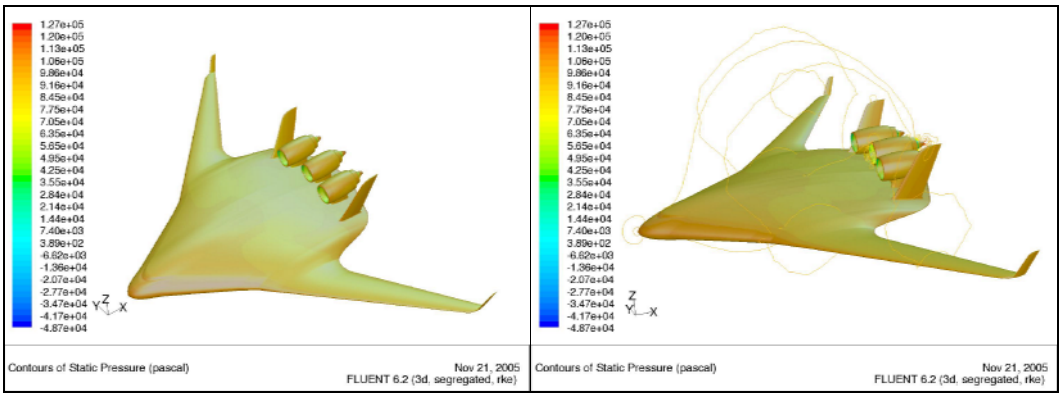

Fig. 4.34 Visualisation of the CFD Results of the Progressive BWB Model

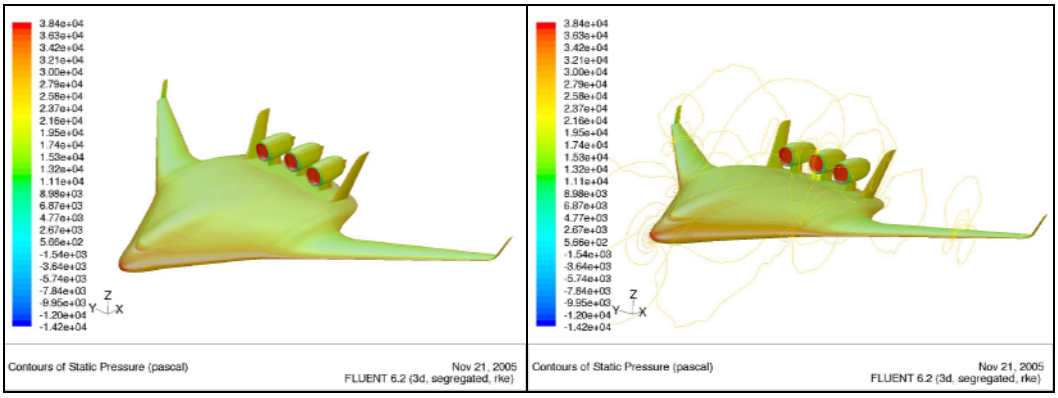

Fig. 4.35 Pressure Distribution of the Optimised BWB Model

According to Fig. 4.34 and Fig. 4.35, the static pressure distribution of the optimised BWB shows that the colour pattern of the upper surface is changed smoothly and this pressure is distributed over the whole wingspan-wise area. Moreover, the optimised BWB configuration has a lower pressure indicated by the green colour area on the upper wing compared to the progressive BWB. This means that the model can generate a higher lift than the previous BWB models.

The detailed description of the optimised BWB model was analysed according to airflow impact on the surfaces showed with contour lines of static pressure and turbulent kinetic energy (k). In Fig. 4.36 the pressure distribution and the flow separating locations were identified with these contour lines. On the upper surface of the 16 m spanwise extension a large increase in drag and separations were identified by the contour lines of turbulent kinetic energy. This difference in the kinetic energy can

show that flows create turbulent eddies (cascade processes) and it dissipates energy (i.e. heat which supplies from mean motion to turbulent and molecular motions on the area). Because of the modification of the 16 m spanwise area, the wing design had a problem because the two different airfoils were joined in this area. In addition to this, the engines and tails have energy dissipations. To solve these negative issues several techniques are possible, such as removing the tails and modifying the vertical control system on the winglets, and for the engines' propulsion system to be integrated within the aft body. However, these advanced ideas have not been included in this BWB configuration, because weight estimations of the BWB components could not be assumed and the structural analysis has not been completed.

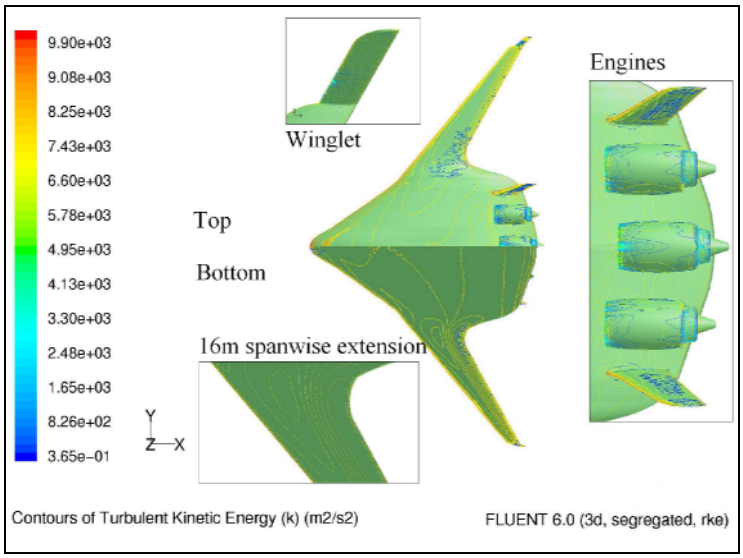

Fig. 4.36 Contour Lines of Pressure Coefficient (Citrus Colour) and Turbulent Kinetic Energy (k)

In regards to the turbulent kinetic energy, Fig. 4.37 shows the results of the comparison of the A380 and the optimised BWB design based on the horizontal axis. In the comparison of both configurations, the plots of kinetic energy of the BWB model gather around the aft body from approximately 35 m (the location of the engines) to 45 m (the end of the body), but the results of the A380 model of kinetic energy were plotted on the wide range of the overall length, especially at the locations of the engines, winglet and tails. Moreover, the winglet of the BWB model creates a turbulent flow (as shown by the

blue colour area on the winglet in Fig. 4.36). In this case of the winglet, this consequence is attributed to a failure of the mesh quality in the grid solution. However, the plotted results of turbulent kinetic energy show, the BWB design has been proved more aerodynamically efficient, because the BWB configuration performs with less energy dissipations.

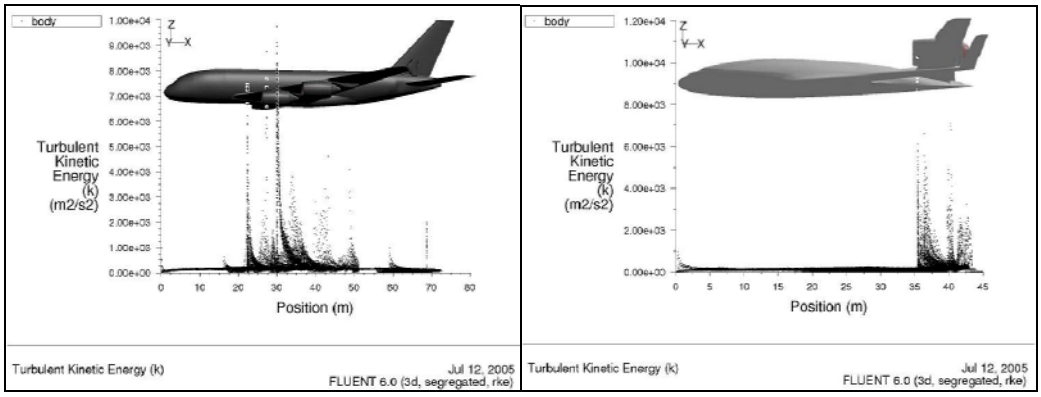

Fig. 4.37 Plots of Turbulent Kinetic Energy (k)
(Left: Airbus A380, Right: the Optimised BWB Model)

Fig. 4.38 shows the scaled residuals of the optimised BWB model with several parameters. In this research CFD simulations were calculated with approximately 1,000 iterations to obtain accurate aerodynamic models in Fluent. The average processing hour of these CFD calculations was approximately 150 hours calculating through the Realisable k-ε turbulence model.

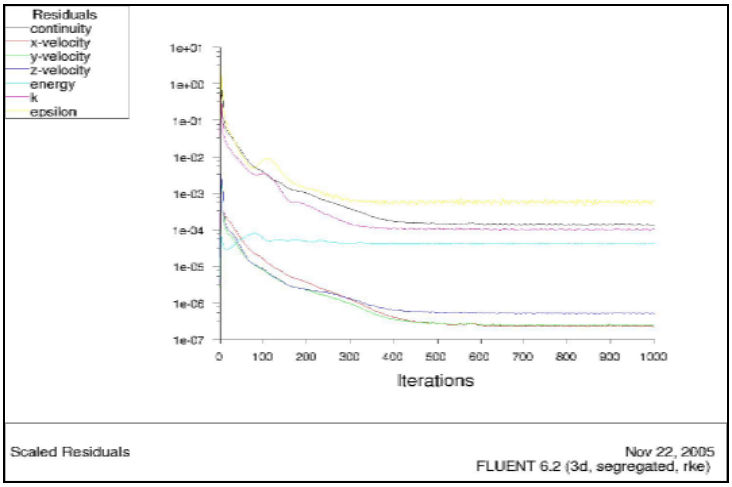

Fig. 4.38 Scaled Residuals of the Optimised BWB Model

4.3 Inspection of the CFD Results Comparing to the RNG k-ε Turbulence Model

To analyse and critique the CFD results of the optimised BWB configuration calculated by the Realisable k-ε model, the optimised BWB model aerodynamic features were recalculated through the RNG k-ε model in Fluent. Using a different turbulent model methodology for CFD simulation, the CFD results were compared and analysed. However, the RNG k-ε turbulence model consumes more than 1.5 CPU time and requires 1.2 times more memory than the standard model. Therefore, this RNG k-ε model has not been utilised through CFD solver in this project because of PC limitations.

The RNG model is more responsive to the effects of rapid strain and streamlines curvature than the standard k-ε models, which explains the superior performance of the RNG model for certain classes of flows. The optimised BWB model was simulated through fluid behaviour by the RNG model for approximately 500 hours. In regards to this processing time in this case, the RNG model was not suitable to calculate aerodynamic features of the BWB configuration, because the BWB configuration needed to have shape design optimised and to have CFD results examined several times through the process. Time saving was a significant to work with CFD analysis and the relevant studies in this research.

Fig. 4.39 shows the CFD results calculated by the RGN k-ε model in Fluent. In comparing the CFD results of the BWB configuration calculated through the Realisable k-ε model, the colour pattern of the static pressure on the surface is similar to the others, as shown in Fig. 4.35.

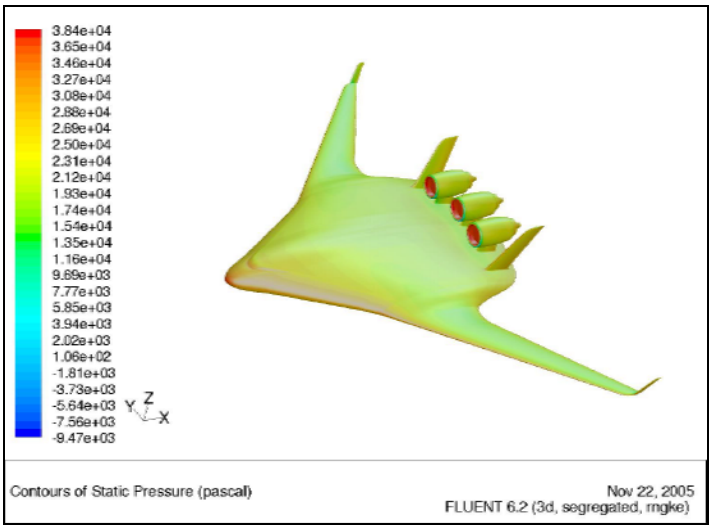

Fig. 4.39 CFD Result of the Optimised BWB Model by the RGN k-ε Model

The comparison of CFD results of the optimised BWB model using the different equations is presented in Table 4.11. In the CFD results, the both turbulent models produced similar values with only several percent differences in the C_L, C_D and L/D ratio. According to the C_M, the BWB model which was calculated through the RGN k-ε model was approximately 30 percent higher than through the Realisable k-ε model.

Table 4.11 Comparison between the Realisable and the RGN k-ε Models of CFD Results

	Momentum Coefficient C_M	**Lift Coefficient C_L**	**Drag Coefficient C_D**	**L/D**
Optimised BWB Model with Realisable k-ε Model	-0.002445	0.15770	0.00736	21.43
Optimised BWB Model with RGN k-ε Model	-0.001727	0.15096	0.00693	21.80

4.4 Control Stabilities of BWB Concept Design

A BWB configuration is an unconventional aircraft and several functions are totally different to existing aircraft. The BWB concept design does not have horizontal tails and also sometimes no vertical tails. Therefore, the BWB configuration requires new flight operation methodologies such as flight control system (i.e. stability functions of the conventional tube-and-wing design are not feasible for the BWB flight mission).

The stability control methodology required for the BWB concept is similar to the control systems of the B-2 stealth bomber (Fig. 4.40). To meet the needs of the control functions of the B-2 bomber, the split rudders (Red colour), outboard elevons (Blue colour), middle elevons (Green colour), inboard elevons (Yellow colour) and the gust load alleviation system (GLAS) are installed to fly efficiently. The elevons which have a similar function to the elevators and ailerons on conventional aircraft change the pitching momentum and rolling momentum while rotating along the horizontal axis. Additionally, the elevons with rudders stabilise the yawing motion of the aircraft (rotation along the vertical axis). Also, the advanced computational technology enables the tailless aircraft to stabilise using a sophisticated fly-by-wire system which means that the computer automatically applies stability control via the electric actuator. The B-2 bomber also utilises the GLAS of the small wedge shaped flap to counteract air turbulence forces (aerospaceweb.org 2005 & Harris 2005).

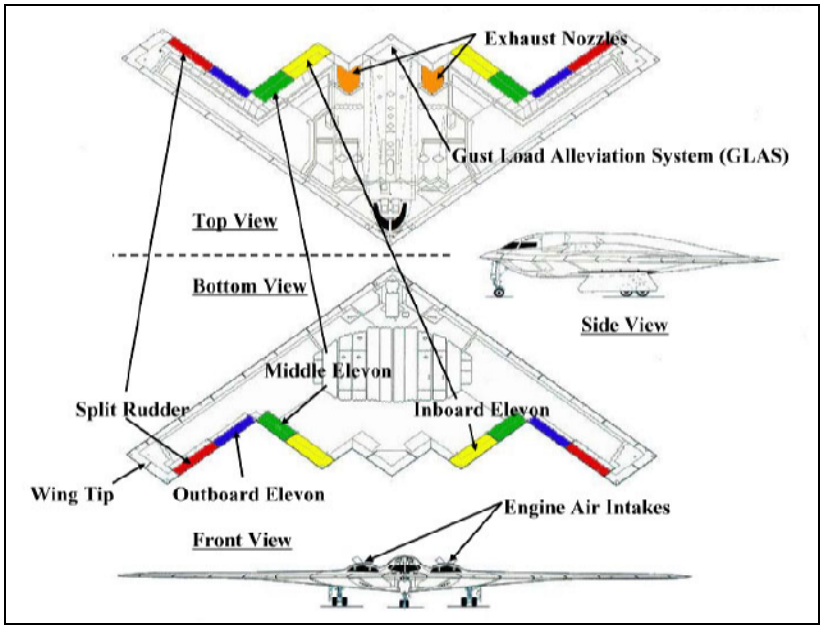

Fig. 4.40 Stability Control System of B-2 Stealth Bomber

An illustration of the stability control system required for the BWB configuration is shown in Fig. 4.41. The BWB configuration would employ inboard elevons, middle elevons and outboard elevons to stabilise its pitching, rowing and yawing motions and would likely use the same mechanisms as the

B-2 stealth bomber. The BWB design has two vertical tails with rudders allowing the rudders to easily provide yawing motion. From several colour portions on the BWB design, the outboard (Blue colour) and middle elevons (Green colour) work as ailerons and flaps to create a friction for yawing motion during flight segments. Moreover, the three jet engines may provide a controlling function as by adjusting engine thrust, and through thrust vectoring using nozzles effective pitching control can be applied. However, this control mechanism using elevons has not been fully researched for application to large commercial BWB aircraft. To data this flight control system has only been utilised for the military aircraft (i.e. the B-2 stealth bomber).

To meet the needs of a control system for the BWB configuration, a fly-by-wire system would be required to stabilise the pitching and rolling motions during flight operation. The control system requirements with fly-by-wire will be achieved for the BWB configuration, because Airbus aircraft already employ this control system for all conventional aircraft. From a structural perspective, however, the components' strength and arrangement of the system will be more complicated and difficult to design it for BWB design in this case.

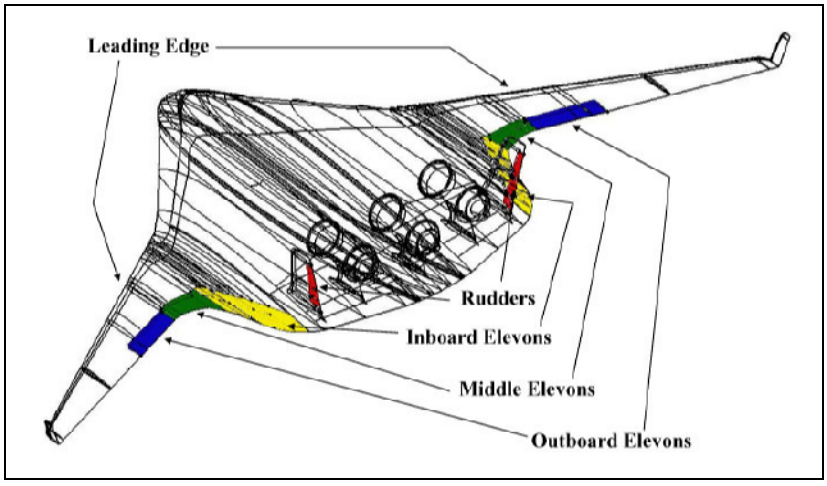

Fig. 4.41 Prediction of the BWB Control System

With the optimised BWB design (CATIA geometry), the locations of the centre of gravity (C.G.) on each component were calculated as shown in Fig. 4.42. This figure shows that the C.G. location of the

cabin compartment with furnishing and floor weights is 22.94 m from the nose, the fuselage C.G. is located at 23.27 m from the front including the weight of two tails, the location of the wing C.G. was calculated as 25.03 m from the front, and the C.G. of the engines is located at 39.30 m from the nose. These C.G. locations were calculated from the solid and surface models of the optimised BWB model using CATIA. In further design, the C.G. locations will be calculated more accurately through including the detail of the component designs. In this conceptual design phase, the C.G. location of the whole BWB configuration was assumed to be 23.00 m from the front. In addition to this, the aerodynamic centre of the BWB configuration was estimated to be at the location of 22.00 m from the front (Fig. 4.15 & Fig. 4.42). However, these locations were estimations only from the conceptual design. With the locations of aerodynamic centre and centre of gravity for aircraft design, it is a significant parameter to analyse a control stability of the configuration, such as longitudinal and lateral stabilities with aircraft momentum of inertia.

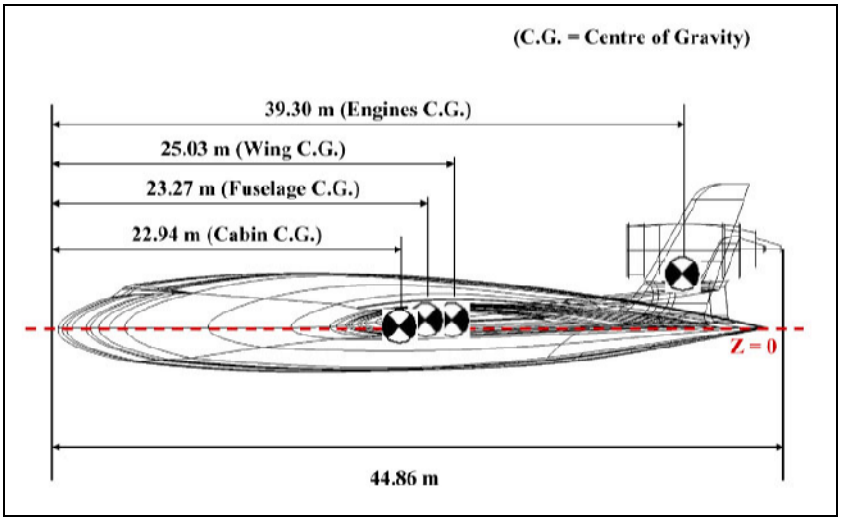

Fig. 4.42 C.G. Locations of the BWB Configuration

4.5 Implication for Human-BWB Aircraft Relations

From the CATIA models and the CFD results, the BWB offers greater structural, aerodynamic and effective flight operation than the A380. Also, advantages and disadvantages have been identified regarding specifications of the BWB concept, such as the wide cabin layout. According to the cabin

layout (Fig. 4.7), the cabin width is 24 m which is approximately 3 times wider than the A380, and 555 passengers can be accommodated together on one floor with 3 travel classes (potentially more than 700 passengers could be carried with all economy class layout).

The major negative impacts on human health in the BWB concept design are caused by the small numbers of installed windows possibly causing more motion sickness. Other health problems are no different to general air travel in commercial aircraft.

The windows on aircraft have a positive effect for the travellers, helping them to relax have comfortable viewing and enjoy natural sun light in flight. However, it is a difficult in the BWB layout to install many windows on the surface as conventional aircraft, because the cabin is located within the wing and the structural strength will be lower if windows are employed on the surfaces. Therefore, the LCD may be substituted for typical aircraft windows to be shown outside view as well as the entertainment programme during flight (Aerospace Medical Association 2001).

In regards to the wider cabin design, the flight motion has influence on the traveller during flight. For example, passengers sitting on the edge of the cabin are more likely to suffer motion sickness, especially when the BWB aircraft is climbing, turning and approaching the runway, because the vertical motion of the passenger is steeper than the conventional aircraft by bank angle. In this particular case, a passenger on the BWB aircraft sitting in a seat which is 12 m from the centre line (i.e. the passenger seats at the edge of cabin) will be moved up ±3 m from the level flight on the Z axis (Fig. 4.43) if the aircraft is turning at a 30 degrees bank angle (e.g. On the A380 the passenger will be moved approximately ±2 m higher than the level flight), and also the passenger will feel more acceleration through the centrifugal force.

To help remedy these negative factors, the BWB aircraft design needs new developments for traveller

comfort through structure and flight control arrangements. For example, a lower bank angle can be recommended to control passenger's vertical motion for passenger comfort during flight.

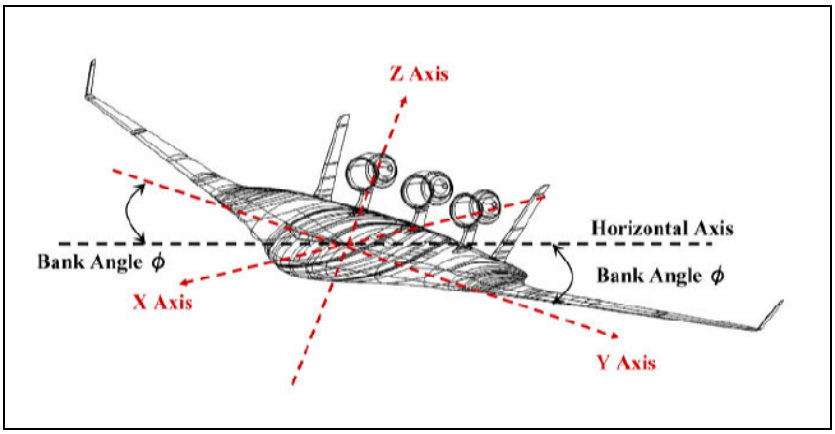

Fig. 4.43 Typical Flight Rotation Profile with the BWB Configuration

To conclude, there are important issues involved in the design of a new configuration from a non-engineering perspective in BWB concept design. The BWB configuration may produce several health problems for passengers, such as motion sickness, pulmonary embolism (caused by space restriction) and claustrophobia (exacerbated by less windows). These symptoms should be considered along with aircraft design, especially for commercial aircraft. In this case, installing windows is important for passenger comfort during flight, or windows should be substituted with a LCD monitor system.

Chapter 5 Conclusions

In recent years, international air tourism has increased significantly, especially in travel to East Asia, the Pacific, and the Middle East regions. According to the WTO (World Tourism Organisation) Tourism 2020 Vision, international travel numbers are expected to increase to over 1.6 billion people by 2020, which is twice the current number (WTO 2005). With this massive increase in air travel demand, the BWB aircraft configuration as a very large airfreight transport vehicle may be looked at favourably as a potential mainstream airliner for the high-density hub to hub routes in the near future.

The BWB configuration was compared to the Aerodynamic performance of the simplified A380 using CFD simulation based on the same flight mission requirements, and the L/D ratio of the A380 was calculated with the Bernoulli's equation. Since the results of aerodynamic performance based on the aircraft models, the capabilities of the BWB configuration offer more potential than the current A380 prototype. The BWB aircraft, according to the NASA's weight estimation methodology based on the FEA and the supporting practical aircraft data suggest that this is the most revolutionary aircraft concept of recent decades.

The differences in design procedures of the BWB configuration (Appendix 6) are the cabin and fuselage sections compared to the cylindrical style of conventional aircraft. However, the cabin-fuselage compartment was assembled with typical wing structural instruments but the CFRP pressurised shell design provides for 555 passengers with its wider accommodation. The empty weight of the BWB was similar to the weight of the A380, but the required fuel weight of the BWB is 45 percent less and the TOGW of the BWB (420 tonnes) is 24 percent lighter than the A380 (560 tonnes) within the same flight mission segment. With the improvements in BWB aircraft performances, the more effective fuel consumption was obtained through superior flight performance of the BWB

capabilities. From the CFD results of aerodynamic parameters, the BWB configuration proved to have the aerodynamic features superior to conventional aircraft, because the BWB design (21.43 of the L/D) achieved 1.5 times higher L/D ratio than the A380 (13.97 of the L/D). This remarkable aerodynamic performance of the BWB configuration is that approximately 21 of L/D ratio was achieved in flight (e.g. the conventional aircraft normally achieve approximately 15 of L/D ratio). Moreover, the flight features of small drag value and less engine thrust requirement predict to perform with less noise emission, and make it a more environmentally-friendly vehicle. Overall the CFD results and the component weight estimations, the BWB configuration demonstrates many advantages, such as in structural and aerodynamic characteristics, better than conventional aircraft with the same flight mission profile.

In conclusion, from the conceptual point of view, the BWB design has been demonstrated to be more attractive than the conventional aircraft. From these results of BWB conceptual design, a preliminary design phase (i.e. more detailed designs as structure and systems) will be required in further research. Moreover, the other significant area will be FEA equals to CFD analysis of the BWB configuration that will illuminate structural design difficulties and make the weight estimation more practical and more credible.

With these numerous advantages, combined with forecast dramatic rise in demand for passenger aircraft, the BWB concept aircraft offers the potential to become the standard commercial aircraft in the next generation - while being more fuel effective and environmentally-friendly at the same time.

References

Aerosite 2005, Aerosite Boeing Blended Wing Body (BWB), *Aerosite.net*, Accessed 21st January 2005, <http://www.aerosite.net/bwb.htm>.

Aerospace Medical Association 2001, USEFUL TIPS FOR AIRLINE TRAVEL, *Aerospace Medical Association*, Accessed 13th July 2005, <http://www.asma.org/pdf/publications/Trip_For_Travelers2001.pdf>.

aerospaceweb.org 2005, Northrop Grumman B-2 Spirit Intercontinental Strategic Bomber, *Aerospaceweb Organisation*, Accessed 22nd November 2005, <http://www.aerospaceweb.org/aircraft/bomber/b2/b2-schem-01.gif>.

AIAA 2003, *AIAA AEROSPACE DESIGN ENGINEERS GUIDE*, 5th Edition, American Institute of Aeronautics and Astronautics, Inc., Reston, pp. 2-2-2-12.

Airbus Company 2005a, A380 Technology and innovation, *Airbus Company*, Accessed 28th September 2005, <http://www.airbus.com/en/aircraftfamilies/a380/innovation.html>.

Airbus Company 2005b, Latest features, *Airbus Company*, Accessed 28th September 2005, <http://www.airbus.com/en/myairbus/airbusview/technologicalleadership.html>.

Airbus Deutschland GmbH 2005, Presentation, *Safeair Organisation*, Accessed 30th September 2005, <http://www.safeair.org/safeair/prt/airbus_d.htm>.

AIRBUS S.A.S 2004, *A380 Facility Planning Manual Maintenance Facility Planning MFP, PRELIMINARY ISSUE, Issue. January 2004*, TECHNICAL DATA SUPPORT AND SERVICES, France.

Aircraft Aerodynamics and Design Group 2004, Component Weights, *Department of Aeronautics and Astronauts in Stanford University*, Accessed 11th December 2004, <http://adg.stanford.edu/aa241/structures/componentweight.html>.

aircrash.org 2001, The more things change, the more they remain the same, *Aircrash Organisation*, Accessed 2nd October 2005, <http://www.aircrash.org/burnelli/n30.htm>.

aircrash.org 1996, NASA/McDonnell Douglas Blended-Wing-Body from McDonnell Douglas "Presentation Packet", *Aircrash Organisation*, Accessed 7th January 2005, <http://www.aircrash.org/burnelli/bwb.htm>

AirlinesGate 2000, AIRLINERS SPECIFICATIONS, *AirlinesGate*, Accessed 10th November 2005, <http://airlinesgate.free.fr/jets.htm>.

AIRLINERS.NET 2005, Aircraft Data and History, *Luleå University of Technology*, Accessed 10th February 2005, <http://www.airliners.net/info/>.

aerostories 2005, Horten Two brothers, one wing., *aerostries*, Accessed 20th September 2005, <http://aerostories.free.fr/constructeurs/horten/page2.html>.

Alinghi 2005, Alinghi, *Team Alinghi*, Accessed 15th October 2005, <http://www.alinghi.com/en/>.

Altair Engineering 2005a, Altair HyperMesh 7.0, *Altair Engineering Inc.*, Accessed 26th September 2005, <http://www.altair.com/software/hm.htm>.

Altair Engineering 2005b, Altair HyperWorks, *Altair Engineering Inc.*, Accessed 26th September 2005, <http://www.altair.com/software/hw.htm>.

Amano, K. 2001, *Conceptual Aircraft Design*, 1st Edition, Tokai University, Kanagawa, Written in Japanese.

Aumann, P. 2001, 'MEGAFLOW: Parallel complete aircraft CFD', *PARALLEL COMPUTING, Computing*, No. 27, pp. 415-440, Accessed 26th January 2005, Science@Direct.

Bluefox9 2005, Commercial Aircraft Information, *Alair Commercial Airplanes' Alair Aircraft Trading Site*, Accessed 14th February 2005, <http://www.alair.com>.

Birch, S. 2001, Nuclear-powered aircraft, *SAE International*, Accessed 30th September 2005, <http://www.sae.org/aeromag/techupdate/05-2001/>.

Boeing Company 2005, 737 technical specifications, *Boeing Company*, Accessed 4th February 2005, <http://www.boeing.com/commercial/737family/technical.htm>.

Boeing News Release 2006, Boeing Phantom Works to Lead Research on X-48B Blended Wing Body Concept, Accessed 10th May 2006, <http://www.boeing.com/phantom/news/2006/q2/060504b_nr.html>.

Bolsunovsky A.L., Buzoverya N.P., Gurevich B.I., Denisov V.E., Dunaevsky A.I., Shkadov L.M., Sonin O.V., Udzhuhu A.J., Zhurihin J.P. 2001, 'Aircraft Design', Volume 4, Number 4, December 2001, pp. 193-219 (27), Elsevier Science.

Bowers, A. 2000, Blended-Wing-Body: Design Challenges for the 21st Century, *THE WING IS THE THING (TWITT) Meeting*, Accessed 2nd October 2005, <http://www.twitt.org/BWBBpwers.html>.

Bradley, R. K. 2004, 'A Sizing Methodology for the Conceptual Design of Blended-Wing-Body Transports', *NASA*, Paper No. NASA/CR-2004-213016.

Briganti, R. 2004, 'BOUSSINESQ MODELLING OF BREAKING WAVES: DESCRIPTION OF TURBULENCE', *COASTAL ENGINEERING*, pp. 402-414, Accessed 20th September 2005, Science@Direct.

Briganti. R, Bellotti. G, Musumeci. R, Foti. E & Brocchini. M. 2004, 'BOUSSINESQ MODELLING OF BREAKING WAVES: DESCRIPTION OF TURBULENCE', *COASTAL ENGINEERING 2004*, pp. 402-414, Accessed 20th September 2005, Science@Direct.

British Aircraft 2005, Armstrong Whitworth A.W.52, *British Aircraft*, Accessed 20th September 2005, <http://www.britishaircraft.com.au/aircraftpage.php?ID=124>.

Brzezinski, A. Garza, C.T. Thrower, J. &Young, B. 2003, *Term 3 Final Report Boeing Blended Wing Body Project 16.100: Aerodynamics, Boeing Company*, Accessed 10th May 2005, Massachusetts Institute of Technology, <http://ocw.mit.edu/.../16-100Fall2002/FFE4BBE5-C4F7-4544-91D6-C3 AD004ABEDD/0/Team3FinalReport1.pdf>.

Buescher, G. 2001, '747X vs. A380 How to Reduce Airport Congestion?', *AOE 4984, Configuration Aerodynamics*, March 2001, Accessed 10th December 2004, <http://www.aoe.vt.edu/~mason/Mason_f/A380Buescher.pdf>.

BWB World 2005, Information of HK1, *BWB World*, Accessed 20th September 2005, <http://www2s.biglobe.ne.jp/~FlyingWing/JapaneseTaillessPlane/Kayaba-1.html>, Written in Japanese.

Cowles, W. G. Parolimi, N. & Sawley, L. M. 2002, 'CFD Makes Waves in the America's Cup', *Fluent News*, Vol. 11, Issue 2, pp. 20-21.

Cumpsty, N. 2003, *Jet Propulsion: A Simple guide to the aerodynamic and thermodynamic design and performance of jet engines*, 2nd Edition, Cambridge University Press, Port Melbourne, pp.1-79.

Dassault Systemes 2004, CATIA V5R14, *Dassault Systemes*, Accessed 19th August 2004, <http://www.3ds.com/products-solutions/plm-solutions/catia/overview/>.

Drela, M. 2001, *XFOIL 6.94 User Guide*, Aircraft, Inc., Harold Youngren.

Dykins, H. D. 1976, 'A WING FOR THE AIRBUS', *Physics in Technology 7*, pp.246-253. Accessed 30th November 2005, < http://www.iop.org/EJ/abstract/0305-4624/7/6/303>.

eHow 2005, How to Estimate Your Walking Speed, eHow.com, Accessed 9th November 2005, <http://www.ehow.com/how_8939_estimate-walking-speed.html>.

Engine Alliance Company, 2005, About Engine Alliance, Engine Alliance LLC, Accessed 28th September 2005, <http://www.enginealliance.com/aboutintro.html>.

FAA 2005a, Federal Aviation Administration, The Federal Aviation Administration, Accessed 4th October 2005, <http://www.faa.gov>.

FAA 2005b, Current FAR by Part, *The Federal Aviation Administration*, Accessed 7th October 2005, <http://www.airweb.faa.gov/Regulatory_and_Guidance_Library/rgFAR.nsf/MainFrame?OpenFrameSet>.

Fluent Inc. 2005a, GAMBIT CFD Preprocessor, *Fluent Inc.*, Accessed 26th September 2005, <http://www.fluent.com/software/gambit/index.htm>.

Fluent Inc. 2005b, FLUENT: The World's Leading Commercial CFD Software, *Fluent Inc.*, Accessed 26th September 2005, <http://www.fluent.com/software/fluent/index.htm>.

Fluent Inc. 2003d, *FLUENT User's Guide: FLUENT 6.1 Documentation*, Fluent Inc., 2003-01-25.

Fluent Inc. 2005e, TGrid CFD Preprocessor, *Fluent Inc.*, Accessed 26th September 2005, <http://www.fluent.com/software/tgrid/index.htm>.

GloablSecurity.org 2005, Military: A-12 Avenger II, *GlobalSecurity.org*, Accessed 4th March 2005, < http://www.globalsecurity.org/military/systems/aircraft/a-12-specs.htm>.

Guynn, D. M. Freeh, E. J. & Olson, D. E. 2004, 'Evaluation of a Hydrogen Fuel Cell Powered Blended-Wing-Body Aircraft Concept for Reduced Noise and Emission', *NASA*, Paper No. NASA/TM-2004-212989.

Harris, T. 2005, How Stealth Bombers Work, *Howstuffworks*, Accessed 23rd November 2005, <http://science.howstuffworks.com/stealth-bomber2.htm>.

Hepperle, M. 2005, The Eppler Code «PROFIL», *Aerodynamics for Model Aircraft*, Accessed 10th November 2005, <http://www.mh-aerotools.de/airfoils/methods.htm>.

Hinterberger, C. García-Villalba, M. & Rodi, W. 2005, 'Large eddy simulation of flow around the Ahmed body', *Computer Systems Support at the University of Iowa*, Accessed 17th October 2005, <http://css.engineering.uiowa.edu/ ~me_160/Lab/LESahmedcarrodi.pdf>.

History of Northrop Corporation 2005, Occurrence, *BWB World*, Accessed 10th March 2005, <http://www2s.biglobe.ne.jp/~FlyingWing/Northrop_Chronicle.html>, Written in Japanese.

Horten Bros's Flying Wing 2005, BWB Aircraft Series of Horten Brother, *BWB World*, Accessed 10th March 2005, <http://www2s.biglobe.ne.jp/~FlyingWing/Ho_Bros.html>, Written in Japanese.

Houghton, L. E. & Carpenter, W. P. 2003, *Aerodynamics for Engineering Students*, 5th Edition, Heinemann-Butterworth, Oxford.

Howe, D. 2001, 'Blended wing body airframe mass prediction', *Process Mechanical Engineers*, Vol. 215, Part. G, pp. 319-331.

ICAO 2005, Making an ICAO Standard, *International Civil Aviation Organisation*, Accessed 4th October 2005, <http://www.icao.int/m_top.html>.

Ikeda, T. & Bil, C. 2005a, 'Aerodynamic Analysis of a Blended Wing Body Aircraft Configuration', *11th Australian International Aerospace Congress, Melbourne, 13-17th March, 2005*.

Ikeda, T. & Bil, C. 2005b, 'Aerodynamic Optimisation of a Blended Wing Body Configuration', *Society of Instrument and Control Engineers 2005 Annual Conference, Okayama, 8-10th August, 2005*.

Ikeda, T. & Bil, C. 2005c, 'Numerical Methods for Aerodynamic Analysis of Blended-Wing-Body (BWB) Aircraft Configuration', *7th Biennial Engineering Mathematics and Applications Conference, Melbourne, 25-28th September, 2005*.

INTA 2005, INTA-NATIONAL INSTITUTE FOR AEROSPACE TECHNOLOGY; Space Technology Serving Society., *Instituto Nacional de Tecnica Aerospacial*, Accessed 17th October 2005, <http://www.inta.es/index.asp>.

JET Composites 2005, AIRBUS: A380 technology & innovation, *JET Composites*, Accessed 29th September 2005, < http://www.jeccomposites.com/news/newsfiche.asp?id=1805&>.

Kennedy, R. & Rand, R.T. 2003, 'Emirates selects GE-PW Engine Alliance to power 23 A380 jumbo jets', Press Releases, United Technology Corp., 8th December 2003, <http://www.pratt-whitney.com/pr_120803.asp>.

Kim, D. & Saunders, D. J. 2003, 'Embedded Wing Propulsion Conceptual Study', *Vehicle Propulsion Integration Symposium, Warsew, Poland, 6-9th October, 2003*, Paper No. NASA/TM-2003-212696.

Kim, S-E. 2005, 'LES is More', *Fluent News*, Vol. 14, Issue 1, pp. 5-7.

Kim, S-E. & Mohan, S. L. 2005, 'PREDICTION OF UNSTEADY LOADING ON A CIRCULAR CYLINDER IN HIGH REYNOLDS NUMBER FLOWS USING LARGE EDDY SIMULATION' *24th International Conference on Offshore Mechanics and Arctic Engineering, 12-16th June, 2005*, Halkidiki, Paper No. OMAE 2005-67044.

Ko, A. Leifsson, T. L. Mason, W. Schetz, A. J. Grossman, B. & Haftka, R 2003, 'MDO of a Blended-Wing-Body Transport Aircraft with Distributed Propulsion', *AIAA's 3rd Aviation Technology, Integration, and Operation (ATIO) Forum, Denver, Colorado, 17-19th November, 2003*, AIAA, Paper No. AIAA-2003-6732.

Krajnović, S. & Davidson, L. 2004, 'Large-Eddy Simulation of the Flow Around Simplified Car Model', *2004 SAE World Congress, Detroit, Miami, 8-11th March*, 2004, SAE Paper No. 2004-01-0227.

Kroo, I. & Shevell, R.S. 2005, *Aircraft Design: Synthesis and Analysis*, Version 1.1, Desktop Aeronautics, Inc., Stanford, January 2006. Accessed 10th July 2006, <http://adg.stanford.edu/aa241/AircraftDesign.html>.

Kucukgokoglan, S. Aroussi, A. & Pickering, J. S. 2000, 'PREDICTION OF INTERACTIONS BETWEEN BOURNERS IN MULTI-BURNER SYSTEMS', *International Centre for Heat and Mass Transfer, International Symposium on Multiphase Flow and Transport Phenomena, Tekirova, Antalya, 5-10th November, 2000*.

Lanfrit, M. 2005, 'Best practice guidelines for handling Automotive External Aerodynamics with FLUENT', *Fluent Deutschland GmbH*, Version 1.2.

Lee, S. 2003, 'Conceptual Investigation of Flying Wing Double Deck Configuration', 2003, Written in German.

Leung, K.H. M. Liu, C-H. Chan, H.S. A. Leung, Y.C. D. Yam, W.C. Ng, S.P. Vrijmoed, L.P. L. 2005, 'Prediction of transient turbulent dispersion by CFD-statistical hybrid modelling method', *Atmospheric Environment*, Vol.39, pp. 6345-6351, Accessed 17th October 2005, Science@Direct.

Li, C. Zeng, J. & Zhou, S. 2004, 'Convergence Analysis of Generalized Schwarz Algorithms for Solving Obstacle Problems with T-Monotone Operator', *Computers and Mathematical with Applications*, Vol. 48, Issue 3-4, pp. 373-386.

Liebeck, H. R. 2005, NASA/ McDonnell Douglas Blended-Wing-Body, *Aircraft Organisation*, Accessed 7th January 2005, <http://www.aircrash.org/burnelli/bwb.htm>.

Makino, M. 1980, *Aerodynamics*, 5th Edition, Sangyoutosho, Tokyo, Written in Japanese.

Mathey, F. 2005, 'Turbulence Brings up the Rear', *Fluent News*, Vol.14, Issue 1, pp. 10-11.

Melbourne Airport 2005, Melbourne & the A380, Media releases 6th April 2005, *Melbourne Airport Inc.*, Accessed 11th November 2005,
< http://www.melbourne-airport.com.au/about_airport/media_releases_item.asp?id=248>.

Monash University 2005, FLYING WING, Monash University, Accessed 20th December 2005,
<http://www.ctie.monash.edu.au/hargrave/northrop.html#top>.

Monge, F. 2002, 'European External Aerodynamics Projects at INTA', *Fluent News*, Vol. 11, Issue 2, p. S3.

Mukhopadhyay, V. 2005, 'Blended-Wing-Body (BWB) Fuselage Structural Design for Weight Reduction', *46th AIAA/ASME/ASCE/AHS/ASC Structures, Structural Dynamics and Materials Conference, Austin, Texas, 18-21st April, 2005*, CASI, Report No. AIAA Paper 2005-2349.

NASA 2005, NASA Dryden Technology Facts - Winglet, *National Aeronautics and Space Administration*, Accessed 13th January 2005, <http://www.nasa.gov/lb/centers/dryden/about /Organizations/Technology/Facts/TF-2004-15-DFRC.html>.

NASAexplores 2005, X-Planes Explained, *NASA Express Lessons and Online Resources*, Accessed 5th March 2005, < http://www.nasaexplores.com/show2_articlea.php?id=03-065>.

National Transportation Safety Board 2000, 'Emergency Evacuation of Commercial Airplanes', *National Transportation Safety Board*, Safety Study NTSB/SS-00/01, Washington D.C.

netcomposites 2005, A380 World's Largest Commercial Aircraft, Successfully Completes Maiden Flight, *netcomposites*, Accessed 29th September 2005, <http://www.netcomposites.com/news.asp?2942>.

Oki, Y. & Masunaga, A. 2003, 'Prediction of High-Lift Flows Using Two-Dimensional Navier-Stokes Code with Sparat-Allmaras Turbulence Model and Unstructured Multigrids', *Transactions of the Japan Society for Computational Engineering and Science*, Paper No. 20030025.

Österheld, C., Heinze, W. & Horst, P. 2001, 'Preliminary Design of a Blended Wing Body Configuration using the Design Tool PrADO', *CEAS Conference on Multidisciplinary Aircraft Design and Optimisation, Köln, 25-26th June, 2005*.

Pachidis, A. V. 2005, INVESTIGATION OF A FEUL CELL-POWERED BLENDED WING BODY AIRLINER WITH BOUNDARY LAYER RE-ENERGIZATION, *Institution of Mechanical Engineers*, Accessed 20th February 2005, <http://www.imeche.org.uk/aero/pdf/pachodis.pdf>.

pilotfriend 2005, The Northrop Flying Wing and the B2 bomber, *pilotfriend*, Accessed 20th September 2005, <http://www.pilotfriend.com/century-of-flight/Aviation%20history/jet%20age/Northrop%20wing.htm>.

Purdue School of Aeronautics and Astronautics 2005, Rolls Royce Trent family, *Purdue University*, Accessed 11th February 2005, <http://roger.ecn.purdue.edu/~propulsi/propulsion/jets/tfans/trent.html>.

Qantas 2005, Checked Baggage, *Qantas Airways Limited*, Accessed 4th October 2005, <http://www.qantas.com.au/info/flying/beforeYouTravel/baggageChecked>.

Qin, N., Vavalle, A., Le Moigne, A., Laban, M., Hackett, K. & Weinerfelt, P. 2004, 'Aerodynamic considerations of blended wing body aircraft', *Aerospace Science and Technology*, No. 40, pp. 321-343, Accessed 23 February 2005, Science@Direct.

Quabeck, H. 2005, Herzlich willkommen auf unserer Homepage, *HQ-Modellservice*, Accessed 10th November 2005, <http://www.hq-modellflug.de/>, Written in German.

Raymer, P. D. 1999, *Aircraft Design: A Conceptual Approach*, 3rd Edition, American Institute of Aeronautics and Astronautics, Inc., Washington. D.C.

Reckzeh, D. 2002, 'Aerodynamic design of the high-lift-wing for a Megaliner aircraft', *Aerospace Science and Technology*, No. 7(2003), pp. 107-109, Accessed 11th August 2004, Science@Direct.

Rodriguez, L. D. 2000, 'A MULTIDISCIPLINARY OPTIMIZATION METHOD FOR DESIGNING INLETS USING COMPLEX VARIABLES', *AIAA*, Paper No. AIAA-2000-4875, Texas.

Rolls-Royce Company 2005, Trent 900, *Rolls-Royce Company*, Accessed 7th January 2005, <http://www.rolls-royce.com/civil_aerospace/products/airlines/trent900/intro.jsp>.

Sandilands, B. 2002, 'Aircraft: Blended Wing', *Aircraft & Aerospace - Asia Pacific*, October 2002, pp. 28-30.

Shih, T. Zhu, J. & Lumley, L. J. 1995, 'A new Reynolds stress algebraic equation model', *Computer Methods in Applied Mechanics and Engineering*, Vol. 125, Issue 1-4, pp. 287-302.

Smith, H. 2000, 'COLLEGE OF AERONAUTICS BLENDED WING BODY DEVELOPMENT PROGRAM', *The 22nd International Council of the Aeronautical Science, Harrogate, 28-31st August, 2000*, International Council of the Aeronautical Sciences.

Steinke, S. 2001, 'AIRBUS STUDIES FUTURE AIRLINER CONCEPTS', *FLUG REVUE January 2001*, pp. 21-22, Online Journal, Accessed 30th September 2005, <http://www.flug-revue.rotor.com/FRheft/FRH0202/FR0101e.htm>.

Stößel, B 2005, Airbus A380, *private pilot*, Accessed 10th November 2005, <http://www.flybernhard.de/ueb_eng.htm?http://www.flybernhard.de/a380_e.htm>.

Sweetman, B. 1992, *Northrop B-2 Stealth Bomber: The Complete History, Technology, and Operational Development of the Stealth Bomber*, Motorbooks International, Osceola.

The MathWorks 2005, Matlab Documentation, *The MathWorks Inc.*, Accessed 1st October 2005, <http://www.mathworks.com/access/helpdesk/help/techdoc/learn_matlab/learn_matlab.html>.

Torenbeek, E. 1991, 'Aerodynamic Performance of Wing-Body Configuration and the Flying Wing', *SAE International*, SAE Technical Paper – Document Number: 911019, April 1991.

Torikai, T. & Kuze, S. 1999, *Structural Aircraft Design*, 4th Edition, Japan Aeronautical Engineer's Association, Tokyo.

Trapp, J. & Zores, R. 2005, NACA 4 Digits Series, *the Institute of Fluid Mechanics of the German Aerospace Center (DLR)*, Accessed 10th November 2005, <http://www.pagendarm.de/trapp/programming/java/profiles/NACA4.html>.

Wei, G & Kirby, T. J. 1994, 'A Time-Dependent Numerical Code for Extended Boussinesq Equations', *Journal of Waterway, Port, Coastal, and Ocean Engineering*, Vol. 121, Issue. 5, pp. 251-261.

Willems, N. Easley, T. J. & Rolfe, T. S. 1981, *STRENGTH OF MATERIALS*, McGraw-Hill Book Company, New York, pp. 297-307.

WTO 2005, Long-term Prospects: Tourism 2020 Vision, *World Tourism Organisation*, Accessed 13th July 2005, <http://www.world-tourism.org/facts/2020/2020.htm>.

Yang, D. X. Ma, Y. H. & Huang, N. Y. 2003, 'Prediction of homogeneous shear flow and a backward-facing step flow with some linear and non-linear k-ε turbulence models', *Communications in Nonlinear Science and Numerical Simulation*, Vol. 10, Issue 3, pp. 315-328.

Appendix

Appendix 1: Comparison of Three Aircraft (Airbus A380, Boeing B747-400 and B777-300)
(Source: Melbourne Airport Inc., Media Release 6th April 2005)

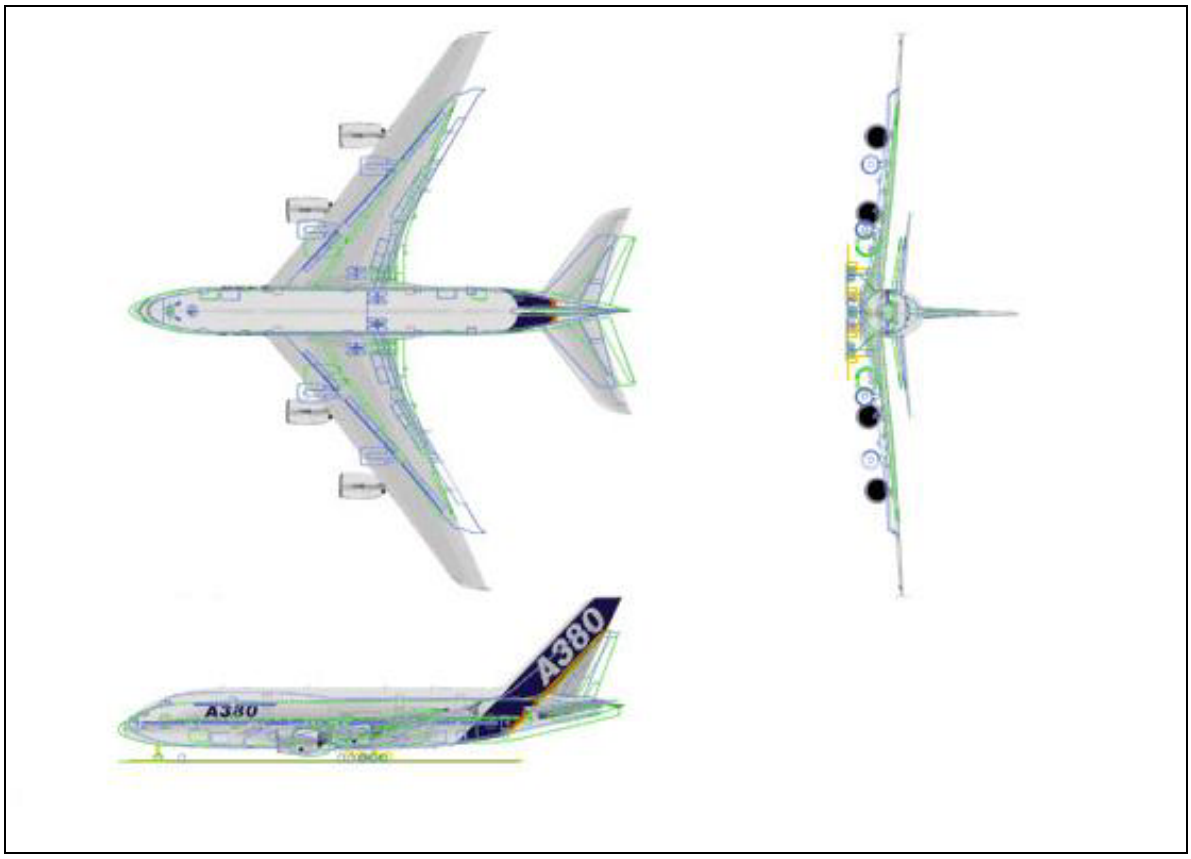

Aircraft Picture: Airbus A380-800, Blue Line: Boeing B747-400, Green Line: Boeing B777-300

Table Specifications of Three Aircraft

	Airbus A380-800	**Boeing B747-300**	**Boeing B777-300**
Overall Length (m)	73.0	70.7	73.9
Wingspan (m)	79.8	64.5	60.9
Height (m)	24.1	19.3	18.5

Appendix 2: Specification of Trent 900

(Source: Rolls-Royce Website: http://www.rolls-royce.com)

www.rolls-royce.com

Trent 900

Leading the way on the Airbus A380

As the fourth generation in the Trent family, the Trent 900 will feature the same successful three-shaft architecture as its Trent predecessors and its detailed design will reflect 20 million hours of Trent engine service experience.

The Trent 900 is the leading engine on the A380 and is proving an excellent engine on test, meeting and beating the next generation targets Rolls-Royce set the engine. The first engine ran to schedule in March 2003 and the flying test bed first flight was also on time in May 2004. The engine was certificated to plan in October 2004, leading to the Trent 900 powered first flight of the A380 in April 2005. The Trent 900 has also been selected as the launch engine for the aircraft, which enters service in 2006, with Singapore Airlines.

The Trent 900 offers the lowest risk route to low fuel burn, high reliability and low operating costs. Delivering high economic efficiency to A380/Trent 900 operators. The Trent 900 takes a demonstrated Trent maintainability advantage to the next stage and is the only engine on the A380 transportable whole in a Boeing 747F.

Although initially operating in commercial service at 70,000lb thrust, the Trent 900 was certificated at a rating of 80,000lb, allowing margin for growth. It has reached 93,000lb thrust during test bed running.

The Trent 900 is the lightest and most environmentally friendly engine on the A380. It is the quietest and cleanest engine option for the A380 and betters all current and proposed legislation in the environmental fields of noise and emissions. Trent 900 certification tests have shown it to have the world's lowest large turbofan emissions per lb thrust.

Etihad Airways recently became the sixth airline to opt for the Trent-powered A380s, joining Singapore Airlines, Lufthansa, Qantas, Virgin Atlantic and Malaysia Airlines. This further strengthens the Trent 900s market share to 51% with 84 firm and option orders, and with the Trent 900 now selected by six out of the nine operators to have made engine selections, the Trent 900 is the engine of choice on the A380.

Engine Specification

SL 0.25Mn, flat-rated to 30°C/86°F	
Thrust	70,000-76,500lb (Certificated up to 80,000lb)
Bypass ratio	8.7-8.5
Inlet mass flow	2655-2745lb/sec
Fan diameter	116in
Length	179in
Weight	14,190lb
Stages	Fan, 8 IPC, 6 HPC, 1 HPT, 1 IPT, 5 LPT
Certification	29th October 2004
EIS	2006

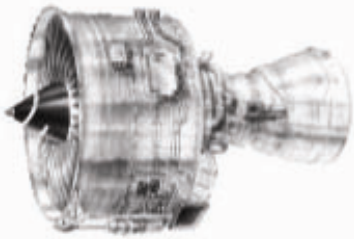

Rolls-Royce

Appendix 3: Explanation of Evacuating Time Estimation of BWB Configuration

----- **Definitions** -----

* The passenger (the location of the smile mark in Fig. 4.8) is 30 m far from the emergency exit A, and will evacuate from the emergency exit A.

* When making a queue, this situation is assumed that each person keeps approximately 1 m distance between forward and backward people, which was considered based on the experience.

* With the BWB cabin layout as Fig. 4.7, a number of passengers between 233 passengers (minimum passenger number of the bottom 4 modules in economy class) and 270 passengers (maximum: the half number of all passengers) is assumed to utilise the exit A.

* The main aisle may allow making two lines, because the width is approximately three times bigger than conventional aircraft.

----- **Time Estimation** -----

With these definitions with extra passengers, the situation of the passenger (Fig. 4.8) may substitute to other situation, such as the passenger is in the bottom of 85 meters' queue (2 lines and 300 passengers) as Fig. A. To be the first of the queue, the passenger will take approximately 60 seconds based on the average walking speed. In addition, the total evacuation time of the passenger including to move to safety place that will be approximately 80 seconds (20 seconds extra of ground activity).

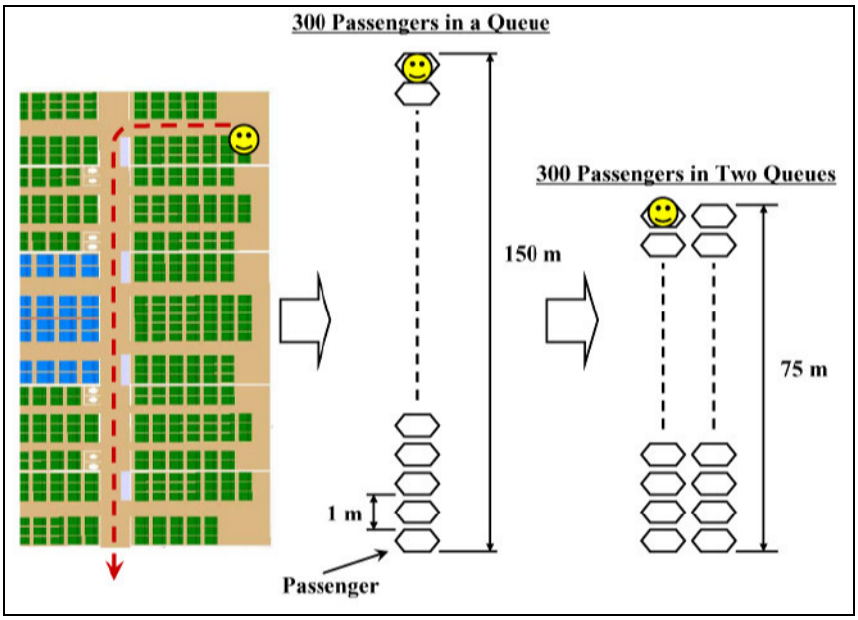

Fig. A Description of the Passenger Situation

Appendix 4: Excel Data of BWB Weight Estimation

	m^2	ft^2	Number	Degree	lb	kg	ft
W_{Sref}	717.82	7,726.90	---	---	---	---	---
W_{Swet}	1,871.85	216,887.00	---	---	---	---	---
W_{Nult}	---	---	4.00	---	---	---	---
W_{b}	---	---	---	---	---	---	259.19
W_{λ}	---	---	0.19	---	---	---	---
$W_{(t/c)ave}$	---	---	---	---	---	---	48.10
$W_{\Lambda ea}$	---	---	---	33.50	---	---	---
TOGW	---	---	---	---	1,234,600	559,900	---
ZFW	---	---	---	---	782,650	354,940	---
cos33.5	0.83389						
Cabin Layout	517.92	5,575.10	---	---	---	---	---
Fuselage	2,311.14	24,878.04	---	---	---	---	---
Lamda	0.5		cos45	0.707		$(t/c)_{ave}$	36.24
Span Length	5.44						
V_{S}	169.88	374.58	---	---	---	---	---
V_{b}	---	---	---	---	---	---	28.54
V_{Nult}	---	---	4	---	---	---	---
$V_{(t/c)ave}$	---	---	---	---	---	---	14.4
$V_{\Lambda ea}$	---	---	---	30	---	---	---
cos30	0.86603						

The maximum load factor of 4.0 was chosen for the BWB conceptual deign. Typical transport aircraft is utilised the positive value of 2.5-3.8 and the negative value of -1.0 (Table 2.7). However, the value was considered with unknown factors in new design.

Appendix 5: Specifications of PC Facilities

1. SGI UNIX Server

---

4 500 MHZ IP35 Processors, CPU: MIPS R14000 Processor Chip Revision: 1.4

FPU: MIPS R14010 Floating Point Chip Revision: 1.4

Processor revision: 1.4. Scache: Size 2 MB Speed 250 MHz DDR Tap 0xa

Main memory size: 4,096 Mbytes, Instruction cache size: 32 Kbytes, Data cache size: 32 Kbytes

2 Memory at Modules: 2,048 MB

---

2. Windows Platform

Machine: Hewlett-Packard HP Compaq

Monitor: Hewlett-Packard HP 7500

System: Microsoft Windows 2000 5.00.2195 Service Pack 4

Computer: Intel® Pentium® 4 CPU 2.80 GHz

AT/AT COMPATIBLE 515,568 RAM

Appendix 6: Overview of BWB Aircraft Configuration

Image of BWB Airliner

※ Flight Operation Profile

Mach Number	0.85
Altitude	11,000 m
Endurance	8,000 nautical miles (15,000 km)
Passenger	555 (Three Classes Layout)

CFD Result of BWB Configuration

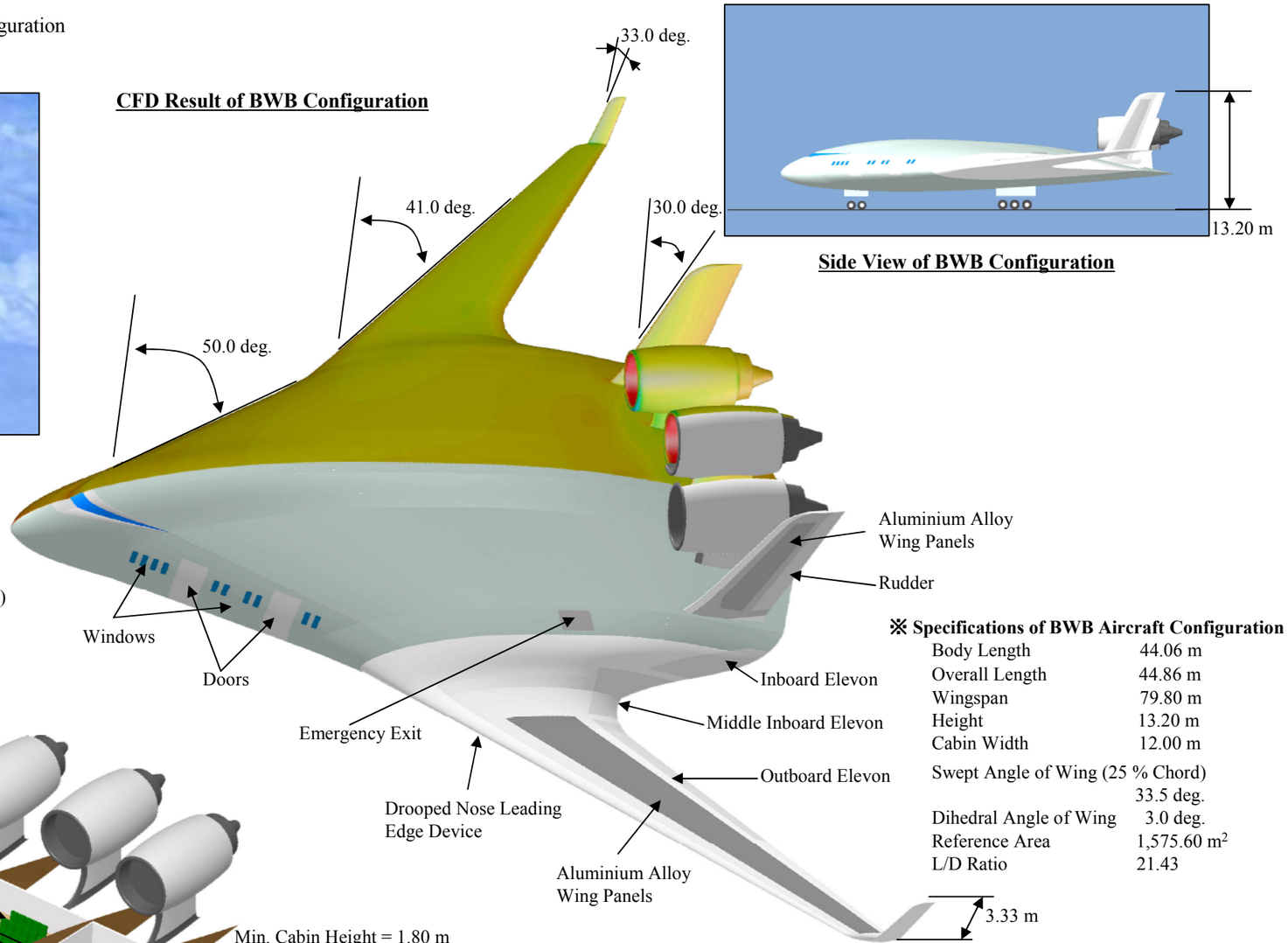

Side View of BWB Configuration

※ Specifications of BWB Aircraft Configuration

Body Length	44.06 m
Overall Length	44.86 m
Wingspan	79.80 m
Height	13.20 m
Cabin Width	12.00 m
Swept Angle of Wing (25 % Chord)	33.5 deg.
Dihedral Angle of Wing	3.0 deg.
Reference Area	1,575.60 m^2
L/D Ratio	21.43

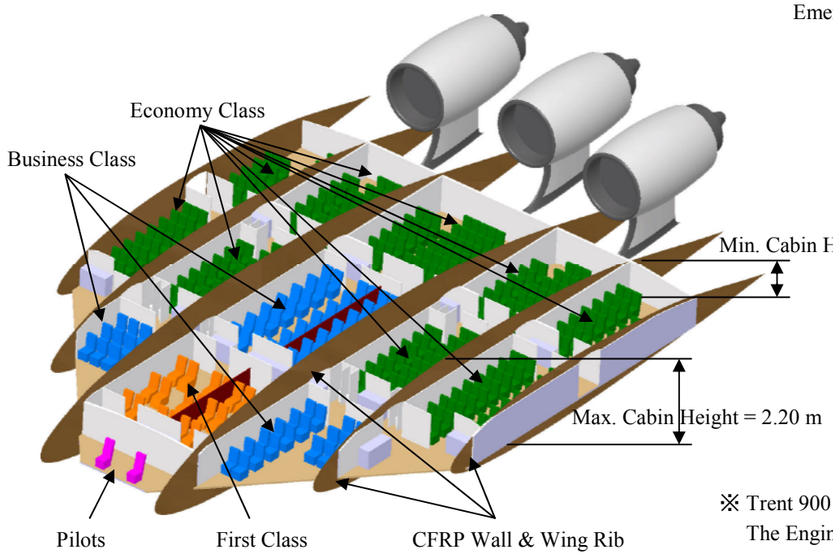

Cabin Design of BWB Configuration

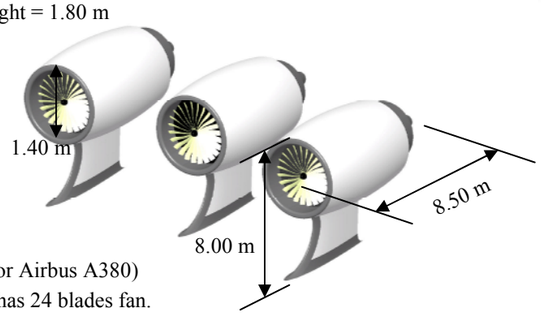

※ Trent 900 (for Airbus A380)
The Engine has 24 blades fan.

Propulsion Design of BWB Configuration

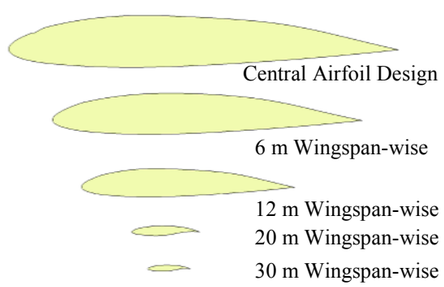

Airfoil Sections of BWB Configuration